Chem Soc Rev

REVIEW ARTICLE

View Article Online
View Journal | View Issue

Cite this: *Chem. Soc. Rev.*, 2017, **46**, 2237

Fluorescent chemical probes for accurate tumor diagnosis and targeting therapy

Min Gao,[ab] Fabiao Yu,*[ac] Changjun Lv,[c] Jaebum Choo*[d] and Lingxin Chen*[ac]

Received 13th December 2016

DOI: 10.1039/c6cs00908e

rsc.li/chem-soc-rev

Published on 20 marzo 2017. Downloaded on 11/05/2026 19:46:09.

Surgical resection of solid tumors is currently the gold standard and preferred therapeutic strategy for cancer. Chemotherapy drugs also make a significant contribution by inhibiting the rapid growth of tumor cells and these two approaches are often combined to enhance treatment efficacy. However, surgery and chemotherapy inevitably lead to severe side effects and high systemic toxicity, which in turn results in poor prognosis. Precision medicine has promoted the development of treatment modalities that are developed to specifically target and kill tumor cells. Advances in *in vivo* medical imaging for visualizing tumor lesions can aid diagnosis, facilitate surgical resection, investigate therapeutic efficacy, and improve prognosis. In particular, the modality of fluorescence imaging has high specificity and sensitivity and has been utilized for medical imaging. Therefore, there are great opportunities for chemists and physicians to conceive, synthesize, and exploit new chemical probes that can image tumors and release chemotherapy drugs *in vivo*. This review focuses on small molecular ligand-targeted fluorescent imaging probes and fluorescent theranostics, including their design strategies and applications in clinical tumor treatment. The progress in chemical probes described here suggests that fluorescence imaging is a vital and rapidly developing field for interventional surgical imaging, as well as tumor diagnosis and therapy.

1. Introduction

Cancer is an extremely aggressive disease that involves uncontrolled cell growth and cell division. The incidence and death rate associated with cancer remain high,[1] and the mechanisms of the development and recurrence of tumors in humans are still not yet fully understood.[2] Therefore, cancer therapy faces huge challenges in modern medical technology. Precise detection of tumors should be the first consideration. The primary

[a] *Key Laboratory of Coastal Environmental Processes and Ecological Remediation, Yantai Institute of Coastal Zone Research, Chinese Academy of Sciences, Yantai 264003, China. E-mail: fbyu@yic.ac.cn, lxchen@yic.ac.cn*
[b] *University of Chinese Academy of Sciences, Beijing 100049, China*
[c] *Department of Respiratory Medicine, Affiliated Hospital of Binzhou Medical University, Binzhou 256603, China*
[d] *Department of Bionano Engineering, Hanyang University, Ansan 426-791, South Korea. E-mail: jbchoo@hanyang.ac.kr*

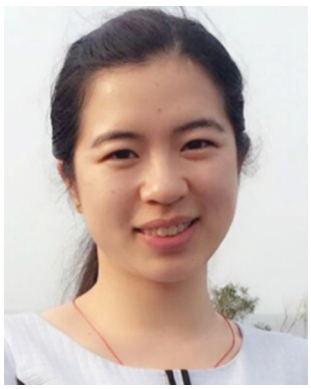

Min Gao

Min Gao is currently a doctoral candidate, under the guidance of Prof. Lingxin Chen, at Yantai Institute of Coastal Zone Research, Chinese Academy of Sciences, and has been since 2015. She received her MS degree in analytical chemistry at Department of Chemistry, Qufu Normal University, in 2015. Her current research interests focus on the development of functional fluorescent probes for bioimaging, cancer specific imaging and targeted therapy.

Fabiao Yu

Fabiao Yu is currently an associate professor at Yantai Institute of Coastal Zone Research, Chinese Academy of Sciences. He received his PhD, joint-educated, at Dalian University of Technology, and Dalian Institute of Chemical Physics, Chinese Academy of Sciences, in 2013. His research interests focus on functional probe molecules (fluorescence and phosphorescence analysis), theranostics, and organic functional materials.

Published on 20 marzo 2017. Downloaded on 11/05/2026 19:46:09.

challenge for the diagnosis and treatment of tumors is finding effective ways to discriminate the boundaries between the tumor and healthy surrounding tissue at the cellular level. Early diagnosis and treatment of a tumor can increase the survival rate to 90%. However, a precancerous lesion has a small volume and its morphology is atypical. Therefore, the lesion is difficult to identify with the naked eye. Technologies that can indicate the molecular boundary between tumor and healthy tissue are necessary to precisely identify diseased tissue and exploit the unique characteristics of tumors. Traditional clinical approaches of surgery, radiotherapy, chemotherapy, and immunotherapy need to be further improved because untargeted therapies can damage both normal cells and cancerous cells, thereby causing serious side effects and poor quality of life and prognosis. Therefore, accurate diagnosis of the tumor is required before starting therapy.

Changjun Lv

Changjun Lv is now a vice president in Binzhou Medical University. He is a professor and serves in Affiliated Hospital of Binzhou Medical University as a chief physician. He received his MD from China Medical University in 1995. He is skilled in the diagnosis and treatment of respiratory diseases, especially in the diagnosis of interstitial lung diseases. He is an expert with China's State Council special allowance due to his excellent performance in clinical work. His research interests include diagnosis and therapy of idiopathic pulmonary fibrosis, drug developments, and theranostics.

It seems likely that bioimaging technologies will meet this challenge. To date, *in vivo* medical imaging has made great advances in locating and discriminating tumor lesions as a result of developments in the engineering of imaging devices and the chemistry of imaging probes.[3] Several imaging diagnostic technologies have been applied in clinical medicine to reveal underlying disease and to assess prognosis and treatment, including magnetic resonance imaging (MRI), X-ray radiography, computed tomography (CT), positron emission tomography (PET), ultrasonography (US), and optical imaging. However, novel imaging tools with high sensitivity are urgently required because of the relatively low concentrations of target analytes *in vivo*. Traditional imaging modalities like CT, MRI, and US lack sufficient specificity and sensitivity, which can be attributed to background tissue noise, tissue metabolism, and the limited resolution and depth of signal penetration. PET is highly sensitive, but widespread application of this imaging modality is limited by its poor spatial and temporal resolution and the stringent safety regulations for radioactive compounds.[4] Compared with the conventional strategies of CT, MRI, and radioisotope imaging, an optical-based imaging approach can increase the target-to-background ratio by employing optical probes with unique features of (1) simultaneous multicolor imaging and (2) signal activation in the tumor. Therefore, optical imaging, such as fluorescence and bioluminescence imaging, offers the promise of accurate tumor diagnosis through non-invasive, real-time, and high-resolution imaging. Fluorescence bioimaging as a technique to visualize specific organelles in live cells[5–10] and whole animals[11,12] has become a powerful supporting tool for biological research,[13–16] and even for clinical utilization such as in the emerging field of fluorescence-guided surgery.[17–21] Additionally, fluorescence bioimaging can capture specific molecular information on tumor structure and tumor metabolism. Fortunately, these probes are also low cost, non-radioactive, simple and quick to use. In particular, near-infrared (NIR) fluorescence bioimaging probes with NIR absorption and emission profiles can

Jaebum Choo

Jaebum Choo has been in the faculty of the Bionano Engineering Department at Hanyang University, since 1995. He obtained his PhD in laser-induced spectroscopy at Texas A&M University, in 1994. In 2015, He became a Baik Nam Distinguished Professor due to his excellent academic achievements. He served as a President of Korea Biochip Society, in 2015. His current research programs are centered on the development of ultra-sensitive optical detection systems for rapid and accurate in vitro diagnostics. He has given 120 invited lectures in the USA, Europe and Asia, and has published over 220 research papers in refereed journals and 4 book chapters.

Lingxin Chen

Lingxin Chen has been a professor at Yantai Institute of Coastal Zone Research, Chinese Academy of Sciences, since 2009. He obtained his PhD in analytical chemistry at Dalian Institute of Chemical Physics, Chinese Academy of Sciences, in 2003. During 2004–2009, he worked at Department of Chemistry, Tsinghua University, and Department of Applied Chemistry, Hanyang University, respectively. His research interests include the studies of novel properties of materials such as functionalized nanoparticles & functional probe molecules for developing nanoscale biochemical analysis methods and molecular imprinting-based sample pretreatment technology. He has published 3 academic books, 200 research papers and topical reviews.

 This journal is © The Royal Society of Chemistry 2017

Published on 20 marzo 2017. Downloaded on 11/05/2026 19:46:09.

maximize tissue penetration while minimizing the absorbance of heme in hemoglobin and myoglobin, water, and lipids.[22–29] Recently developed NIR probes for fluorescence-guided surgery have shown great progress in determining the tumor margin and executing lesion resection.

The other challenge for tumor therapy is how to improve the drug therapeutic efficacy with minimum side effects due to the non-specific distribution of small molecular drugs *in vivo*. Undoubtedly, the rapidly growing class of chemotherapeutic drugs has achieved clinical success. However, the severe side effects of many drugs, including poor bioavailability, rapid blood/renal clearance, non-selective accumulation, uncontrollable drug release, bone marrow depression, severe multidrug resistance, and gastrointestinal disorders, have decreased the drug efficacy and caused tremendous pain to patients. The new nano-carriers that have rapidly emerged as drug delivery systems may overcome these limitations.[30–38] The drug delivery mechanism of nano-carriers depends on enhanced permeability and retention (EPR) effects. The anticancer drugs are either conjugated to the nano-carriers or packaged as nano-capsules. These combinations demonstrate better tumor penetration and controllable drug release at the target site compared with free drugs.[39–41] However, these conjugates have several disadvantages that cannot be ignored, such as the potential cytotoxicity of the heavy metal component or surface-coated materials, high cost, and difficulties in reproducibility and quantification.[42,43] Compared with nanoparticle-based therapeutic agents, small molecular fluorescent probe-based therapeutic agents are becoming preferred chemotherapeutic candidates.[3,44–50] These small fluorescent theranostic agents exhibit improved photophysical properties and can be easily modified by chemical synthesis.[51,52] The structural architecture of these systems is often relatively simple and compact: a desirable fluorophore, a tumor targeting ligand, and a masked antitumor drug. The intact theranostic agent is delivered through the circulation to accumulate in the tumor through the action of the targeting ligand. After being triggered to release drug *in situ*, the fluorophore emits fluorescence for monitoring of pharmacokinetics, tumor therapy, and tumor prognosis (Fig. 1).

In this review, we describe the entities that have been elegantly established to date, and aim to provide an up-to-date and concise overview of the design, application, and development of small molecular-weight fluorescent imaging agents and fluorescent theranostics for tumor diagnosis and therapy. We summarize the criteria governing the choice of the targeted receptor, modification of the targeting ligand, employment of the conjugating linker, utilization of the fluorophore, and optimization of the therapeutic drug. We discuss the strategies for integrating a targeting ligand with a suitable fluorophore and the desired linker-cleavage chemical reaction for selective release of the masked cytotoxic drug after endocytosis into tumor cells. We also address the issue that the development of fluorescent imaging agents is currently limited by the availability of NIR fluorophores.

2. Fluorescent probes for tumor diagnosis

The early diagnosis of preinvasive and metastatic tumor cells in patients is critical for the success of tumor therapy and improvement of survival rates. The fluorescence bioimaging approach,

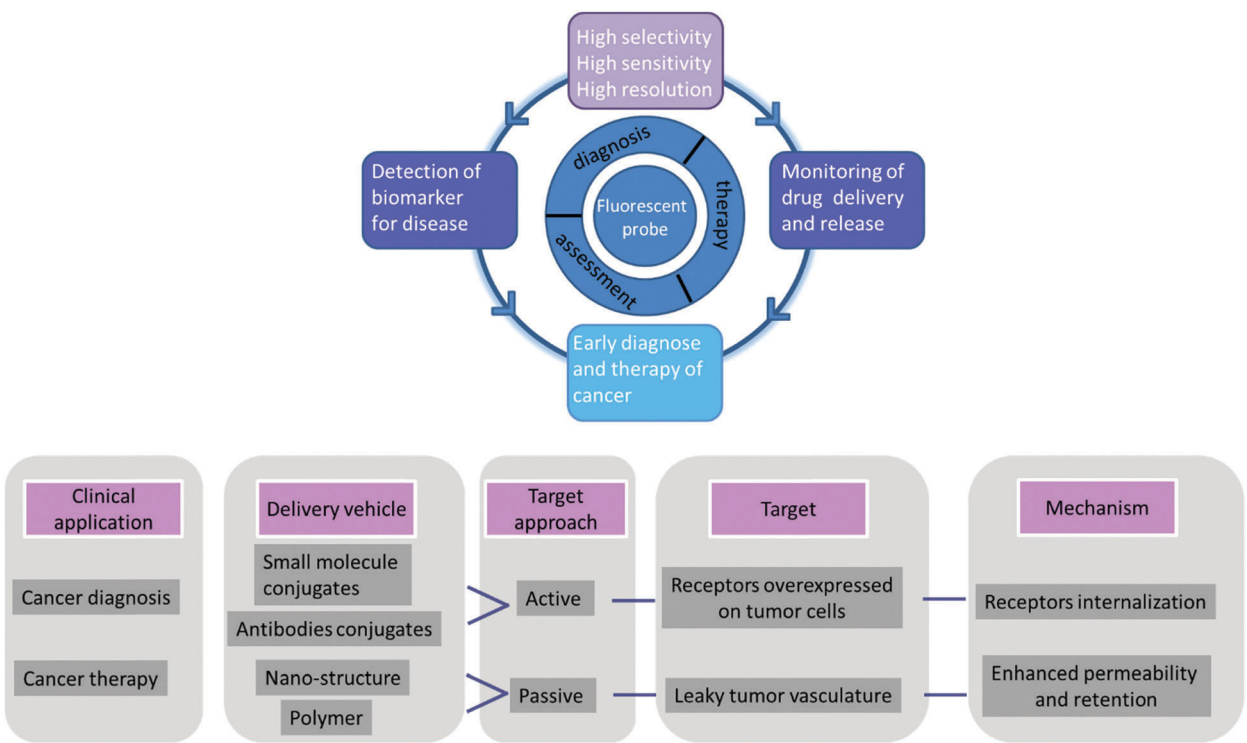

Fig. 1 Summary of applications of fluorescent probes in diagnosis and therapy.

Published on 20 marzo 2017. Downloaded on 11/05/2026 19:46:09.

which is emerging as a promising non-invasive, real-time, and high-resolution modality, can be employed for the early diagnosis of tumors. Fluorescent signals can provide molecular information on tumor tissues that is related to the tumor anatomical structure and metabolism. There is an urgent need to establish stable, efficient, and safe multifunction fluorescence systems to accelerate the achievement of accurate and personalized medicine. A successful fluorescent probe must meet several requirements for medical imaging, including wavelength, brightness, biostability, photostability, specific tissue accumulation, and pharmacokinetics. Conventionally, one approach is to simply and directly conjugate the fluorophore with a ligand that can bind to a certain cellular surface receptor: a so-called active imaging probe (Fig. 2). The imaging mechanism relies on accumulation and retention of the probe at the target site as a contrast agent. This approach is helpful for tumor imaging, but the non-bound probe must be quickly cleared from the circulation *via* excretion. An activatable imaging probe can be employed to achieve highly specific delivery; this type of probe is only activated within the targeted tumor cells, for example by a tumor-specific enzyme. Such probes are non-fluorescent or weakly fluorescent in the unactivated state, but become strongly fluorescent after activation by the relevant molecular trigger. Thus, the target-to-background ratio is higher than that of active probes. The activation mechanisms of activatable probes mainly depend on enzyme digestion and quenching effects. After removal of the quencher moiety, the released fluorophores will immediately emit fluorescence (Fig. 2). However, the fluorescent probes that are currently employed in intraoperative imaging systems for clinical fluorescence imaging are untargeted fluorophores including indocyanine green,[53] methylene blue,[54] 5-aminolevulinic acid,[55] and fluorescein.[56] In this section, we classify these probes according to their conceived structures and functions.

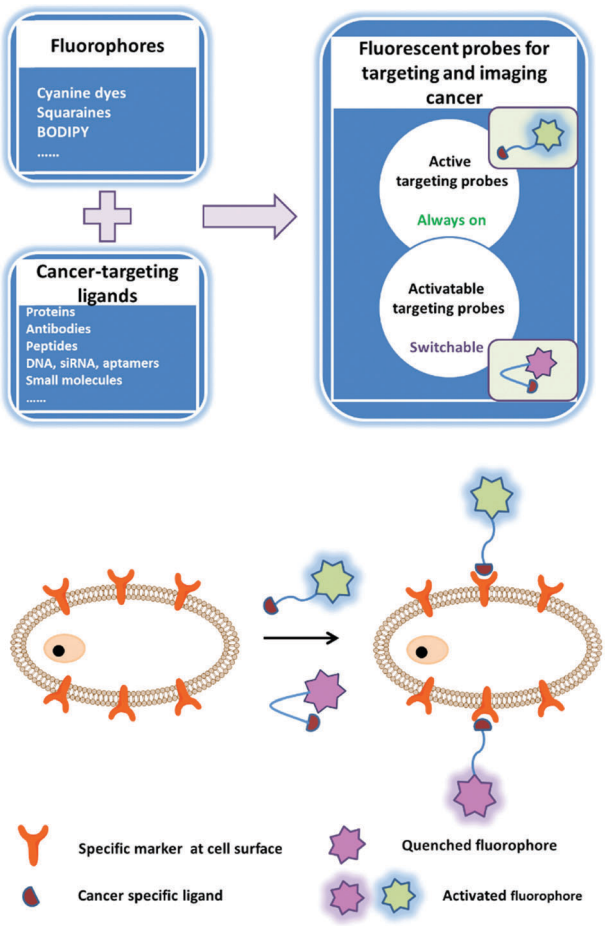

Fig. 2 Strategies of fluorescent probes for tumor diagnosis.

2.1 NIR imaging fluorophores

Near-infrared (NIR) light can penetrate tissue more deeply and minimize the interference from background autofluorescence, which greatly facilitates *in vivo* imaging of the molecular processes.[22–24,57–59] However, suitable fluorophores for tumor imaging must possess good hydrophilicity, stable photostability, high quantum yield, and excellent sensitivity in biological systems. Recent developments in cyanine dyes, squaraine, phthalocyanines, porphyrin derivatives, and BODIPY dyes have made them good candidates for tumor imaging (Fig. 3).

Shi and Chung *et al.* identified a class of NIR fluorescence heptamethine cyanines (**1–3**) for tumor imaging.[60,61] These small molecular dyes could be taken up and accumulated in tumor cells without requiring chemical conjugation with tumor-specific targeting ligands. The recognition mechanism was mediated by hypoxia-induced HIF-1α and specific organic anion transporting polypeptides (OATPs). This simple and direct strategy had no limitation to specific tumor cell types. The unique properties of **1** for selective imaging of the sentinel lymph node (SLN) in animals are very important because the SLN is the first barrier that prevents tumor cell metastasis from the lymph node. Real-time images from the injection site toward the SLN were achieved within 5 min, and the retention time could be up to 2 weeks. After conjugation of **2** with a positron-emitting radionuclide, the NIR dye **4** showed improved deep-tissue tumor detection with fluorescence imaging and PET/CT scans.[62] The above NIR dyes can be actively taken up and accumulated in cancer cells within 30 min. *In vivo* NIR imaging was achieved over a period of 24 h.

The fluorescence emission that lies in the first near-infrared window (NIR-I; 650–900 nm) is far superior to visible wavelengths, but a fluorophore that emits within the second near-infrared window (NIR-II; 1000–1700 nm) exhibits a greater improvement in imaging quality, such as decreased tissue autofluorescence, reduced photon scattering, and low levels of photon absorption.[63–66] However, NIR-II fluorophores are often constrained by slow metabolism and long retention in the reticuloendothelial system. Hong *et al.* synthesized a soluble NIR-II emitting probe (**5**) for imaging the mouse lymphatic vasculature and sentinel lymphatic mapping near the tumor.[66] The fluorescent signal in 4T1 xenograft tumors was observed within 10 min after intradermal injection of **5-PEG**. The probe **5-PEG** was excreted through the kidneys within 24 h. Dye **5** also allowed targeted imaging of tumors *in vivo* when conjugated with an anti-epidermal growth factor receptor (EGFR) antibody.

 This journal is © The Royal Society of Chemistry 2017

Published on 20 marzo 2017. Downloaded on 11/05/2026 19:46:09.

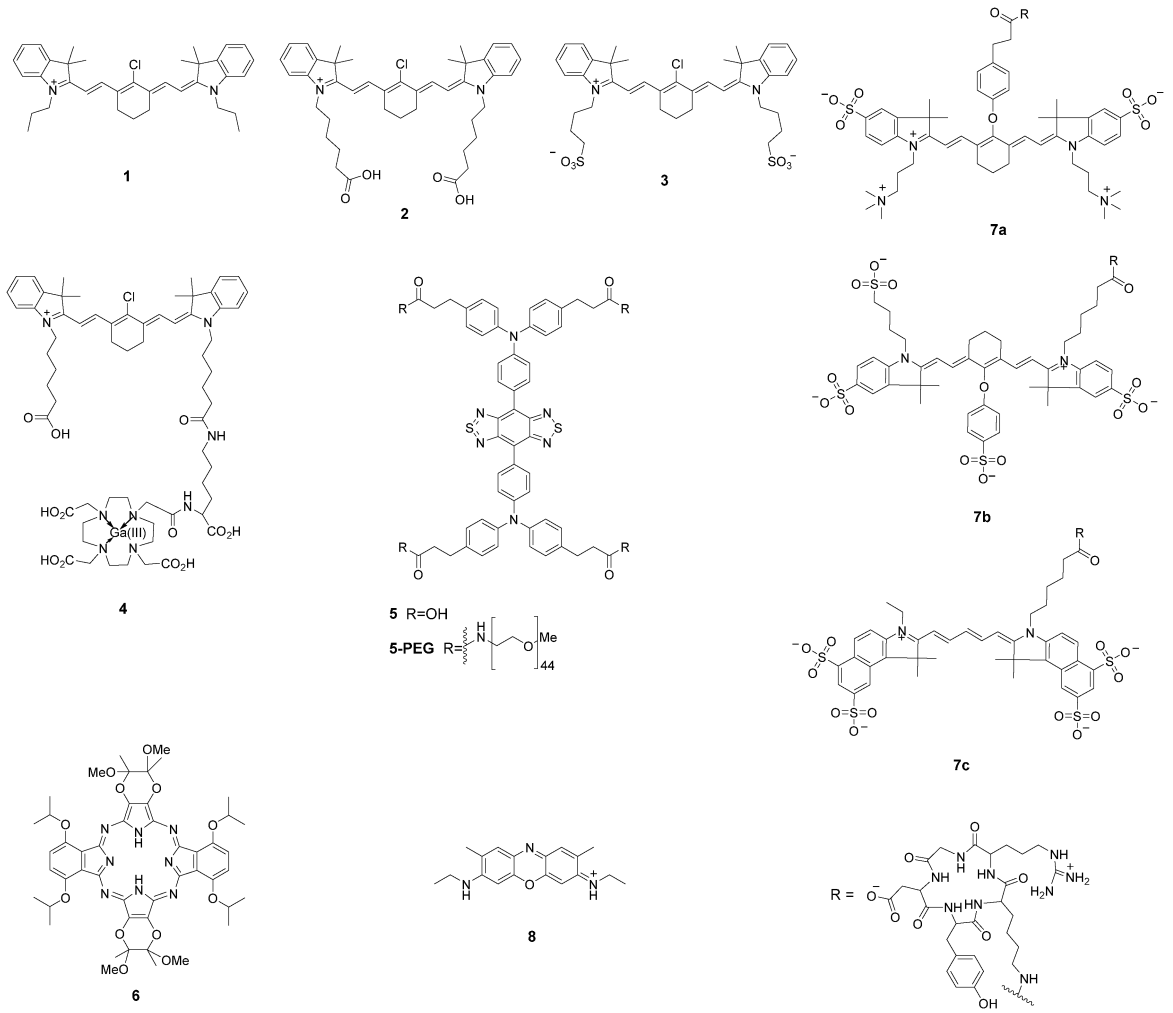

Fig. 3 NIR imaging fluorophores.

Hoffman *et al.* reported a chiral NIR porphyrazine (**6**) for accumulation in tumor cells.[67] The porphyrin derivative was composed of four bridged pyrrole subunits linked through nitrogen atoms. Compound **6** was taken up by cells into the lysosomes through low-density lipoprotein (LDL) receptor-mediated endocytosis. LDL is preferentially associated with highly proliferative tumor cells over normal cells, therefore this NIR fluorescent probe enabled excellent contrast imaging between tumor and surrounding tissue. *In vivo* studies revealed that **6** was preferentially taken up and retained in MDA-MB-231 human breast cell xenografts in mice. The retention of **6** in the tumors continued to increase up to 48 h after injection.

A chemical compound with well-balanced charge would result in a more hydrophilic molecule with low non-specific targeting properties. Frangioni *et al.* introduced zwitterionic properties into NIR fluorophores to improve the signal-to-background ratio for diagnostic and therapeutic applications.[68] Conjugates of the zwitterionic heptamethine indocyanine with cyclic peptide cyclo(RGD-yK) (**7a–c**) showed good behaviors *in vitro* for cell binding assays, histology, and immunoblotting and *in vivo* for xenograft tumor targeting and image-guided surgery. Real-time intraoperative melanoma detection was achieved 4 h after intravenous injection into mice. A real-time intraoperative thrombus could be detected at 30 min.

Accidental transection or injury of nerves leads to significant morbidity of numbness, pain, or paralysis. Choi *et al.* evaluated an oxazine derivative (**8**) to navigate peripheral nerve structures in rats and swine.[69] The pharmacokinetic data suggested that the targeted fluorophore rapidly penetrated and was retained in nerves. The fluorescent labeled nerve was clear enough for discrimination for 3–4 h during complicated nerve surgery. The dye provided a nerve-targeted signal in the brachial plexus, sciatic nerve, and recurrent laryngeal nerve for up to 12 h after a single intravenous injection.

2.2 Probes integrating tumor-targeting ligands

Tumor targeting capability of fluorescent imaging probe is crucial for the accurate diagnosis of tumors. Common strategies for targeting ligand-based imaging probes involve exploitation of certain cell surface receptors that are overexpressed in cancerous cells (Fig. 2). There are a number of ligands (*e.g.*, small molecules, peptides, proteins, antibodies, and aptamers) with a high

Published on 20 marzo 2017. Downloaded on 11/05/2026 19:46:09.

intrinsic affinity for tumor targets that can be considered in the design of imaging probes. The probe is targeted to tumor cells through conjugation of a certain ligand, which accordingly reduces the delivery to normal cells and the associated collateral toxicity. Such strategies involve direct conjugation between the desirable fluorescent dyes and the ligands to produce a suitable imaging probe. This type of fluorescent probe can be targeted and bind to the tumor, while surplus probe will be excreted from the blood circulation. In this regard, an activatable imaging probe has the potential to further improve the signal-noise ratio.

2.2.1 Small molecules as tumor targeting ligands

A. Prostate-specific membrane antigen. Prostate-specific membrane antigen (PSMA) is a type II membrane glycoprotein that is highly expressed in the neovasculature of tumors.[70,71] PSMA-specific antibodies,[72] aptamers,[73] peptides,[74] peptide derivatives,[75] and other small molecules[76,77] have been developed as targeting ligands. Slusher *et al.*[78] described a high-affinity, single nucleophile-containing, small-molecule imaging probe (**9**) targeting the active site of the PSMA enzyme. The probe was obtained by conjugation of a tetra-sulfonated NIR heptamethine indocyanine fluorescent derivative with (2-[[(3-amino-3-carboxypropyl)(hydroxy)phosphinyl)-methyl]pentane-1,5-dioic acid) (GPI). GPI itself was a potent inhibitor with a K_i of 9.0 nM, but the probe showed greater than 20-fold improvement in affinity (0.4 nM). The specificity of binding of **9** to cell-surface PSMA was tested not only in human prostate cancer cell lines LNCaP and PC-3, but also in human prostate cancer xenograft tumors in athymic mice.

Berkman *et al.*[79,80] reported fluorescent probes **10** and **11** for imaging PSMA-expressing cells. The fluorophore of compound **10** was fluorescein. Compound **10** could effectively label cell membranes of LNCaP cells due to interactions with PSMA. Co-localization studies of **10** with transferrin-Texas Red showed that **10** was located in the perinuclear region. Moreover, **10** could be retained within endosomes for up to 150 min without loss of the signal. The IC_{50} values of GPI and fluorescent conjugate **10** were 14 nM and 0.35 nM, respectively. Obviously, the dye-conjugate showed greater inhibitory potency against PSMA. The fluorescent probe **11** was developed by conjugation of NIR Cy5.5 with GPI. The probe exhibited high potency against PSMA with IC_{50} of 0.55 nM.

In addition, Pomper *et al.*[81] described a PSMA-binding NIR probe **12** for targeting PSMA in mice. The fluorophore of compound **12** was a heptamethine indocyanine derivative. Probe **12** demonstrated a PSMA inhibitory activity of 0.37 nM. The pharmacokinetic behavior of **12** *in vivo* was acquired at an array of post-injection time points. The probe had clearly accumulated in the tumor at 18.5 h, and the fluorescence could be imaged repeatedly over 70.5 h.

Kozikowski *et al.*[82] outlined a strategy of directly conjugating a PSMA inhibitor and doxorubicin (**13**) for locating prostate cancer cells by targeting PSMA. The antiproliferative action of **13** was poor without compromising the binding affinity.

B. Cyclooxygenase-2. Cyclooxygenase-2 (COX-2) is a crucial biological mediator in the etiology of inflammation and cancer. This enzyme is absent or present at low levels in normal cells but has high expression levels in inflamed tissues as well as many premalignant and malignant tumors.[83] COX-2 has been used as an ideal imaging biomarker for cancer cells. Many fluorescent probes have been engineered to target COX-2.

Marnett *et al.* reported a series of fluorescent probes (**14**, **15**) that efficiently targeted COX-2 in cells *in vitro* and *in vivo*.[84–87] The design strategy for these optimized candidates was based on a rhodamine-derived fluorophore with selective COX inhibitors (Fig. 4). *In vitro* experiments in 1483 head and neck squamous cell carcinoma (HNSCC) cells showed that compound **14** localized at the perinuclear regions of membraneous structures that appeared to be endoplasmic reticulum or Golgi. Lipopolysaccharide-activated RAW264.7 macrophages showed stronger fluorescence labeling due to immunological stress. These probes showed preferential accumulation in inflammatory lesions and tumors. Inflammation was induced with carrageenan in C57BL/6 mice and images were acquired 3 h after injection of the probes. The probes were then employed to image human tumor xenografts. Levels of fluorescence in the tumor required 3 h to reach near maximal levels and remained relatively high for at least 24 h. The authors also summarized the structure–activity relationship (SAR) effects between fluorophores and linkers.[85] The SAR study revealed that indomethacin conjugates were superior COX-2-targeted agents compared with other carboxylic acid-containing nonsteroidal anti-inflammatory drugs (NSAIDs) or COX-2-selective inhibitors. The 2′-trifluoromethyl analog of indomethacin is a potent and selective COX-2 inhibitor. The same group synthesized and evaluated the fluorescence imaging probe **15** with improved ability to inhibit COX-2 in inflammatory tissues and human tumor xenografts.[86] Kinetic analysis revealed that **15** was a slow and tightly binding inhibitor of COX-2. Application of the NIR COX-2-targeted probe **15** could improve imaging signal-to-noise in cancer detection. Probe **15** exhibited selective and potent COX-2 inhibition of purified protein and in human cancer cell lines. Time course imaging studies conducted from 3 h to 7 days post-injection showed a gradual decrease of the fluorescent signal in 1483 HNSCC tumors.

Peng *et al.* developed two-photon activatable fluorescent probes **16–19** for imaging COX-2 in cells and *in vivo*.[88–91] All of these free probes existed in the folded state. This molecular configuration led to quenching of fluorescence due to photo-induced electron transfer (PET) between the fluorophores and the inhibitor of COX-2. Strong fluorescence would be emitted after binding of the probe to COX-2. The imaging probe **16** could target the Golgi apparatus of tumor cells.[88] It stained cancer cells within 0.5 h and fluorescence intensity remained almost unchanged in cells for at least 6 h. This probe allowed imaging of sarcoma 180 tissue slices at a depth from 0 to 650 μm. The enzyme COX-2 is expressed at low levels (<0.085 μg mL^{-1}) as a monomer in inflammatory lesions. Each COX-2 monomeric unit is composed of three distinct structural domains. However, in tumor cells and tumor tissues COX-2 is expressed at high levels (>0.085 μg mL^{-1}) and exists as a homodimer. The binding site of enzyme inhibitors is located at the end of a hydrophobic cavity. Peng *et al.* improved their probe (**17**) for a sensitive

 This journal is © The Royal Society of Chemistry 2017

Published on 20 marzo 2017. Downloaded on 11/05/2026 19:46:09.

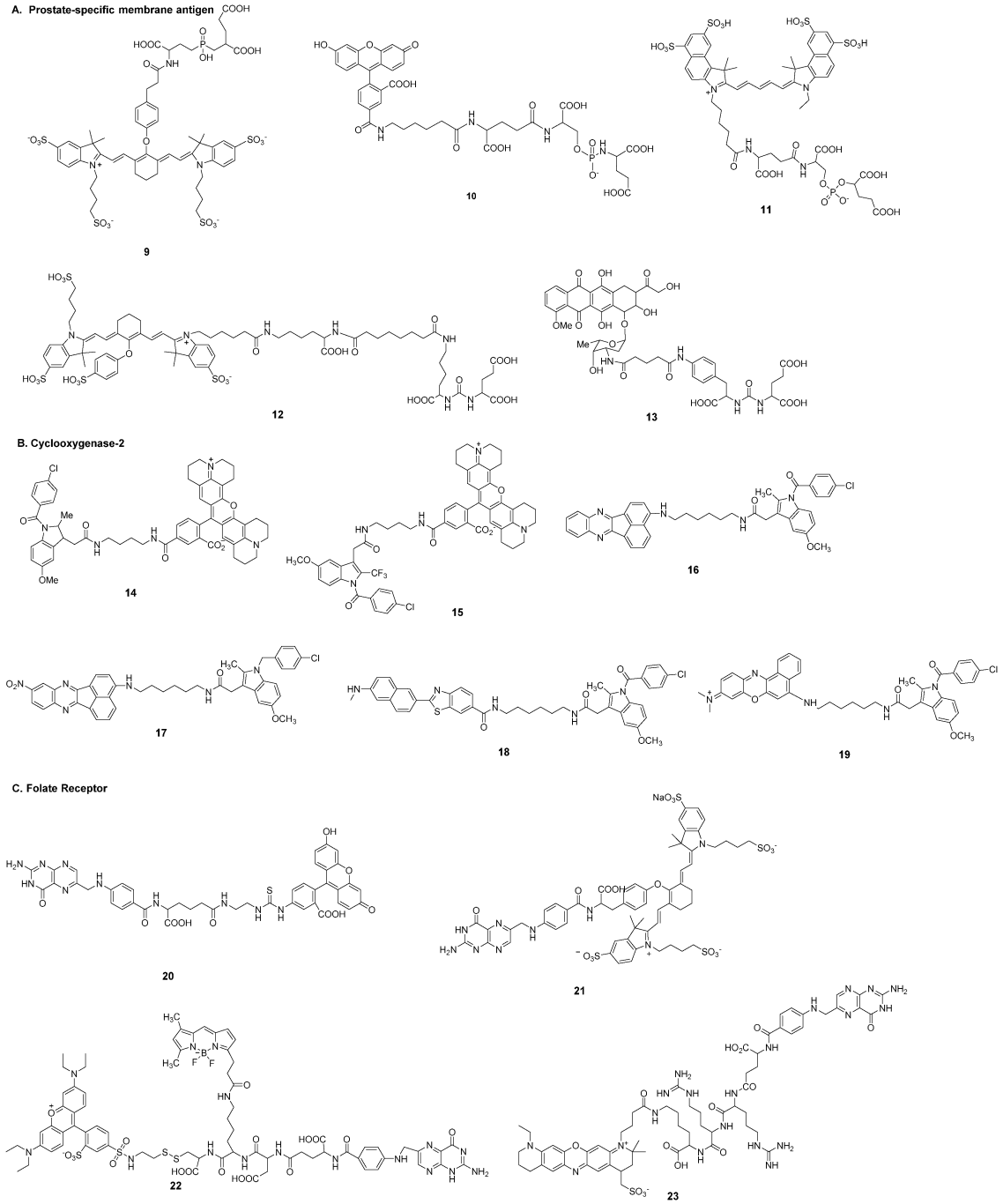

Fig. 4 Small molecules as tumor targeting ligands: A–C.

fluorescence response to environmental changes.[89] The fluorescence of **17** was ''turned on'' in both inflammation and cancer but the fluorescent emission was quite different. Moreover, cancerous tissues, inflamed tissues, and normal tissues could be discriminated *in vivo* by the naked eye. Probe **18** afforded high sensitivity and selectivity for COX-2 with a detection limit of 1.0 nM.[90] Probe **19** was a COX-2-specific NIR fluorescent probe[91] that could be directly applied to native polyacrylamide gel electrophoresis analysis and in-gel fluorescence analysis. This utilization facilitated rapid and sensitive screening of cancer cells without the need for a time-consuming enzyme-linked immunosorbent assay (ELISA).

C. Folate receptor. Folate is essential for the proliferation and maintenance of all cells. Folate has a high affinity for its cell surface folate receptor (FR, K_d: 10^{-10}).[92] The FR is primarily expressed on the healthy apical surface of polarized epithelial cells where it does not readily encounter folate from the bloodstream.[93] Once malignant transformation occurs, these apically restricted receptors will become accessible to folate because

Published on 20 marzo 2017. Downloaded on 11/05/2026 19:46:09.

intercellular junctions are lost during tumorigenesis and the FR is overexpressed over the entire cell surface. This significant upregulation of the FR on tumor cells has already become the main design strategy for folate-based tumor imaging probes.[44,49,92,93]

Low *et al.* described a tumor-targeting folate–fluorescein conjugate (**20**) for imaging of folate receptor-expressing tumors.[93] This probe could be visualized in peritoneal, subcutaneous, and metastatic murine tumor models with 2 h intravenous administration. Folate receptor-mediated transcytosis could not be exploited to deliver this folate conjugate into the brain.[94] Tumor masses exhibited significantly more fluorescence than adjacent normal tissues regardless of autofluorescence of non-injected controls. Excretion of the fluorescein conjugate from non-targeted tissues was achieved mainly through the kidneys within 2 h. Tumor nodules less than 1 cm in size could not be accurately detected with either computer tomography or ultrasound, but the fluorescent probe could locate malignant lesions smaller than 0.5 mm with appropriate optical instrumentation. The overexpression of the folate receptor in 90–95% of epithelial ovarian cancers prompted investigation into the use of this probe in intraoperative specific fluorescence navigation to improve the prognosis of patients with ovarian cancer.[20] Further development of a near-infrared fluorescent probe (**21**) allowed identification of more deeply seated tumors based on the stronger penetration properties of near-infrared dye IR-783 compared with fluorescein.[20,49,95]

Low *et al.* also synthesized a fluorescent folate conjugate (**22**) to label the disulfide bond-reducing process in endosomal compartments.[96] The approach adopted was to directly link folate to two fluorescent dyes *via* a disulfide bond, which engaged in fluorescence resonance energy transfer. Reduction of the disulfide bond resulted in a change in fluorescence from red to green. It was observed that disulfide reduction began in the endosomes and occurred with a half-time of 6 h after folate-FRET endocytosis.

Choi *et al.* developed a folate receptor-specific probe (**23**) for NIR fluorescence imaging of ovarian tumors *in vivo*.[97] The probe was synthesized by conjugating folate to the ATTO655 fluorophore *via* a cathepsin B-cleavable peptide spacer. The fluorescence emission from the fluorophore was effectively quenched by folate. After specific uptake into SKOV3 cells, the tumor-associated cathepsin B enzymes subsequently activated NIR fluorescence emission by cleaving the spacer. Assessment of the tumor targeting of probe **23** in a xenograft mouse model of ovarian cancer showed that fluorescence images could be obtained after 3 h post-injection.

D. Glut5 transporter. Glut transporters are a family of transmembrane proteins that transport sugars such as glucose, fructose, and galactose across the cell membrane. They are expressed in different types of tumor tissues but have distinct substrates.[98] Tumor cells need to overexpress at least one Glut transporter to meet their high levels of energy consumption. Glut5 is a fructose-specific transporter that is expressed at high levels in breast cancer cells but is not dominantly expressed in normal breast cells.[99]

To achieve molecular differentiation between cancerous and normal breast cells, Gambhir *et al.* synthesized two fructose-based fluorescent probes using 7-nitro-1,2,3-benzoxadiazole (**24a**) and cyanine5.5 dye (**24b**) as fluorophores, respectively.[98] Evaluation of the first metabolic pathway of fructose showed the involvement of hexokinases, which could phosphorylate fructose only in the breast cancer cell lines. On the basis of this result, the fluorophore labeling site was chosen in the C-1 position of fructose. The uptake of probe **24a** was dependent on the presence of the fructose-specific transporter Glut5. Probe **24b** with the very bulky fluorophore cyanine5.5 resulted in nonspecific accumulation in breast cancer cells (Fig. 5).

E. Cholecystokin receptor. The cholecystokin 2 receptor (CCK2R) belongs to the family of membrane G protein-coupled receptors. The CCK2R and its tumor-specific splice variant CCK2i4svR are overexpressed in tumors of the pancreas, medullary thyroid, lung, breast, ovary, gastrointestinal tract, and colon.[100–106] The CCK2R has normal organ distributions in the central nervous system and gastrointestinal tract.

Low *et al.* reported a tumor-specific nonpeptidic conjugate (**25**) that could target the CCK2R and its splice variants for use in fluorescence imaging.[107] The conjugate was composed of a sulfonated NIR fluorophore LS-288, a hydrophilic tetrapeptide spacer, and a targeting ligand Z-360 (a benzodiazepine-derived antagonist). The nonpeptidic ligand could bind in a similar manner to the natural ligand and access both the inactive and active states of the receptor. Additionally, the nonpeptidic ligand could not be taken up by a peptide scavenging receptor, thus avoiding unwanted accumulation in the liver and kidneys. Conjugate **25** accumulated in tumor tissue within 2 h following tail vein injection in mice. The results showed that **25** specifically localized to CCK2R-expressing HEK 293 murine tumor cells in both primary tumors and xenografts.

Hilger *et al.* synthesized a CCK2R targeted probe (**26**) by linking a NIR fluorophore DY-754 and a high-affinity minigastrin peptide analog with the sequence H_2N-$(DGln)_6$-Ala-Tyr-Gly-Trp-Met-Asp-Phe-amid *via* a hydrophilic linker.[108] The binding assay demonstrated a high binding affinity for CCK2R-expressing A431 cells. After intravenous injection of the probe, a fast and long-lasting accumulation in tumors was observed. CCK2R expression was clearly identified by fluorescence imaging in the A431/CCK2R xenografts at 8 h post-injection.

F. Carbonic anhydrase IX. Carbonic anhydrases are a family of transmembrane zinc metalloenzymes that exist in 16 different isoforms. These isoforms are distributed in different subcellular organelles where they play catalytic roles and are susceptible to their own specific inhibitors. Carbonic anhydrase IX (CAIX) is normally expressed in the stomach and gallbladder epithelia. However, CAIX can be used as a marker of hypoxia because of its overexpression in solid tumors such as glioblastoma, colorectal, and breast[109–111] and is therefore a potential tumor target.

Neri *et al.* designed and characterized a series of small-molecule fluorescence conjugates (**27a–c**) targeting CAIX.[112] These acetazolamide-based fluorophore conjugates were found

 This journal is © The Royal Society of Chemistry 2017

Published on 20 marzo 2017. Downloaded on 11/05/2026 19:46:09.

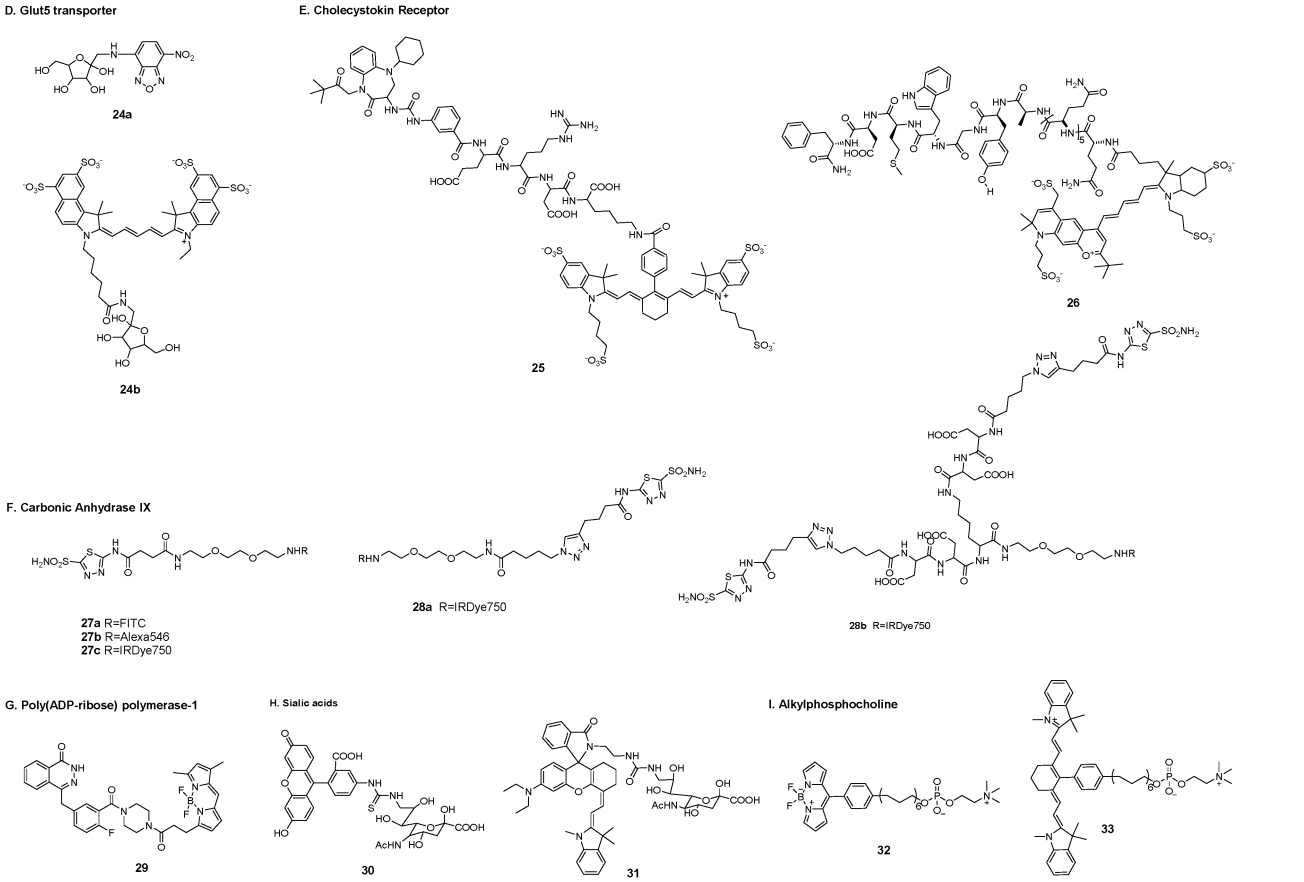

Fig. 5 Small molecules as tumor targeting ligands: D–I.

to preferentially target CAIX-expressing tumor cells. Compound **27c** was used to evaluate biodistribution in a mouse model. The results showed that accumulation of **27c** in the tumor was rapid and efficient at 1 h post-injection; however, the short retention time in the tumor (residence half-life $t_{1/2} \approx 1$ h) suggested that the bivalent inhibitor acetazolamide against CAIX might result in improved CAIX binding affinity compared with its corresponding monovalent counterpart. Neri *et al.* synthesized monovalent and bivalent acetazolamide fluorescence conjugates (**28a–b**) and tested their binding to tumor cells.[113] Their results showed that the bivalent conjugate **28b** efficiently accumulated in CAIX-expressing SKRC52 kidney xenograft tumors with a retention time (>24 h) longer than that of the corresponding monovalent conjugate **28a**.

G. Poly(ADP-ribose) polymerase-1. Poly(ADP-ribose) polymerase-1 (PARP-1), a well-known DNA-binding enzyme, is expressed in human tumors due to a deficiency in DNA repair enzymes, rendering the tumor cells susceptible to the small-molecule PARP1 inhibitor olaparib. Weissleder *et al.* synthesized a fluorescent olaparib derivative (**29**) for single-cell and subcellular pharmacokinetic analysis in murine cancer models.[114,115] They performed high-resolution, temporal *in vivo* imaging of single cells in tumors to measure drug distribution and pharmaceutics in real time, and utilized a quantitative framework to extract and extrapolate single-cell data to be used in predictive models.[114] Compound **29** reached the cellular target compartment, the nucleus, within 6 min *in vivo*. At the whole-body level, **29** had a weighted blood half-life of 18 min. The authors also used these data to validate predictive finite element modeling. Overexpression of PARP-1 was particularly apparent in the nuclei of glioblastoma, but not normal brain tissue. The high expression of PARP-1 in tumors and low expression in healthy tissue made **29** a valuable candidate for the detection and staging of tumors, especially glioblastoma. **29** could also be used to exploit the overexpression of PARP-1 in various other forms of cancer, including breast cancer, melanoma, and brain malignancies.[116]

H. Sialic acids. Sialic acids are anionic monosaccharides located at the termini of cell surface glycans. These derivatives of *N*-acetylneuraminic acid are involved in host–pathogen interactions and cell–cell adhesions. Overexpression of sialic acids on the cell surface has been associated with metastatic potential in a broad spectrum of tumors, suggesting an enhanced metabolic demand for sialic acids by these tumor cells.[117,118]

Han *et al.* reported a 9-fluoresccinylthioureido-9-deoxy-*N*-acetylneuraminic acid (**30**) for high-performance detection of tumors through labeling of sialic acid.[119] Probe **30** could be transferred into the Golgi and metabolically incorporated into glycoproteins *via* a cellular sialylation pathway. The fluorescence

Published on 20 marzo 2017. Downloaded on 11/05/2026 19:46:09.

signal was observed in tumors within 20 min after administration. The off-target probe was quickly eliminated from the circulation. The tumor-to-organ fluorescence ratios remained high up to 10 h post-injection. Implanted H22 hepatocellular carcinoma in the liver could be clearly discerned for tumors with a diameter of 0.2–5 mm. However, the active imaging probe **30** suffered from "always-on" green fluorescence, which limited deep tissue penetration. Han *et al.* next presented a sialylated pH-activatable NIR probe **31** for fluorescence targeted tumor detection.[120] The sialic acid ligand provided effective tumor targeting in H22 hepatocellular carcinoma lesions and the NIR fluorophore underwent lysosomal pH-triggered isomerization to emit fluorescence. The micromilieu of solid tumors is hallmarked by acidic microenvironments due to the accumulation of lactic acid by glycolysis. Therefore, probe **31** displayed a high tumor-to-normal tissue signal contrast. The NIR signal was observed in nude mice 30 min after administration *via* the tail vein, and the signal could be retained for 144 h after injection. Additionally, **31** could effectively convert NIR light into cytotoxic heat to kill tumor cells, suggesting tumor-activatable photothermal therapy.

I. Alkylphosphocholine. Alkylphosphocholine derivatives (APCs) selectively accumulate in many solid tumor cells compared with normal cells.[121] APCs also show suppressive effects on tumor growth and extend survival. APCs target cellular and intracellular membranes, inhibit phosphatidylcholine biosynthesis, interfere with lipid transduction pathways, block the endoplasmic reticular transport of cholesterol, and ultimately disrupt cholesterol homeostasis and membrane lipid raft function.[122,123] Kuo *et al.* developed two APC-based cancer-selective fluorescent probes CLR1501 (**32**) and CLR1502 (**33**) for discriminating tumors from normal brain tissue in fluorescence-guided glioma surgery.[123,124] These two probes provided high tumor-to-normal brain contrast in fluorescence discrimination with glioblastoma multiforme and glioblastoma stem cell-derived xenografts in mouse models. Moreover, **33** showed a superior tumor-to-brain fluorescence ratio compared with 5-aminolevulinic acid, which is the current standard for fluorescence-guided neurosurgery. The tumor fluorescence was readily detected with the indocyanine green fluorescence microscopy technique currently used in the clinic.

2.2.2 Peptides, proteins, and antibodies as tumor targeting ligands. Small molecular weight peptides are the preferred candidates as potential targeting ligands.[125] These peptides possess strong targeting capability as they easily penetrate the cell membrane; alternatively, cell-specific target delivery can be improved by facilitating receptor-mediated endocytosis. Peptides that block signal transduction or interfere with nuclear localization may also have therapeutic effects on tumors. Compared with larger antibodies or proteins, peptides are easily synthesized, effectively penetrate tissues, and are rapidly cleared from the circulation.[125]

A. IL-11 receptor. Interleukin-11 (IL-11) is a multifunctional cytokine in blood cells. The IL-11 receptor alpha-chain (IL-11Rα) is a member of the gp130-dependent receptor group (Fig. 6). IL-11 and IL-11Rα are related to breast cancer development and progression and play crucial roles in bone metastasis of human breast cancer, which indicates poor prognosis.[126] Targeting of IL-11Rα-positive tumors has potential as a useful strategy for noninvasive imaging. Wang *et al.* developed a NIR fluorescence and single photon emission tomography (SPECT) dual-modality imaging probe (**34**) to improve the diagnosis and management of tumors.[127] The targeting moiety was the cyclic nonapeptide c(CGRRAGGSC), which showed a particular affinity for IL-11Rα, the radiotracer was radioisotope ^{111}In complexes, and the fluorescence signal generator was the cyanine dye IR-783. Dual-modality imaging of mice bearing subcutaneous MDA-MB-231 tumors demonstrated uptake of the imaging probe in the tumor 24 h after administration.

B. Vitronectin receptor. Integrins are a family of heterodimeric transmembrane proteins that behave as receptors for specific steric-configuration constrained extracellular ligands.[128,129] Among these integrins, $\alpha_v\beta_3$, the vitronectin receptor, plays important roles in tumor progression, angiogenesis, and metastasis.[129–132] Vitronectin, which contains the arginine–glycine–aspartic peptide sequence (Arg–Gly–Asp, RGD), exhibits a high affinity for $\alpha_v\beta_3$, providing a promising ligand for diagnostic imaging and a therapeutic target in tumors.

Li *et al.* reported the synthesis and characterization of integrin $\alpha_v\beta_3$-targeted peptide cyclo(Lys–Arg–Gly–Asp–Phe) [c(KRGDf)] labeled with NIR cyanine dyes Cy5.5 (**35a**) and IRDye800 (**35b**) for tumor imaging.[133,134] These peptide–dye conjugates showed specificity for human Kaposi's sarcoma (KS1767) cells that overexpress $\alpha_v\beta_3$. Tumors were clearly visualized after intravenous injection at a dose of 6 nmol per mouse. Dynamic fluorescence images obtained over a period of 20 min revealed that **35a** was rapidly taken up by KS1767 tumors after intravenous injection.

Blasberg *et al.* reported an IRDye 800CW-conjugated c(KRGDf) peptide that specifically targeted the overexpressed integrin receptors in murine RCAS-PDGF-driven/tv-a glioblastomas and two human orthotopic glioblastomas (U-87 MG and TS543).[135] The three tumor models exhibited different levels of integrin receptor upregulation. The conjugate could specifically bind the overexpressed integrin receptors in these glioblastomas and visualization of the tumor tissue and tumor margins could be achieved by NIR imaging.

Chen *et al.* used the RGD peptide cyclo(Lys–Arg–Gly–Asp–D-Tyr) [c(RGDyK)] as a targeting ligand to produce a sensitive and semiquantitative NIR fluorescence imaging probe **36**.[136] The conjugate could function as a specific ligand toward the $\alpha_v\beta_3$ integrin receptor in the human glioblastoma cell line (U87MG) and primary human brain capillary endothelial cells (HBCECs) that are known to overexpress $\alpha_v\beta_3$ integrin. *In vivo* three-dimensional imaging showed typical NIR fluorescence images of athymic nude mice bearing subcutaneous U87MG glioblastoma tumors after intravenous injection of optimized doses of **36**. The tumor could be clearly discriminated from the surrounding tissue from 30 minutes to 24 h post-injection, with maximum contrast occurring about 4 h post-injection.

 This journal is © The Royal Society of Chemistry 2017

Published on 20 marzo 2017. Downloaded on 11/05/2026 19:46:09.

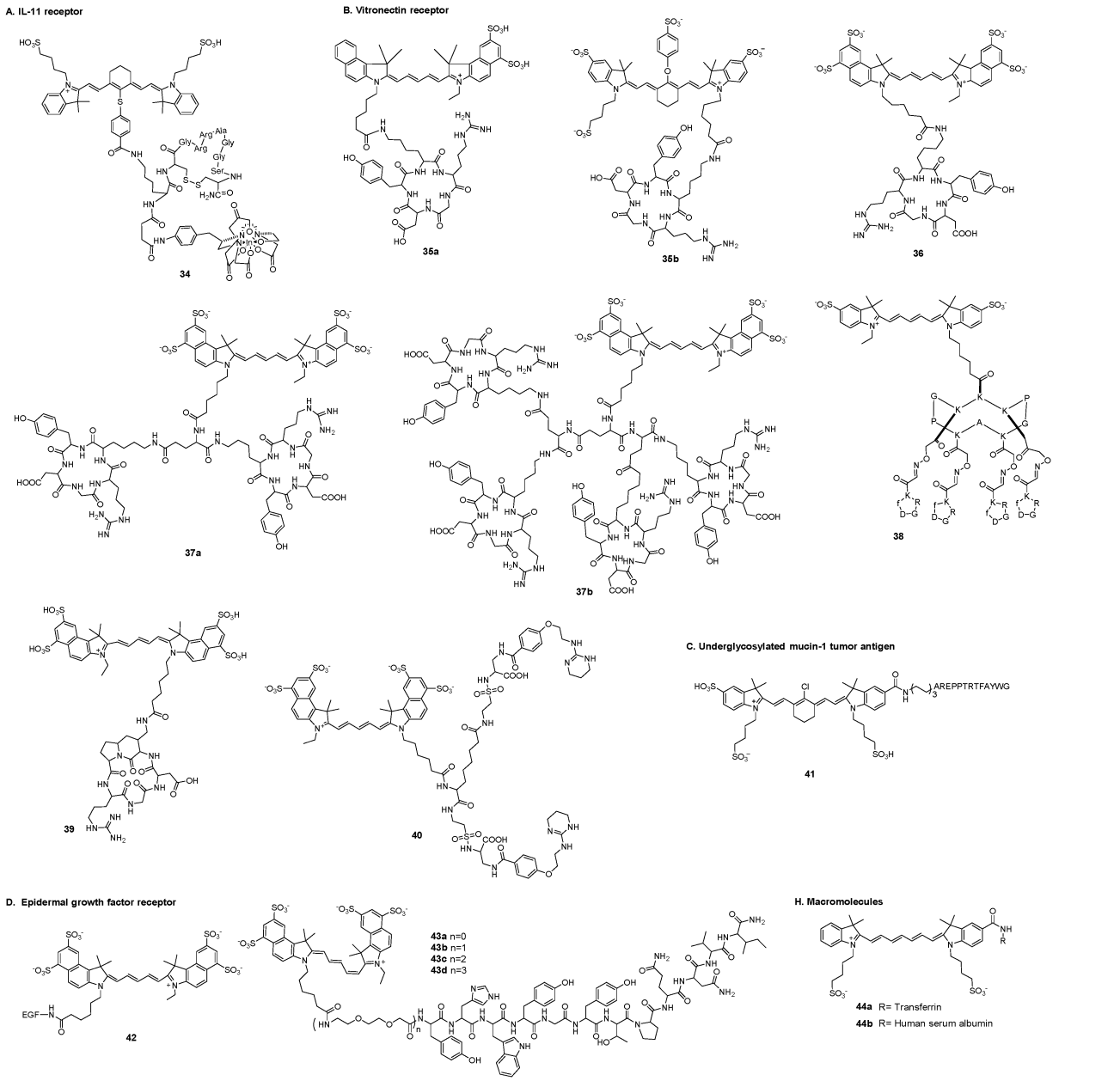

Fig. 6 Peptides, proteins and antibodies as tumor targeting ligands.

Additionally, Cy5.5-conjugated monomeric, dimeric, and tetrameric c(RGDyK) peptides (**37a**, **37b**) were evaluated in subcutaneous U87MG glioblastoma xenograft models and were all suitable for integrin expression imaging.[137]

Coll *et al.* reported the *in vitro* and *in vivo* characteristics of conjugate **38** for targeting and imaging of tumors.[138–140] Four c(RGDyK) peptides were assembled onto the functionalized RAFT scaffold *via* chemoselective oxime ligation. The fluorophore was Cy5. RAFTc(RGDyK)$_4$ could be used as a therapeutic agent in nude mice. RAFTc(RGDyK)$_4$ significantly improved the targeting specificity for subcutaneous tumor masses. Compound **38** could target $\alpha_v\beta_3$-positive human IGROV1 ovarian nodules scattered in the peritoneal cavity of nude mice after intravenous administration. The affinity between the targeting ligand RAFTc(RGDyK)$_4$ and $\alpha_v\beta_3$ was also verified in Swiss nude mice bearing HEK293 (β_1) and HEK293 (β_3).[140]

Forni *et al.* reported a NIR fluorescence RGD cyclic probe **39** for noninvasive detection of $\alpha_v\beta_3$ integrin-overexpressing tumors.[141] The targeting moiety was a functionalized cRGD peptide that preferentially bound the Mn-activated form of integrin, mediating rapid and extensive cell adhesion. The conjugate displayed a high binding affinity for $\alpha_v\beta_3$ integrin on human U-87 MG glioblastoma cells and their xenografts in nude mice. Probe **39** showed broad diffusion in most organs after injection, followed by a progressive increase up to 24 h with specific accumulation in tumors. The low expression of $\alpha_v\beta_3$ integrin on the C6 glioma cell line led to reduced specific accumulation in the tumor. The expression and retention of **39**

Published on 20 marzo 2017. Downloaded on 11/05/2026 19:46:09.

in the tumor area was low compared with that observed in U-87 MG transplantable tumors.

Li *et al.* developed a NIR imaging probe (**40**) based on a bivalent nonpeptide small molecule intergrin $\alpha_v\beta_3$ antagonist for tumor imaging.[142] The $\alpha_v\beta_3$ antagonist 4-[2-(3,4,5,6-tetrahydropyrimidine-2-lamino)-ethyloxy]benzoyl-2-(*S*)-aminoethylsulfonyl-amino-*h*-alanine (IA) and the Cy5.5 fluorophore were conjugated *via* an 8-carbon linker that had the lowest conformational energy for construction of **40**. The bivalent IA contributed to a strong and specific affinity for the detection of tumors and micrometastatic lesions. Whole-animal fluorescence imaging of subcutaneously implanted U-87 xenograft tumors indicated that **40** was specific for the tumor tissue through binding to its integrin receptor. The target-to-background ratio was sufficient to clearly discern the tumor lesions at 7 h post-contrast injection. The intense signal detected at the tumor site could be retained for more than 48 h.

C. Underglycosylated mucin-1 tumor antigen. Underglycosylated mucin-1 tumor antigen (uMUC-1) is one of the early hallmarks of tumorigenesis in a wide variety of tumors.[143] The EPPT peptide with the sequence AREPPTRTFAYWG targeting the uMUC-1 antigen was derived from the CDR3V_β region of a monoclonal antibody.[144] Moore *et al.* developed a conjugate cyanine 7-EPPT peptide (**41**) for tumor imaging.[143] The hydrophilicity of the cyanine fluorophore was increased by introduction of a sulfonic moiety. Removal of the carboxylic acid group would eliminate the possibility of cross-linking with peptides/proteins during conjugation. NIR fluorescence imaging was obtained 24 h after injection of **41**. The results showed specific accumulation in mice bearing human pancreatic adenocarcinoma CAPAN-2.

D. Epidermal growth factor receptor. The epidermal growth factor receptor (EGFR) is a transmembrane glycoprotein. Activation of the EGFR triggers the signal transduction pathways involved in regulating cellular proliferation, differentiation, and survival.[145–147] The EGFR is overexpressed in many tumor cell lines, and is associated with poor prognosis and high mortality. The epidermal growth factor (EGF) is one of the most important ligands for the EGFR.

Li *et al.* reported an EGF–Cy5.5 fluorescent probe (**42**) for the detection of the EGFR in human breast tumor xenografts.[148] The conjugate was conveniently synthesized from EGF and an NHS ester of Cy5.5. The selectivity of EGF–Cy5.5 for the EGFR was established by comparing the binding capability between EGFR-overexpressing MDA-MB-468 tumor cells and EGFR-negative MDAMB-435 tumor cells. NIR fluorescence in mice bearing MDA-MB-468 tumors was still detectable at 96 h after injection of **42** and the signal intensity returned to the background level at 192 h.

Basilion *et al.* developed a series of NIR probes **43a–d** targeting the EGFR for imaging glioblastoma brain tumors *in vivo*.[149] The probes were synthesized by varying the length of the polyethylene glycol (PEG) spacer between the peptide GE11 (YHWYGYTPQNVI) and the fluorophore Cy5.5. The length of the linker critically affected the affinity of the probes for tumors. Probe **43b**, which had one unit of PEG, had the highest apparent affinity for the EGFR in glioblastoma cells and could selectively localize at glioblastoma-derived orthotopic brain tumors. When tested in cultured cell lines that expressed different levels of the EGFR and in orthotopic brain tumors using fluorescence-mediated molecular tomography, the probe could distinguish different tumors expressing various levels of the EGFR.

E. Tyrosine phosphatase μ. Receptor protein tyrosine phosphatase μ (PTPμ) protein transduces signals in response to cell adhesion and is highly expressed in the normal brain. Expression of full-length PTPμ is downregulated in the most aggressive glial tumor, glioblastoma multiforme.[150] Brady-Kalnay *et al.* verified that the extracellular fragment of PTPμ is expressed in the human glioblastoma multiforme tumor margin but not in normal brain tissue. A series of peptides (SBK1-4) were linked to Texas Red, Cy5, and Alexa 750 fluorophores to recognize protein fragments of PTPμ.[150–152] The SBK2 conjugate labeled the main tumor mass of an intracranial animal model of glioma as well as tumor cells at the margin. SBK2 could navigate the margin and recognize dispersing tumor cells up to 4 mm from the main tumor mass. The SBK2 conjugate rapidly accumulated in tumors within 10 minutes, and the fluorescent signal was retained for more than 180 min.

F. Chlorotoxin. Chlorotoxin (CTX) is a 36-amino acid peptide with four disulfide bridges that preferentially binds to glioma cells.[153] The molecular targets of CTX include a lipid raft-anchored complex that contains matrix metalloproteinase-2 (MMP-2), membrane type-1 MMP, the transmembrane inhibitor of MMP-2, the glioma-specific chloride ion channel, and the ClC-3 chloride ion channel.[44]

For intraoperative differentiation of tumor margins or small foci of cancer cells, Olson *et al.* developed a molecular imaging conjugate composed of CTX and Cy5.5.[154] The probe could delineate malignant glioma, medulloblastoma, prostate cancer, intestinal cancer, and sarcoma from adjacent non-neoplastic tissue. Specific binding to cancer cells was facilitated by MMP-2. The fluorescent signal was still higher in xenografts than in non-neoplastic tissue at 14 days after injection. The conjugate was concentrated in the kidneys and was excreted in urine. The Cy5.5 conjugation resulted in a mixture of mono-, di-, and tri-labeled probes because CTX contains three lysine residues.[155] Substitution of the lysines at positions 15 and 23 with either alanine or arginine would result in a Lys27 monolabeled peptide that retained the stability and *in vivo* half-life properties of CTX. The half-life of the Cy5.5-labeled linear peptidic probe was 14 h, whereas that of Cy5.5-labeled cyclized chlorotoxin was 11 h.

Kovar *et al.* developed and tested a targeted NIR probe CLTX-800CW for brain tumors in the mouse model ND2:SmoA1, which spontaneously develops medulloblastoma tumors.[156] Colocalization of hematoxylin and CLTX-800CW in cells at the tumor margin was distinctly visible. Specificity and functionality of the targeted probe for MMP-2-dependent tumor cell targeting were evaluated by examining cultured medulloblastoma, glioblastoma,

 This journal is © The Royal Society of Chemistry 2017

Published on 20 marzo 2017. Downloaded on 11/05/2026 19:46:09.

lung carcinoma, and prostate carcinoma cell lines in a microplate assay.

Butte *et al.* presented a NIR imaging probe BLZ-100, using a standard charge-coupled device (CCD) camera to visualize low levels of BLZ-100 binding to the tumors.[157] BLZ-100 exhibited a high affinity for glioma. After injection of BLZ-100 for 48 h, the orthotopic glioma tumors in mice were effectively discriminated from the surrounding normal brain tissue.

G. Endostatin. Endostatin, a 20 kDa C-terminal fragment of type XVIII collagen, is a potent inhibitor of angiogenesis, lymphangiogenesis, and cancer metastasis.[158] Endostatin can bind to a variety of receptors including the VEGF receptor, integrin, and glypicans. All of these receptors are associated with tumors. Camphausen *et al.* reported an endostatin–Cy5.5 conjugate for imaging tumor *in vivo*.[159] After injection into mice bearing Lewis lung carcinoma tumors, the conjugate selectively migrated to the site of the tumor. Injection of endostatin–Cy5.5 produced a near-infrared fluorescent image within the tumors at 18 h and reached a maximum at 42 h after injection. Intravenous injection provided a peak emission at 3 h, and the fluorescent signal persisted until 72 h. Immunofluorescence imaging of tumor specimens confirmed the intratumoral binding site for endostatin at the tumor vasculature.

H. Macromolecules. Larger particles (usually with diameters <600 nm) can passively accumulate in tumor tissues because of the enhanced permeability and retention (EPR) effect caused by defects or gaps in the tumor vasculature.[160] Licha *et al.* reported serum protein–dye conjugates consisting of transferrin (**44a**) or human serum albumin (**44b**) and the cyanine derivative for tumor imaging.[161] In contrast to **44b**, the transmembrane mechanism of **44a** in HT29 human colon carcinoma cells was mediated by receptor endocytosis. After intravenous injection of both compounds into HT29 tumor-bearing nude mice, maximum fluorescence intensities were reached after 6 h in tumor tissue. However, the contrast between tumor and normal tissue was significantly higher for **44a** than for **44b** at 24 h after injection. **44a** produced fluorescence in viable tumor cells, whereas **44b** fluorescence was observed along connective tissue.

I. Antibodies. Monoclonal antibodies (mAbs) usually have excellent antigen specificity and a higher binding affinity than peptides.[162] Fluorescently-labeled antibodies provide potential strategies to specifically target tumor cell-specific surface epitopes *in vivo* while avoiding off-target effects.[163] Thus, antibody-based fluorescence probes show great promise for broad applications in clinical medicine, such as cancer diagnosis, staging, and therapy response assessment.

Cetuximab is an anti-EGFR antibody that selectively binds to the external domain of the EGFR with a high affinity.[164] Rosenthal *et al.* conjugated cetuximab with a fluorophore Cy5.5 for imaging HNSCC xenografts.[165] Fluorescence images were obtained by time-domain fluorescence imaging and fluorescence stereomicroscopy. Compared with control isotype-matched IgG1–Cy5.5, Cy5.5–cetuximab was specifically accumulated in HNSCC xenografts with significantly higher fluorescence. Tumor xenograft fluorescence was retained for up to 72 h. Fluorescence was detected in multiple HNSCC tumor cell lines with different EGFR expression levels. Moreover, Cy5.5–cetuximab could be detected in small specimens (2 mm).

Warram *et al.* evaluated a fluorescent conjugate cetuximab–IRDye 800CW in both subcutaneous and orthotopic animal models of glioblastoma multiforme.[166] Fluorescence intensities of cetuximab–IRDye 800CW correlated with EGFR expression and vessel density. Fluorescence intensity of the conjugate within the luciferase-positive tumor cell lines was retained for 3 days and offered sufficient fluorescent contrast for surgical resection. Immunohistochemistry was performed to confirm tumor fluorescence, EGFR expression, and vessel density.

Cai *et al.* combined an anti-EGFR Fab and an anti-CD105 Fab (Bs-F(ab)$_2$) by bioorthogonal "click" ligation of *trans*-cyclooctene and tetrazine.[167] Next, the NIR fluorophore ZW800-1 was conjugated to Bs-F(ab)$_2$ for NIRF imaging of mice bearing U87MG subcutaneous xenografts. ZW800-Bs-F(ab)$_2$ showed excellent uptake in tumors and low background in non-target tissues. The probe could delineate the tumor contours and was useful for locating the tumor and guiding removal of the tumor foci and surgical margins.

The fluorescence of indocyanine green (ICG) will be quenched upon binding to mAbs. After endocytosis and internalization, ICG dissociates from the targeting mAbs and the fluorescence emission is recovered. This property can be used to generate activatable probes. Kobayashi *et al.*[168] developed fluorescence probes by combining indocyanine green (ICG) or Cy5.5 with monoclonal antibodies directed at cell surface markers that are overexpressed on tumors (anti-CD25, anti-EGFR1, and anti-HER2). ICG or Cy5.5 was conjugated to the antibodies daclizumab (Dac), trastuzumab (Tra), and panitumumab (Pan). ICG–mAb conjugates performed as improved activatable imaging probes *in vivo* in mice with tumor retention times of over 4 days. Dac–ICG could locate at CD25-expressing tumors, while tumors overexpressing HER1 and HER2 could be traced by Pan–ICG and Tra–ICG, respectively. The same group developed antibody-bound fluorescent probes using humanized anti-PSMA antibody (J591)–ICG in prostate cancer;[169] Pan–Alexa680 and Tra–ICG in breast cancer;[170] Pan–ICG, Pan–PEG4–ICG and Pan–PEG8–ICG in EGFR-positive tumors (MDA-MB-468);[171] PSMA–MB–ICG, PSMA–MB–PEG4–ICG, PSMA–MB–PEG8–ICG, and PSMA–MB–IR700 in prostate cancer;[172] and panitumumab–FNIR-774 and panitumumab–FNIR-Z-759 in MDA-MB-468 tumors.[173]

Inappropriate activation of the mucosal immune system can lead to production of the proinflammatory cytokine TNF-α, which plays a pivotal role in the immunopathogenesis of Crohn's disease. The monoclonal antibody adalimumab exhibits a high affinity to human mTNF. Neurath *et al.* labeled the adalimumab antibody with an FITC fluorophore for *in vivo* imaging of mucosal immune cells in Crohn's disease during colonoscopy.[163] The response time of the probe was 10 min at room temperature. *Ex vivo* confocal imaging revealed specific fluorescence signals for the identification of mTNF-expressing mucosal cells in the inflamed tissue. They quantified the number of immune cells

Published on 20 marzo 2017. Downloaded on 11/05/2026 19:46:09.

expressing mTNF and found that patients with high or low numbers of $mTNF^+$ immune cells showed high or low response rates to adalimumab therapy, respectively.

2.3 Hypoxia-mediated tumor imaging

Hypoxia is one of the features typically observed in malignant solid tumors *in vivo*. Two different biological responses, stabilization of hypoxia-inducible factor-1 (HIF-1) and accelerated bioreductive reaction, are induced by hypoxia. Tumor cells display an elevated level of reductive enzymes such as nitroreductase, DT-diaphorase, and azoreductase. Therefore, tumors can accelerate enzyme-catalyzed one-electron reduction to reduce specific functional compounds containing a nitro group, quinone group, and azo group. This renders these enzymes ideal targets for tumor cells *in vivo*. Several hypoxia-sensitive fluorescent probes have been developed.[174] Here, we summarize the fluorescent probes for potential tumor imaging.

A. Nitro group. Nitroreductase (NTR), which belongs to the family of flavin-containing enzymes, can reduce nitroaromatics to the corresponding amino derivatives in the presence of nicotinamide adenine dinucleotide (NADH). It is well known that the strong electron withdrawing nitro group can quench fluorescence when conjugated to fluorophores, while the fluorescence of fluorophores will return once the nitro group is reduced to the corresponding amine.

Qian *et al.* synthesized a series of nitro fluorescent probes for targeting hypoxia environments in solid tumors.[175] The NIR fluorescence probe (**45**) was linked to a *p*-nitrobenzyl moiety and the fluorophore Nile Blue *via* a carbamate linkage.[176] When activated by NTR and NADH, the *p*-nitrobenzyl moiety of the probe was reduced to form the unstable intermediate *p*-aminobenzyl derivative, which spontaneously released the Nile Blue fluorophore with fluorescence emission at 658 nm. The fluorescence response was completed within 20 min and 2 h when tested in PBS buffer and in hypoxic A549 cells, respectively.

Ma *et al.* reported a series of fluorescent probes for nitroreductase and tumor hypoxia.[177–179] The resorufin fluorophore was decorated with 5-nitrofuran *via* an ether bond (**46**) for imaging the hypoxic status of tumor cells.[177] Upon reduction by NTR and NADH, the nitro group in the probe could be selectively transformed into an amino group, followed by 1,6-rearrangement-elimination to release resorufin. The reduction reaction could be completed within 10 min in buffer. The probe was successfully applied in HeLa and A549 cells with different extents of hypoxia. The response time in cells was 8 h.

Nagasawa *et al.* developed a NIR fluorescent probe (**47**) composed of 2-nitroimidazole and Cy7 dye for *in vivo* imaging of tumor hypoxia.[180] The probe was accumulated to a greater extent in SUIT-2/HRE-Luc pancreatic tumor cells cultured under hypoxic conditions than in cells under normoxic conditions. The fluorescence resonance time was 30 min. *In vivo* imaging of hypoxic cells was performed in tumor-bearing mice inoculated with SUIT-2/HRE-Luc cells. HIF-1 activity in xenografts was monitored by bioluminescence imaging (Fig. 7). After administration to the mouse xenograft model, probe **47** rapidly accumulated in tumors and NIR fluorescence could last for more than 24 h.

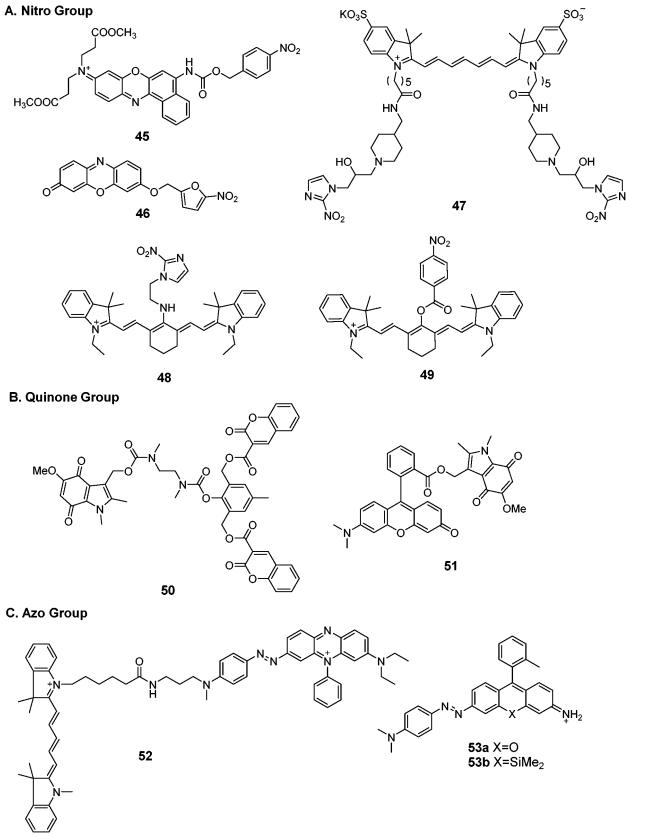

Fig. 7 Hypoxia-mediated tumor imaging.

Tang *et al.* reported a NIR fluorescent probe (**48**) composed of nitroimidazole conjugated to Cy7 fluorophores for monitoring the hypoxia status *via* the detection of NTR.[181] The probe was used to detect intracellular hypoxic levels in HepG2 cells under different oxygen concentrations. The reaction time in the presence of liver microsomes was 15 min. The probe was applied to investigation of the relationship between epithelial–mesenchymal transition in tumor progression and intracellular hypoxic level. The results showed that HepG2 cells displayed downregulation of E-cadherin expression and upregulation of α-SMA expression at low oxygen concentrations.

Li *et al.* reported five NIR fluorescent probes for rapid NTR imaging *in vivo*.[182] The experimental screening results showed that only the *para*-nitrobenzoate group modified Cy7 fluorophore (**49**) probe showed rapidly increased NIR fluorescence for monitoring and bioimaging of NTR. Time-dependent fluorescence emission intensity gave a reaction kinetic time within 200 s in the presence of 1.5 μg mL^{-1} NTR. Probe **49** could be used to monitor NTR in A549 cells under normoxic conditions and different hypoxic conditions. **49** was also transferred into hypoxic A549 tumor-bearing mouse models *via* intratumoral injection. PET imaging confirmed that the A549 tumor in the murine model was a hypoxic tumor. Strong fluorescence in the hypoxic A549 tumor could be observed within 60 s, and this fluorescent signal lasted for more than 30 min.

 This journal is © The Royal Society of Chemistry 2017

Published on 20 marzo 2017. Downloaded on 11/05/2026 19:46:09.

Probe **49** could distinguish the hypoxic tumor from inflamed tissue *in vivo*.

B. Quinone group. The quinone group can also quench the fluorescence of the conjugate system. Under hypoxic conditions, the quinone group undergoes a one-electron reduction process to trigger fluorescence emission. Nishimoto *et al.* synthesized two hypoxia-sensitive fluorescent probes (**50** and **51**) for hypoxia tumor cell imaging.[183,184] Both probes possessed the hypoxia-sensitive indolequinone unit. Probe **50** was composed of two coumarin chromophores and an indolequinone unit, conjugated *via* a 2,6-bis(hydroxymethyl)-*p*-cresol linker. Upon activation by a reduction enzyme, the coumarin chromophore was released with an increase in fluorescence. The response time was 45 min in solution. Probe **50** also worked in cell lysates of the human fibrosarcoma cell line HT-1080 under hypoxia conditions with a response time of 4 h. Probe **51** consisted of an indolequinone unit and a rhodol fluorophore. The indolequinone unit functioned not only as a quenching group on the fluorophore, but also as a hypoxia-sensitive reduction group. The probe emitted fluorescence after enzymatic reduction for 30 min in solution and could produce strong fluorescence in human lung adenocarcinoma A549 cells at 6 h.

C. Azo group. The azo group is a fluorescence quenching group because of its ultrafast conformational change around the N=N bond after photoexcitation; when reduced by reductases under hypoxia this quenching process will be inhibited. Nagano *et al.* exploited azobenzene derivatives as hypoxia-sensitive moieties and developed a NIR fluorescent probe (**52**) for hypoxia detection.[185] The fluorescence increase was triggered by cleavage of the azo bond. The fluorescence regulation mechanism was Förster resonance energy transfer (FRET). After enzymatic reactions under hypoxic conditions, the fluorescence intensities of these probes reached a plateau within 10 min. These probes could distinguish hypoxia in MCF-7 breast cancer cells. Probe **52** could detect hypoxia in mice using an ischemia model of the mouse liver with a rapid *in vivo* fluorescence response within 1 min after vessel ligation. Hanaoka *et al.* conceived a further improvement to azo-based hypoxia sensors.[186] They directly conjugated the azo group to per-rhodamine fluorophores and obtained two probes (**53a** and **53b**). Once reduced under hypoxia, the two probes resulted in free fluorophores. The resultant colorimetric and fluorescent changes could be utilized to indicate different levels of hypoxia. Cellular hypoxia was observed under hypoxic conditions with a time-dependent course. Probe **53a** was localized in the mitochondria, whereas **53b** was localized inside the lysosomes. *In vivo* imaging studies showed that **53a** could visualize retinal hypoxia in a rat model of retinal artery occlusion.

3. Applications of theranostics in tumors

3.1 General strategies and activation mechanism

Fluorescent probes that integrate tumor-targeting ligands have successfully been used to identify and localize tumor masses in tumor diagnosis trials. The next focus is the enhancement of the drug therapeutic efficacy by improving the targeting function of small molecular drugs to achieve accumulation in tumor lesions. Conjugation of these diagnostic tools with small cytotoxic drugs generates a new synergistic system with simultaneous diagnostic and therapeutic capabilities; this field has been termed theranostics. Theranostic agents have the promise of regulating precisely when, where, and how a pharmaceutically active artificial compound is delivered to a single cell. The major features of small conjugate theranostics include targeted accumulation, improved pharmacokinetics, imaging ability, real-time information on treatment, and intraoperative guidance. Such agents can not only increase therapeutic efficacy, but also elucidate underlying disease mechanisms and allow pre- and post-treatment assessment.[50]

The critical features of small conjugate theranostics design include the fluorescence manipulated mechanism, cytotoxic drug selection, regulation of prodrug release, and localization capability. Overall, theranostics aims to improve biodistribution, increase tumor targeting ability, reduce biotoxicity, and minimize side effects. Generally, a small molecular fluorescent conjugate therapeutic should be composed of four moieties: an imaging fluorophore, a chemotherapy drug, a targeting ligand, and an appropriate linker (Fig. 8). These theranostic agents can show increased localization and therapeutic efficacy at the tumor site *via* the specific recognition of receptors that are overexpressed on the surface of tumor cells. After reaching the targeting site, the cleavable linkers are broken and the masked drugs are directly released for therapy. The cleavable linkers are required to behave as stable chemical bonds unless they are selectively activated by a variety of external stimuli signals, such as temperature, light, magnetic field, ultrasound, and electric current. More importantly, the ability to selectively cleave the linkers by endogenous disorder factors, such as biothiols, reactive oxygen and nitrogen species, acidic pH, intracellular redox potential, enzymes, and glucose is even more favorable for the treatment of disease. The requirements of fluorophores and targeting ligands are the same as those of the fluorescent probes used for tumor diagnosis. The fluorescence changes of the imaging fluorophores should illustrate the biodistribution of the therapeutics,

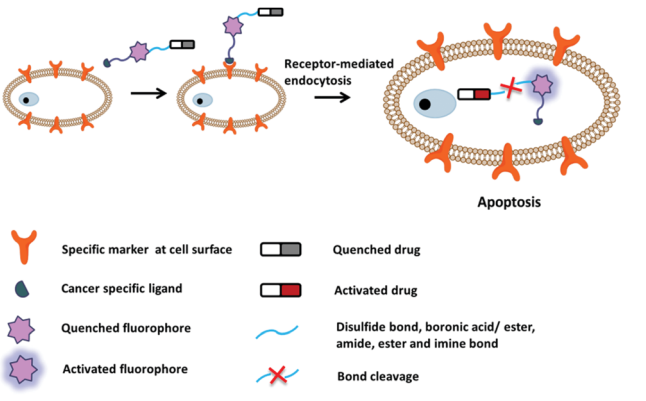

Fig. 8 Design strategy and drug release mechanism.

Published on 20 marzo 2017. Downloaded on 11/05/2026 19:46:09.

tumor lesions, and pharmacokinetics (Fig. 8). Recently, small fluorescent conjugate therapeutics have been developed for tumor diagnosis and therapy. In this section, we discuss the latest developments in these theranostics according to the cleavable mode of the linkers, which essentially form the sluice for drug release and fluorescence emission.

3.2 Thiol-mediated modes

Glutathione (GSH) is the most abundant endogenous biothiol in cells. It participates in various cellular processes, including cell differentiation, cellular metabolism, antioxidant defense, and apoptosis.[187] Normal concentrations of GSH range from 1 to 15 mM depending on the cell type.[188] However, the intracellular GSH level is much higher in tumor cells than in normal cells.[189] The disulfide bond (–S–S–) can be cleaved *via* the reduction of free biothiols.[190] Therefore, GSH seems to be an ideal bioactivator for triggering therapeutics. A cytotoxic drug can be conjugated with a fluorophore *via* a disulfide linker to form a desired therapeutic agent with the specific capability to accumulate in tumor lesions. The therapeutic agent does not release the antitumor drug before it reaches the tumor cells because of the relatively low concentration of GSH in blood circulation and in normal cells (Fig. 9).

3.2.1 Therapeutics with disulfide bonds and targeting ligands. The folate receptor (FR) is a well-known tumor-associated receptor that is overexpressed in many tumors.[92,93] Folic acid is a small compound that binds the FR with a high affinity. Perez *et al.* reported folate–doxorubicin theranostics (**54a**,**b**) for the targeted delivery of a prodrug to cancer cells expressing FR.[191] Doxorubicin (DOX) is a topoisomerase II inhibitor that blocks DNA replication in tumor cells. The authors found that covalent conjugation of folic acid to DOX would mask its fluorescence and cytotoxicity. Here, DOX was masterly chosen as both the prodrug and fluorophore, and folic acid was selected as both the targeting ligand and quencher for DOX. The theranostic agent **54a** could be selectively activated by a high concentration of glutathione (GSH) in A549 cells *via* cleavage of the disulfide linker between DOX and folic acid, allowing monitoring of the theranostic agent's intracellular localization and migration before recovering its cytotoxicity. The control theranostic agent **54b** confirmed the results. Treatment of **54a** with GSH resulted in fluorescence activation within 3 h. The plasma stability of the disulfide linker in mice was 47 h ($t_{1/2}$). Time-dependent viability of A549 cells showed the high and sustained cytotoxicity of **54a**.

Gemcitabine, a commercial antitumor drug, principally functions as a strong inhibitor of a pyrimidine base in DNA replication or as an apoptosis inducer *via* an interaction with ribonucleotide reductase. Kim *et al.* reported the prodrug **55** as an NIR targeted drug delivery system. The theranostic agent included the targeting ligand folate, modified gemcitabine, and a Cy7 fluorophore conjugated with a cleavable disulfide linker.[192] Upon reacting with GSH, the prodrug **55** decomposed into an amino fluorophore derivative and released gemcitabine. The absorption and fluorescence changes could be completed within 2 h in the presence of 0.2 mM GSH. The prodrug **55** exhibited higher cytotoxicity in FR-overexpressing cells than in FR-negative cells, indicating its targeting capability. The biothiol-induced disulfide cleavage occurred in the endoplasmic reticulum and the released gemcitabine diffused into the cell nucleus to form a faulty nucleoside and induce apoptosis. *In vivo* fluorescence imaging confirmed that the prodrug **55** could be selectively taken up by KB tumor tissue that overexpressed the folate receptor.

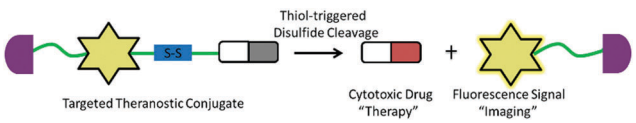

Fig. 9 Thiol-mediated drug release.

Some drugs have been directly connected to folate *via* a disulfide linker to strengthen their targeting abilities as therapeutic agents. Low *et al.* reported a folate–peptide–camptothecin prodrug **56**.[193] The hydrophilic peptide was introduced to improve the water solubility of the prodrug. Release of camptothecin from the folate peptide linker took 1 h in the presence of a 10-fold molar excess of dithiothreitol. **56** showed a high binding affinity for FR-overexpressing KB cells and efficiently released camptothecin to inhibit cell proliferation with an IC_{50} of 10 nM. Leamon *et al.* synthesized a folate–mitomycin C conjugate **57**.[194] The water-soluble conjugate exhibited a high affinity for FR-positive cells. Evaluation of cytotoxicity showed an IC_{50} of 5 nM in FR-positive cells. Goldmacher *et al.* reported the targeting prodrugs folate–maytansinoids (**58a**, **58b**).[195] These prodrugs exhibited a high binding affinity for the folate receptor and folate receptor-mediated internalization. They also showed high cytotoxicity and selectivity for folate receptor-positive KB cells with an IC_{50} of 50 pM.

Biotin is a B-group vitamin with an extreme affinity for avidin proteins. Biotin is a key micronutrient for cellular function and cell growth. Biotin uptake is much higher in rapidly growing tumor cells than in normal cells. Ojima *et al.* used biotin as a tumor targeting ligand in the design of theranostic agents utilizing different anticancer drugs and fluorophores.[196–198] The biotinylated fluorescein coupled with SB-T-1214 *via* the self-immolative disulfide linker formed theranostic agent **59**. Cleavage of the disulfide bond by endogenous GSH would release the anticancer drug and fluorescein. Fluorescent imaging demonstrated that theranostic agent **59** localized at the microtubules. This group developed a versatile platform that consisted of 1,3,5-triazine as the tripod splitter module, both SB-T-1214 and camptothecin as antitumor drugs, biotin as the tumor-targeting moiety, and the disulfide linker.[199] The prodrugs **60a** and **60b** were delivered to cell lines that overexpressed the biotin receptor, such as MX-1, MCF-7, ID8, and L1210FR cells. After activation by GSH, **60a** exhibited IC_{50} values of 3.22–9.80 nM against all biotin receptor-positive cell lines, and 705 nM against biotin receptor-negative WI38 cells. Next, they adopted this strategy to report two tumor-targeting theranostic conjugates **61a** and **61b**.[200] The cytotoxic drug taxoid 3 was conjugated with a fluorine-labeled prosthetic (**61a**) or a fluorophore fluorescein (**61b**) *via* a disulfide bond. Once internalized into tumor cells, the disulfide bond was cleaved by endogenous biothiols and

 This journal is © The Royal Society of Chemistry 2017

Published on 20 marzo 2017. Downloaded on 11/05/2026 19:46:09.

drug release was monitored by PET and fluorescence imaging, respectively. Conjugate **61b** exhibited higher specificity for biotin receptor-overexpressing tumor cells than biotin receptor-negative cells. The recycling of biotin receptors varies among different cell lines, resulting in different rates of conjugate **61b** internalization into cells.

Kim *et al.* developed a tumor-targeting theranostic agent **62** composed of the chemotherapeutic drug gemcitabine, a disulfide linker, a coumarin fluorophore, and a targeting unit biotin.[201] The fluorescence intensity increased after cleavage of the disulfide linker by intracellular thiols. Temporal release of gemcitabine from the prodrug **62** was measured *via* fluorescence changes in the presence of GSH. The function time was 10 min. The prodrug was selectively internalized by biotin receptor-positive A549 cells compared with biotin receptor-negative WI38 cells. Colocalization experiments demonstrated that thiol induced the release of active gemcitabine in the lysosomes. In another study, Kim *et al.*[202] designed a theranostic agent **63** based on a NIR azo-BODIPY fluorophore conjugated with biotin and linked with gemcitabine *via* a disulfide linker. Time-dependent fluorescence changes showed a response time of 30 min in the presence of 5.0 mM dithiothreitol. The time-dependent drug release depended on the available biothiol reactivities (Cys > Hcy > GSH > Trx). The theranostic agent **63** was easily internalized by A549 cells compared with WI38 cells. Co-localization experiments demonstrated that thiol-induced disulfide cleavage of this theranostic agent occurred in the endoplasmic reticulum (ER). Theranostic agent **64** was a cancer targeting conjugate composed of biotin, a naphthalimide fluorophore, and Holliday junction (HJ) inhibitor peptide2 (KWWCRW).[203] Cleavage of the disulfide bond occurred in the ER, releasing the active HJ inhibitor peptide2 drug and the fluorophore.

SN-38 is a topoisomerase I inhibitor and the active ingredient in CPT11 (camptothecin), which is used as a therapeutic agent to treat various carcinomas. The potent antitumor drug SN-38 was connected to a biotinylated rhodol fluorophore through a cleavable disulfide bond linker.[204] The theranostic agent **65** displayed a 32-fold increase in the fluorescence intensity within 10 min after exposure to GSH. The prodrug was internalized effectively within biotin receptor-enriched cells by receptor-mediated endocytosis and showed targeted antiproliferative activity against biotin receptor-positive HeLa and A549 cells as a result of release of SN-38 within these cells (Fig. 10). The antitumor efficacy of **65** was evaluated *in vivo* using a xenograft murine model created by subcutaneous inoculation with HeLa cells. *Ex vivo* optical and fluorescence imaging showed increased fluorescence of the tumor region compared with other organs, confirming the *in vivo* tumor targeting effect of the prodrug.

The Shiga toxin receptor Gb3 is overexpressed on the surface of certain human cancers, including colorectal carcinoma. The cytotoxic drug SN-38 belongs to the class of camptothecin derivatives that inhibit topoisomerase I. Johannes *et al.* designed prodrug conjugates **66a**, **b**, **c**, **d** to deliver the cytotoxic drug SN-38.[205] The disulfide linkage of these prodrugs involves two different spacers with different stabilities in the biological system. One is based on an aromatic ring (**66a**,**b**) and the other on an aliphatic chain (**66c**,**d**). Conjugate **66b** was too unstable to be used *in vivo*; however, conjugate **66d** was completely stable over extended periods of up to 48 h in all media. Enzyme-linked immunosorbent assay (ELISA) analysis of **66d** indicated that cleavage of the disulfide bond became detectable between 6 and 24 h and was essentially complete at 48 h. This slow release should sustain the continued presence of the active principle in dividing tumor cells, with the prodrug being otherwise rapidly cleared from the circulation. The disulfide bond of prodrug **66c** was cleaved in the ER, which functions in cellular redox homeostasis. The ER was close to the nucleus, where the molecular target of hydrophobic SN-38 resides.

In addition to folate and biotin, cyclic peptides are another type of effective tumor targeting ligand. These peptides contain an RGD (Arg–Gly–Asp) sequence, which can be recognized and internalized by a well-known tumor-associated receptor, $\alpha_v\beta_3$ integrin. $\alpha_v\beta_3$ integrin is highly expressed on several activated endothelial cells and plays a predominant role in tumor-induced angiogenesis and growth. Kim *et al.* reported a therapeutic agent **67** that allowed direct, fluorescence-based monitoring of targeted cellular uptake and release of the antitumor drug camptothecin.[206] The results of cellular experiments indicated that conjugate **67** bearing a cyclic RGD peptide targeting subunit was selectively internalized into U87 tumor cells *via* $\alpha_v\beta_3$ integrin-mediated endocytosis. Disulfide bond cleavage occurred in the ER, permitting fluorescence changes of the naphthalimide moiety within 60 min.

3.2.2 Therapeutics without targeting ligands. Although the targeting ligands facilitate internalization of the theranostic agents into tumor cells through receptor-mediated endocytosis, theranostic agents that directly conjugate fluorophores with anticancer drugs have also been developed. Omission of the tumor targeting ligands decreases the overall molecular weight of the theranostic agents, which can accelerate the rate of membrane penetration into tumor tissues. Additionally, the conjugation between fluorophores and drugs can improve the hydrophilicity of more polar drugs, which will increase the passive diffusion across the relatively nonpolar cell membrane.

Wender *et al.* presented three disulfide-based luciferin-transporter conjugates (**68a–c**) to establish operationally facile methods to quantify drug-conjugate delivery, linker cleavage, and drug release in real time in cellular assays.[190] The disulfide-carbonate linkers of these conjugates were stable without affecting the rapid release of luciferin and drug (within minutes) in cells through disulfide cleavage. The half-lives of the conjugates (**68a–c**) were 3 h, 11 h, and 33 h, respectively, and depended on cyclization of the intermediate thiol with the carbonate. When the conjugates **68b** and **68c** were incubated with prostate tumor cells transfected with the luciferase gene, strong luminescence of luciferin could be observed within 1 min.

Zhu and Guo *et al.* developed novel activatable theranostics (**69a** and **69b**) based on the dicyanomethylene-4*H*-pyran NIR fluorophore for *in vivo* and *in situ* monitoring of drug delivery and cancer chemotherapy in living animals.[207] The biologically abundant thiols in tumor cells triggered cleavage of the

Published on 20 marzo 2017. Downloaded on 11/05/2026 19:46:09.

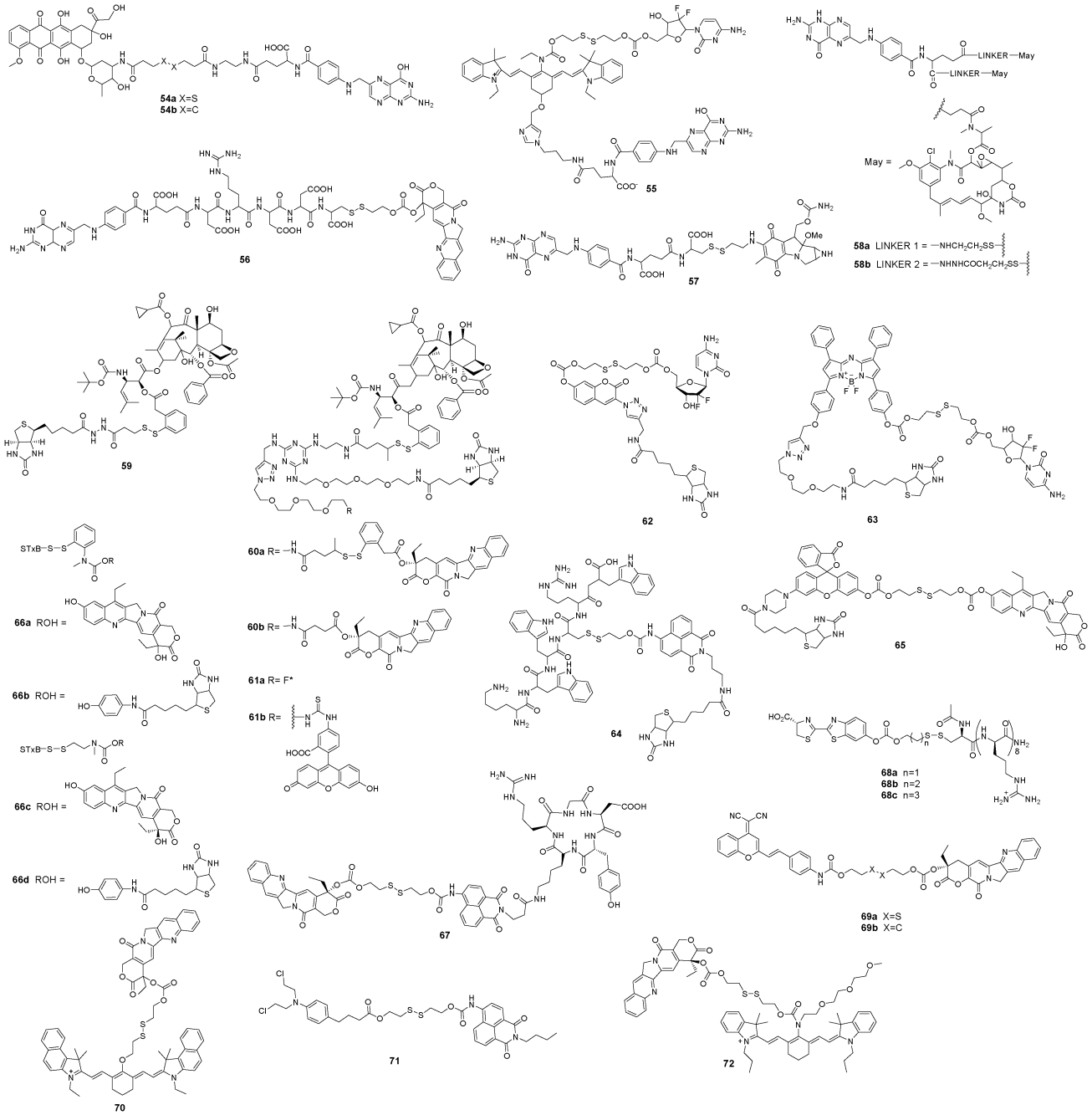

Fig. 10 Theranostics based on thiol-mediated release.

disulfide linker, leading to the release of camptothecin and emission of NIR fluorescence. These theranostics showed similar cytotoxicity with significant *in vitro* antitumor activity against several cell lines including BCap-37, HepG2, MCF-7, HeLa, KB, and KB200. However, the cytotoxicity of **69a** was slightly higher than that of camptothecin and 2-fold lower than that of **69b**. The prodrug **69a** and its polyethylene glycol–polylactic acid (PEG–PLA)-encapsulated nanoparticles all displayed significantly potent cancer therapy and fewer side effects compared with free camptothecin. Loading of PEG–PLA nanoparticles increased the tumor localization properties and prolonged the plasma retention time of the prodrug. The theranostic prodrug **70** contained camptothecin and NIR cyanine dye, linked by a disulfide bond.[208] Cleavage of the disulfide bond resulted in generation of the active drug and induced a remarkable fluorescence shift. This change of wavelength provided dual fluorescent channels for real-time imaging of the activation and biodistribution process of the prodrug. After intravenous injection of **70** for 24 h, the prodrug predominantly accumulated and was activated in tumor lesions. Loading the theranostic prodrug in PEG–PLA nanoparticles would improve the therapeutic efficacy and reduce the side effects of comptothecin.

 This journal is © The Royal Society of Chemistry 2017

Published on 20 marzo 2017. Downloaded on 11/05/2026 19:46:09.

Chlorambucil (CLB) is a DNA alkylating agent that causes DNA damage in the nucleus. Zhou *et al.* developed a theranostic agent **71** composed of the potent anticancer drug CLB, a disulfide linker, and a fluorescent naphthalimide moiety.[209] The prodrug **71** underwent thiol-induced disulfide bond cleavage in HeLa cells with release of the naphthalimide moiety.

Cheng *et al.* reported a therapeutic agent **72** containing a cyanine-amide moiety as the NIR fluorophore, camptothecin as a model antitumor drug, and a disulfide bond as the cleavable linker.[210] The disulfide bond was cleaved by dithiothreitol within 120 min, with release of the active drug and NIR dye. The results of the real-time monitoring of drug release by recording NIR fluorescence changes *in vitro* and *in vivo* demonstrated potential applications in quantitative assessments in live cells and semi-quantitative measurements in live animals.

3.3 H_2O_2-mediated release

Reactive oxygen species (ROS) exhibit highly physiological activities and play key roles in several physiological processes including cellular redox homeostasis, cell differentiation, cell proliferation, and cell signaling.[211–214] ROS include hydrogen peroxide (H_2O_2), hydroxyl radicals ($HO^{\bullet}$), hypochlorous acid (HOCl), the superoxide anion (O_2), and singlet oxygen ($^1O_2$). Compared with normal cells, tumor cells exhibit elevated intrinsic oxidative stress due to the dysregulated production of ROS (mainly as H_2O_2). Given this special feature of tumor cells, increased concentrations of ROS have been recognized as trigger switches for the development of ROS-activated theranostics. Among ROS, the chemical lifespan of H_2O_2 is relatively stable, which allows establishment of significant steady-state concentrations in tumor cells. These factors make H_2O_2 a preferred candidate for the development of ROS-activated theranostics. Such theranostics generally contain two separate functional domains: (i) a H_2O_2-response moiety, and (ii) a cleavable linker system. Once triggered by H_2O_2, the drug is released with a large increase in cytotoxic potency (Fig. 11).

Nitrogen mustard, one of the DNA cross-linking agents, exhibits severe cytotoxicity but has poor selectivity for cancer cells *versus* normal cells. Peng *et al.* synthesized two prodrugs of nitrogen mustard coupled with aryl boronic acids (**73a**) and their pinacol esters (**73b**) to reduce the toxicity of cross-linking agents against normal cells.[215] The aryl boronic acids and their pinacol esters can be cleaved by H_2O_2. These prodrugs were effectively activated in tumor cells. The ability and selectivity of these prodrugs to inhibit tumor cell growth was evaluated and both compounds inhibited various types of tumor cells at 10 μM.

Kim *et al.* developed a H_2O_2-activated theranostic agent **74**.[216] Compound **74** was activated by H_2O_2-mediated boronate oxidation, resulting in the release of the coumarin fluorophore for monitoring fluorescence and activation of the chemotherapeutic drug camptothecin for inhibition of tumor cell growth. The fluorescent signal of coumarin showed that **74** was localized in lysosomes. *In vivo* therapeutic activity was evaluated after intratracheal administration of **74** into mice bearing metastatic lung tumors.

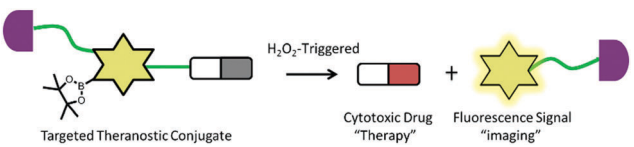

Fig. 11 H_2O_2-mediated drug release.

Kim *et al.* next developed a mitochondria-targeted antitumor theranostic agent **75** that was activated by overexpressed H_2O_2 in mitochondria and led to self-monitored apoptosis of tumor cells to achieve precise tumor treatment.[217] The theranostic agent **75** consists of four parts. The fluorophore ethidium can preferably localize in mitochondria for detection of the intrinsic apoptosis caused by the 5′-deoxy-5-fluorouridine drug moiety. Ethidium emits weak fluorescence in aqueous solution unless intercalated into double-stranded RNA or DNA. The tumor-targeting unit biotin would mediate accumulation of **75** at the tumor site. Aryl boronic acid esters were the H_2O_2 activator. **75** could be activated by endogenously produced mitochondrial H_2O_2 in tumor cells and then release the drug 5′-deoxy-5-fluorouridine to induce apoptosis. *In vitro* experiments showed that **75** displayed high uptake in biotin receptor-positive human lung tumor A549 cells compared with biotin receptor-negative WI-38 cells. *In vivo* xenografts revealed that **75** could inhibit tumor progression and cure tumor-bearing mice (Fig. 12).

3.4 Enzyme-activated release

Real-time detection of drug release would enable *in vivo* studies of pharmacokinetics, pharmacodynamics, and cell permeation pathways. A desirable activation mechanism for drug release depends on the unique physiologic characteristics of tumor cells. As various enzymes are typically overexpressed in tumor cells, utilization of overproduced enzymes as trigger switches for the development of enzyme-activated theranostics has been considered.

Shabat *et al.* reported the prodrug system **76** containing a 7-hydroxycoumarin with a hydroxymethyl substituent spacer, the chemotherapeutic drug melphalan as the end-unit, and phenylacetamide as the cleavable linker.[218] The phenylacetamide could be cleaved by the enzyme penicillin-G-amidase (PGA) for release of drug in cells. In the presence of PGA, **76** exhibited cytotoxicity toward the cells with IC_{50} of 2.5 μM. The prodrug **77** achieved selective activation in tumor cells. The proteolytic enzyme cathepsin B was employed to trigger the dipeptide Phe–Lys linker. **77** was more than 7.5-fold more toxic toward starved cells (IC_{50} = 4 μM) than non-starved cells (IC_{50} = 30 μM). The increased cytotoxicity of **77** was attributed to elevated expression of proteolytic enzymes, including cathepsin B. Human umbilical vein endothelial cells incubated with **77** showed cytoplasmic accumulation of activated coumarin.

DT-diaphorase, a cytosolic flavoenzyme, plays essential roles in the cellular antioxidant system. DT-diaphorase levels are markedly higher in a number of tumor tissues than normal tissues.[219] DT-diaphorase has been employed as a trigger to activate quinone antitumor drugs and acts as a valuable biomarker for efficient drug delivery.

Published on 20 marzo 2017. Downloaded on 11/05/2026 19:46:09.

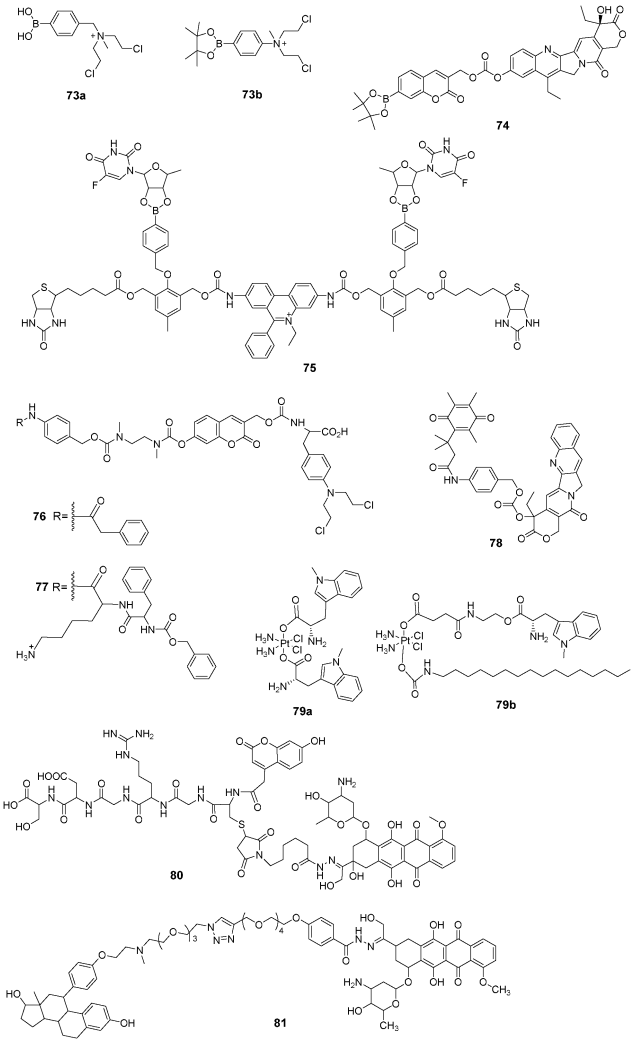

Fig. 12 H_2O_2, enzyme, and pH-triggered theranostics.

DT-diaphorase was developed to produce therapeutic NO by metabolizing a nitric oxide (NO) prodrug.[220] In addition, Wu *et al.* reported a DT-diaphorase-activatable theranostic prodrug **78**.[221] **78** was composed of an antitumor drug camptothecin (CPT), a self-immolative linker, and a quinone propionic acid trigger group. As a result of a photoinduced electron transfer (PET) process between CPT and the quinone propionic acid moiety, the fluorescence of CPT was almost quenched. After reduction by DT-diaphorase, the active CPT recovered its fluorescence emission. CPT release could be monitored by real-time detection of fluorescence. The prodrug exerted high cytotoxicity towards DT-diaphorase overexpressing cell lines.

Indoleamine-2,3-dioxygenase (IDO) is an immunosuppressive enzyme present in human tumors that can be used as a tumor immunotherapeutic target. Lippard *et al.*[222] presented tumor immunochemotherapy Pt(IV) prodrugs **79a** and **79b** for combining immunomodulation and DNA cross-link-triggered apoptosis. The conjugates include the IDO inhibitor (D)-1-methyltryptophan ((D)-1-MT) and the Pt agent cisplatin. After being preferentially targeted to IDO, (D)-1-MT and cisplatin were released inside tumor cells. The release of (D)-1-MT would enhance T-cell proliferation and the generation of cisplatin would concomitantly induce DNA damage in tumor cells. Dynamic blood stability experiments of **79b** in Balb/c mice revealed $t_{1/2}$ of 1 h, and the human blood stability study showed $t_{1/2}$ of 2.2 h.

3.5 pH-triggered theranostics

The tumor cell micromilieu is highly acidic (pH 6.0–7.0), mainly as a result of glycolysis and hypoxia.[223] Growth of solid tumors requires large amounts of nutrients such as glucose; however, highly efficient glycolysis will induce intracellular acidification due to the generation of lactic acid. In addition, the extracellular diffusion effect of CO_2 is discharged by tumor tissue hypoxia, producing carbonic acid with H_2O.

Zhang *et al.* designed a pH-responsive prodrug (**80**) for real-time monitoring of drug release in the tumor mass.[224] The prodrug contains three parts: a coumarin fluorophore, a targeting moiety GRGDS oligo-peptide that can be recognized by $\alpha_v\beta_3$ integrin, and doxorubicin, which functioned not only as an antitumor drug but also as a fluorescent quencher for coumarin. The GRGDS moiety promoted selective uptake of the prodrug into tumor cells that overexpressed $\alpha_v\beta_3$ integrin. The hydrazone bond in the prodrug could be cleaved in the endosomes/lysosomes (pH 5–6) of tumor cells and the activated doxorubicin induced cell apoptosis. In addition, the fluorescence of coumarin was recovered. *In vitro* studies showed approximately 93.8% release of drug at pH 5.0 and only 40.7% release at pH 7.4. Merged fluorescence images indicated that this prodrug was internalized and cleaved in endo/lysosomes.

Hanson *et al.* synthesized a therapeutic agent of steroidal anti-estrogen and doxorubicin (**81**).[225] This prodrug reduced the side effects of doxorubicin and the targeted drug delivery of steroidal anti-estrogen improved its efficacy. Fluorescence microscopy studies in MCF-7 cells that overexpress the estrogen receptor (ER) suggested that the uptake process was controlled *via* a membrane ER-mediated mechanism, resulting in cellular accumulation of doxorubicin. Once the prodrug entered the acidic cytoplasm of tumor cells, hydrolysis of the pH-sensitive hydrazone linker released free doxorubicin to kill the tumor cells.

3.6 Light-activated theranostics

As an alternative to chemotherapy, a new modality termed photodynamic therapy (PDT) has been successfully applied in the clinic for the treatment of a variety of tumors and other diseases.[226] Photoresponsive theranostics allows precise control of drug release, including location, timing and dosage, through an active ''phototrigger''.[227] The primary components of photoresponsive theranostics include a photosensitizer, a masked drug, a photo-switched linker, light, and molecular oxygen. All of these elements are required in PDT to produce reactive oxygen species and release cytotoxic drugs for killing of tumor cells (Fig. 13).

Berkman *et al.* reported PSMA inhibitor conjugates of pyropheophorbide-a (**82** and **83**) for targeted photodynamic therapy of prostate tumors.[228,229] Compared with PSMA-negative PC-3 cells, the prodrug **82** selectively induced apoptosis in PSMA-positive

 This journal is © The Royal Society of Chemistry 2017

Published on 20 marzo 2017. Downloaded on 11/05/2026 19:46:09.

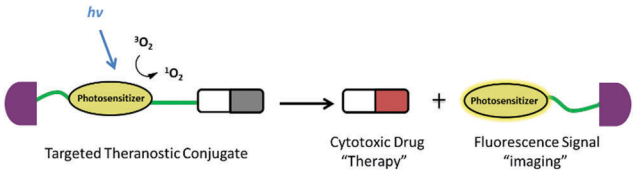

Fig. 13 Light-activated drug release.

LNCaP prostate tumor cells *via in vitro* targeted photodynamic therapy. Fluorescence labeling showed that conjugate **83** was specifically localized in PSMA-positive LNCaP cells, but not PSMA-negative PC-3 cells. Studies with specific caspase inhibitors revealed that conjugate **83** mediated apoptosis through the caspase-8/-3 pathway in PSMA-positive LNCaP cells; after 4 h of PDT treatment with **83** the activities of caspases-8, -9, and -3 were increased.

Ju *et al.* reported a pH-activatable aniline-substituted azaboron-dipyrromethene as a photosensitizer for efficient photodynamic therapy and therapeutic monitoring (**84**).[230] To achieve high accumulation in tumors, compound **84** was encapsulated in a cyclic RGD peptide-functionalized poly(ethylene glycol)-*block*-poly(lactic acid) and methoxyl poly(ethylene glycol)-*block*-poly(lactic acid) nanomicelle (Fig. 14). After activation by the physiologically acidic pH in the tumor, **84** exhibited strong phototoxicity by producing $^1O_2$ and emitted fluorescence. The fluorescence at the tumor increased gradually and reached a maximum at 8 h post-injection. The high fluorescence level could be maintained for more than 16 h after injection.

Choi *et al.* developed a folate–photosensitizer conjugate (**85**) *via* a protein linker for photodynamic therapy.[231] The NIR fluorescence emission of the photosensitizer was quenched when folate was removed by the tumor-associated lysosomal enzyme cathepsin B. KB cells were implanted into mice as a xenograft model to assess the utility of conjugate **85** for *in vivo* fluorescence imaging and photodynamic therapy. Strong fluorescence signals were observed at the tumor site at 3 h post-injection and could be maintained for up to 24 h.

You *et al.* synthesized three double activatable prodrugs of the CA-4, SN-38, and coumarin system (**86a–c**) that were first activated by intracellular esterase and then drug release was induced by light irradiation.[232] A photo-cleavable aminoacrylate-linker and a deactivated photosensitizer allowed the spatiotemporally controlled release of drugs by visible light irradiation. When the prodrug **86a** was irradiated with very low intensity light (540 nm, 8 mW cm^{-2}) for 30 min up to 99% of the coumarin was released.

NIR light has great potential for spatiotemporally controlled release of therapeutic agents due to its deep tissue penetration. You *et al.* demonstrated that the aminoacrylate group could be cleaved to release parent drugs after oxidation by $^1O_2$ when activated by NIR light.[233] The prodrugs of combretastatin A-4 (**87a–c**) contain core-modified porphyrin as a NIR photosensitizer to generate $^1O_2$. The aminoacrylate linker of **87a** was broken by tissue-penetrable NIR light (690 nm), releasing the antitumor drug. The prodrug **87a** exhibited a significantly better antitumor effect after irradiation than **87b**. The prodrug **87c** was designed for *in vivo* fluorescence imaging after cleavage of the aminoacrylate group in mice. The prodrug **88a** was developed to achieve multifunction activity, including the release of drug, fluorescence imaging, and photodynamic therapy.[234] The compound **88b** was designed as a pseudo-prodrug to assess the effects of photodynamic therapy and confirm the potential application of the prodrug **88a** *in vivo*. The time-dependent distribution of **88a** was investigated using Balb/c mice with SC tumors (colon-26 cells, 4–6 mm in length).

You *et al.* expanded their NIR light activatable strategy by integrating a tumor-targeting folic acid group into the prodrug systems (**89a–e**).[235] The photosensitizer and fluorophore was phthalocyanine. The light switch was aminoacrylate with variable polyethylene glycol chains. Compared with the lipophilic prodrugs **89a** and **89b**, the hydrophilic prodrugs **89c** and **89d** had higher cellular uptake in SC colon-26 tumors. The prodrug **89e** without folic acid indicated the effectiveness of tumor targeting.

Singh *et al.*[236] developed a targeted photoresponsive prodrug **90** containing biotinylated coumarin and chlorambucil, in which the phototrigger was directly attached to the drug. The prodrug **90** could be selectively taken up by MDA-MB-231 cells. The release time of active chlorambucil was 20 min after light irradiation. Biotin-mediated accumulation could significantly increase the efficiency of intracellular drug delivery in the MDA-MB-231 cell line.

The tropomyosin receptor kinase C (TrkC) receptor is normally expressed in neurons, but is overexpressed in highly metastatic tumor cells such as neuroblastoma, glioblastoma, thyroid cancer, melanoma, and breast cancer.[237–244] The TrkC receptor could be used as a potential molecular target for chemotherapeutics. Burgess *et al.* reported fluorescence conjugates for PDT based on a synthetic peptidomimetic (including isoleucine and tyrosine side chains) targeting ligand.[245] Conjugate **91a** composed of a peptidomimetic and a boron dipyrromethene (BODIPY) fluorophore for tumor imaging was selectively accumulated in TrkC receptor-expressing tumor tissues. Intracellular imaging studies showed that **91a** was internalized into lysosomes, and behaved as the natural TrkC ligand neurotrophin-3 when internalized *via* the TrkC receptor. The diiodo-BODIPY could perform as a photosensitizer to produce triplet oxygen for PDT. Conjugate **91a** induced significant photocytotoxicity in TrkC-expressing NIH-3T3 fibroblasts and SY5Y neuroblastoma cells compared with TrkC-negative cells. The biodistribution of conjugate **91a** was tested in mice bearing 4T1 tumors. Fluorescence was maintained at a high level for up to 72 h after intravenous administration. The isomeric conjugate **91b** that could not bind TrkC was used as a control probe.

The application of PDT to lesions in deep tissue is often hampered by light penetration, as well as absorption and scattering by biological tissues. Wang *et al.* developed a PDT system in which the photosensitizer was activated by bioluminescence instead of an external light source.[246] In this PDT system, luminol (**92a**), hydrogen peroxide, and horseradish peroxidase were used as bioluminescent molecules. Cationic oligo (*p*-phenylene vinylene) (OPV, **92b**) was used as the photosensitizer. The activation

Published on 20 marzo 2017. Downloaded on 11/05/2026 19:46:09.

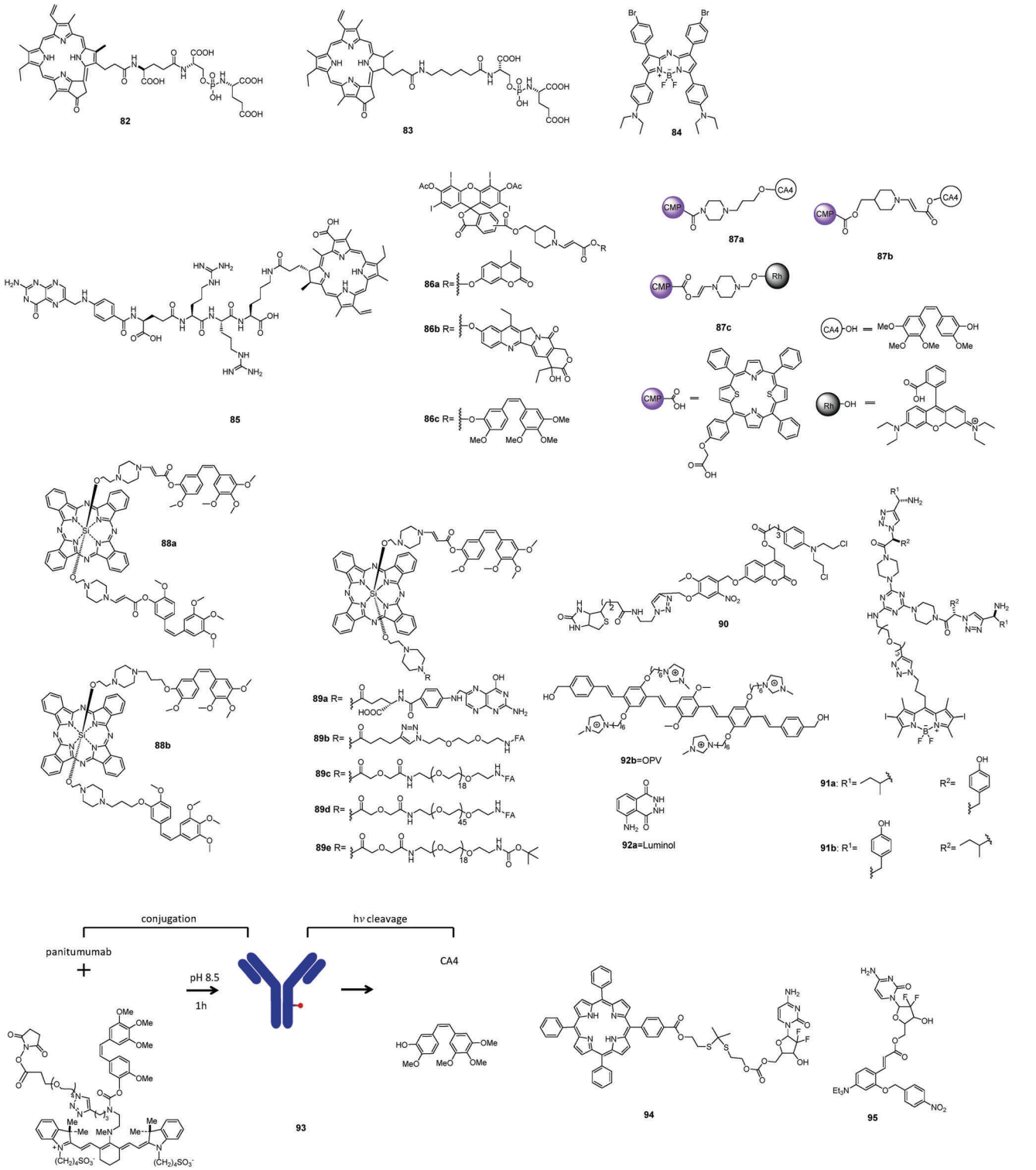

Fig. 14 Light-activated theranostics.

mechanism was bioluminescence resonance energy transfer (BRET). The blue bioluminescence generated from luminol excited OPV to produce reactive oxygen species to kill cancer cells and pathogenic microbes. The cationic **92b** could bind to the HeLa cell surface. This BRET system could function in deeper tissues.

Schnermann *et al.* reported NIR light-mediated cleavage of antibody-drug conjugate **93** based on cyanine photocages.[247] The conjugate includes a heptamethine cyanine fluorophore as the caging component, the drug combretastatin A4, and panitumumab (Pan), a clinical monoclonal antibody to the human epidermal growth factor receptor (EGFR). The fluorescence

 This journal is © The Royal Society of Chemistry 2017

Published on 20 marzo 2017. Downloaded on 11/05/2026 19:46:09.

signal offered a useful marker for accumulation of conjugate **93**. Loss of the fluorescence signal after excitation by light at 690 nm indicated drug release. The consequence of irradiation with NIR light was evaluated in mice bearing A431 tumors.

Tumor-associated M2-type macrophages are correlated with tumor invasion and metastasis. The biomarker CD206 is specifically expressed in M2 macrophages. Liu *et al.* reported a CD206-targeting photoimmunotherapy agent generated by conjugating a monoclonal anti-CD206 antibody with the near-infrared phthalocyanine dye IRDye700.[248] Upon light irradiation, this agent suppressed proliferation of sorafenib-resistant 4T1 tumors and prevented lung metastasis.

Zhang *et al.* developed a photosensitive prodrug **94** for fluorescence imaging-guided photodynamic therapy and chemotherapy of tumors.[249] The prodrug included a fluorescent photosensitizer *meso*-tetraphenylporphyrin (TPP) and an antitumor drug gemcitabine. Upon irradiation with low-energy red light, TPP generated $^1O_2$. Subsequently, $^1O_2$ mediated cleavage of the thioketal linker, which resulted in the cascaded release of gemcitabine and combination therapy against tumor cells. The prodrug was formulated in PEG–PLA to form uniform micelles to enhance the plasma stability and endow tumor-targeting activity. Strong fluorescence was detected in tumor lesions after 48 h post-injection, displaying significantly enhanced tumor accumulation and good tumor retention.

Zhang *et al.* developed an anticancer theranostic prodrug (**95**) based on hypoxia and a photo dual activation process.[250] The photo-activated group (*o*-hydroxyl E-cinnamic ester) of the prodrug was modified using a hypoxic trigger 4-nitrobenzyl group, which was directly attached to the anticancer drug gemcitabine. In hypoxic MCF-7 cells, the hypoxic trigger was reduced by nitroreductase and underwent a 1,6-rearrangement-elimination reaction to remove the masked group. Subsequent UV irradiation would induce isomerization and intramolecular esterification processes leading to the formation of a coumarin fluorophore and the release of gemcitabine. The theranostic prodrug exhibited significant cytotoxicity against MCF-7 cells.

3.7 Aggregation-induced emission-based theranostics

Aggregation-induced emission (AIE) is a unique photophysical process that is induced by a series of silole or tetraphenylethene derivatives that are non-emissive in dilute solutions but become highly emissive in solid or aggregated states.[251] Fluorescent probes with AIE characteristics possess unparalleled advantages in biological detection compared with traditional fluorescent probes. On one hand, they can achieve brighter fluorescence as a result of more AIE active molecules binding to the target analytes without aggregation-induced fluorescence quenching. On the other hand, the feature of a drastic enhancement in the fluorescence intensity associated with an aggregation event can be used as a method of quantitative detection (Fig. 15).

Tang *et al.* presented a series of theranostic agents based on AIE characteristics (Fig. 16).[252–254] The theranostic prodrug **96** was a targetable theranostic Pt(IV) prodrug for monitoring and assessing drug-induced cell apoptosis.[252] The targeting ligand was a cyclic arginine–glycine–aspartic acid (cRGD) tripeptide

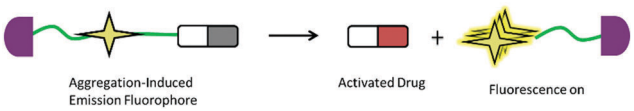

Fig. 15 AIE-based theranostics.

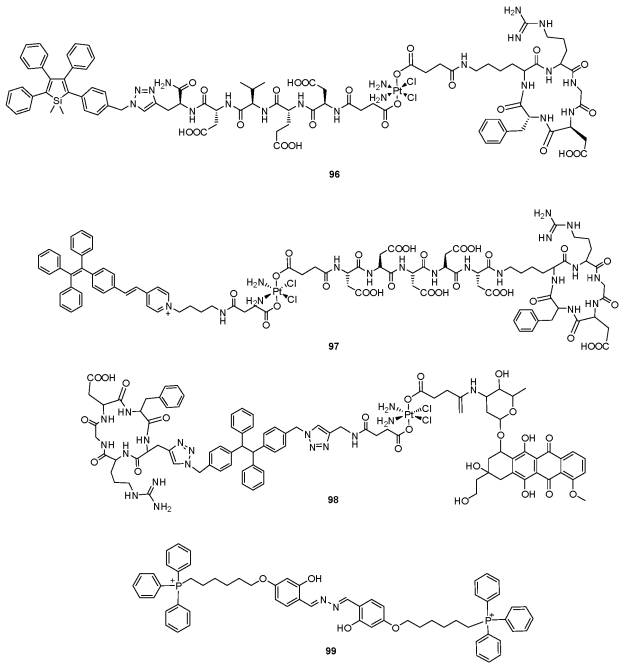

Fig. 16 Theranostics based on aggregation-induced emission.

for intergrin $\alpha_v\beta_3$ that was overexpressed on the surface of tumor cells. The prodrug was a nontoxic Pt(IV) complex that was reduced to toxic Pt(II) in tumor cells. Asp–Glu–Val–Asp (DEVD)-conjugated tetraphenylsilole (TPS) that possessed AIE characteristics was used as an apoptosis sensor. The prodrug **96** selectively accumulated in tumor cells that overexpressed $\alpha_v\beta_3$ integrin and then released the toxic drug Pt(II) to induce apoptosis. Subsequently, caspase-3 cleaved the apoptosis unit TPS-DEVD and triggered the AIE fluorescence.

A targeted theranostic Pt(IV) prodrug **97** based on an AIE luminogen for *in situ* monitoring activation of the platinum(IV) prodrug was developed.[253] The theranostic prodrug consisted of nontoxic Pt(IV) complexes, a tetraphenylethene pyridinium unit with AIE properties, a short hydrophilic peptide with five aspartic acid (D5) units to ensure its water solubility, and a cRGD tripeptide as the targeting ligand. Prodrug **97** could be selectively taken up by MDA-MB-231 cells that overexpressed $\alpha_v\beta_3$ integrin. The theranostic prodrug **98** contained a targeted cRGD moiety, a tetraphenylene (TPE) derivative, a fluorescent antitumor drug doxorubicin (DOX), and a chemotherapeutic Pt(IV) prodrug. **98** was selectively taken up by tumor cells that overexpressed $\alpha_v\beta_3$ integrin accompanied by the release of two drugs: Pt(II) and DOX. The fluorescence of TPE recovered, followed by the separation of TPE and DOX.[254]

The outer membrane of mitochondria has a more negative potential in tumor cells.[255] Triphenyl phosphonium cation

Published on 20 marzo 2017. Downloaded on 11/05/2026 19:46:09.

(TPP) facilitates penetration of the phospholipid bilayers in mitochondria due to the positive charge on the phosphonium and three lipophilic phenyl groups.[256] Liu *et al.* presented a mitochondrial targeting probe (**99**) formed by conjugation of a salicyladazine fluorophore with the mitochondria-targeting TPP.[257] The fluorescence manipulation mechanism involved both AIE and excited-state intramolecular proton transfer processes, which could enhance the imaging contrast and the signal-to-noise ratio. The probe exhibited no fluorescence in culture media but fluorescence was activated after its accumulation in the mitochondria of tumor cells. The probe could induce the generation of reactive oxygen species and affect essential cancer cell progression, leading to tumor cell apoptosis.

3.8 NIR dye-based theranostics

NIR hemicyanine dyes are desirable candidates for the development of fluorescence imaging probes due to their photophysical properties, biocompatibility, and low toxicity to living systems.[258] Heptamethine indocyanine dyes are often utilized for lesion targeting and imaging. However, these dyes are lipophilic cationic molecules that can preferentially accumulate in the mitochondria of tumor cells, therefore some cyanine probes show activity in photodynamic therapy. These types of dyes have promise as candidate theranostic agents.

Shi *et al.* developed a class of near infrared (NIR) heptamethine indocyanine dyes that preferentially accumulated in tumor cells for *in vivo* imaging.[45,259–263] The probe **100** not only preferentially accumulated in a broad spectrum of tumor cells for *in vivo* tumor targeting and imaging, but also had unique photodynamic therapeutic properties.[261] This probe avoided the problems of chemical conjugation with tumor-specific ligands and photosensitizers. Changes in the lipophilicity of heptamethine indocyanine dyes would increase their mitochondrial toxicity. A series of IR-808 analogs (**101a–c**) was developed for simultaneous cancer-targeted NIR imaging and potent anticancer activities.[262] The theranostic agent **101a**, a butyl ester derivative of IR-808, showed preferential accumulation in the mitochondria of A549 cells and PDT activity. The tumor inhibition effect of **101a** was better than that of cyclophosphamide. The tumor selective NIR dye IR-780 (**1**) also exhibited efficient anti-tumor activity by targeting drug-resistant cell populations.[263] IR-780 preferentially accumulated in the mitochondria of drug-resistant human lung tumor cells (A549/DR) and blocked the self-renewal and migration ability of A549/DR cells. The IR-780 dye showed tumor targeting ability and inhibited tumor recurrence in a mouse syngeneic Lewis lung carcinoma xenograft model.

Shi *et al.* synthesized a mitochondria-targeting theranostic agent (**102**) for synchronous photodynamic therapy and photothermal therapy.[264] The theranostic agent **102** was screened from a panel of heptamethine cyanine dyes modified with various *N*-alkyl side chains. This NIR fluorescent dye could clearly visualize the margins of tumors, which is greatly helpful for imaging-guided surgical operations. **102** exhibited synchronous photodynamic and photothermal therapy effects on multiple cancer cells by targeting mitochondria (Fig. 17). The theranostic agent preferentially accumulated in tumor lesions *via* organic-anion transporting polypeptide (OATP)-mediated active transport and was retained in mitochondria because of its lipophilic cationic properties.

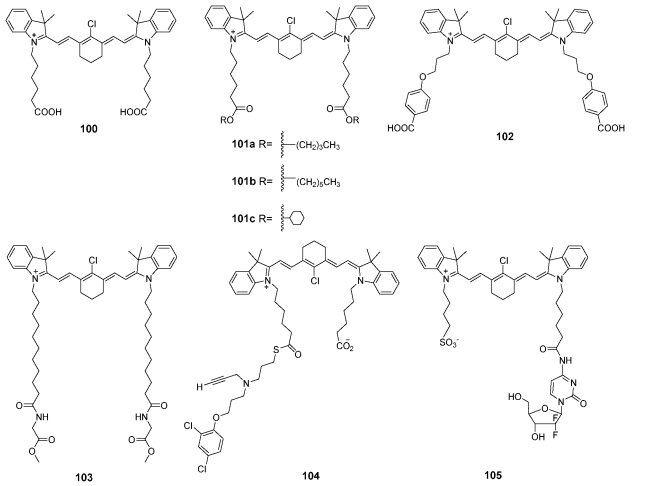

Fig. 17 Theranostics based on NIR dyes.

Shi *et al.* developed a NIR therapeutic autophagy-enhancer (**103**) to kill tumor cells.[265] **103** preferentially accumulated in the mitochondria of tumor cells in a glycolysis-dependent and organic anion transporter polypeptide-dependent manner. **103** killed tumor cells *via* inducing excessive autophagy both *in vitro* and *in vivo*, which is mediated through the reactive oxygen species (ROS)-Akt-mammalian target of the rapamycin (mTOR) pathway. Translocase of inner mitochondrial membrane 44 (TIM44), a novel autophagy-related gene, correlated positively with CRC development and prognosis. Downregulation of TIM44 resulted in the induction of autophagy and cell death through the TIM44-SOD2-ROS-mTOR pathway.

Mitochondria-bound monoamine oxidase A (MAOA) can catalyze the degradation of monoamine neurotransmitters and dietary amines. High MAOA levels are associated with prostate cancer progression and poor prognosis for patients.[266] Shih *et al.* demonstrated a tumor-targeting NIR hemicyanine–MAOA inhibitor conjugate (**104**) as a theranostic agent for the treatment and diagnosis of prostate cancer.[266] The fluorophore of this theranostic agent could be taken up and localized in tumor cells. The MAOA-targeting moiety was derived from the MAOA inhibitor clorgyline. The theranostic agent **104** accumulated in human PCa LNCaP cells and localized in the mitochondria to inhibit the activity of overexpressed MAOA. *In vivo* and *ex vivo* imaging of tumor xenografted mice demonstrated that **104** possessed tumor-targeting properties and antitumor efficacy.

The delivery of diagnostic and therapeutic agents for detection and therapy of brain tumors is hindered by the blood brain barrier (BBB) and the blood tumor barrier (BTB) between brain tumor cells and microvessels. Chung *et al.* synthesized an IR-783–gemcitabine conjugate **105** as an imaging and therapeutic agent for the detection and treatment of human brain tumors and brain metastases.[267] The targeting mechanism was mediated by activation of the tumor hypoxia-inducible factor 1α/OATP signaling pathway. Conjugate **105** could penetrate the BBB/BTB

 This journal is © The Royal Society of Chemistry 2017

Published on 20 marzo 2017. Downloaded on 11/05/2026 19:46:09.

and accumulate in intracranial human tumor and brain tumor metastases of a human prostate tumor model within 24 h.

3.9 Metal complex-based theranostics

Metal complexes are widely used in antitumor theranostic agents because of their favorable pharmacological profiles *in vitro* and *in vivo*. Ruthenium (Ru) (III) complexes have been identified as leading candidates due to their good photochemical and pharmacological properties. Several Ru(III) complexes, such as NAMI-A, ([Him][*trans*-$RuCl_4$(DMSO)(im)], im = imidazole), KP1019, (^{146}-[*trans*-$RuCl_4(ind)_2$], ind = indazole), and its Na^+ analogue (KP1339), have been developed. NAMI-A and KP1339 have successfully entered clinical trials.[268]

Spiccia *et al.* demonstrated the use of coordinatively saturated and substitutionally inert polypyridyl Ru(II) compounds **106a–d** as theranostic drugs.[269] The derivatives **106c** and **106d** exhibited enhanced cytotoxicity toward all six cell lines tested: human cervical tumor HeLa, breast carcinoma MCF7, osteosarcoma U2OS, ovarian carcinoma A2780, and cisplatin-resistant ovarian carcinoma A2780–CP70 cells. The complex **106c** was mainly targeted to mitochondria, whereas **106d** was primarily located in the outer cellular membrane. The anticancer activity of **106c** was similar to that of cisplatin. **106c** exerted its toxicity through a mitochondria-related pathway. The mitochondrial membrane potential of tumor cells was impaired as early as 2 h after the introduction of **106c**.

Mao *et al.* designed three fluorescent Ru(II)–polypyridyl complexes **107a–c** targeting histone deacetylase inhibitors (HDACs) as antitumor agents.[270] These antitumor agents showed relatively high quantum yields, large stokes shifts, and long emission life times. The fluorescence regulation mechanism was a metal-to-ligand charge transfer process. Treatment of HeLa cells with complex **107c** significantly increased the acetylation of histone H3 in a dose- and time-dependent manner. Confocal microscopy images illustrated that **107c** accumulated in the nuclei. Cell apoptosis induced by **107c** was determined to involve mitochondrial dysfunction and the production of reactive oxygen species. The compounds **108a–c** based on cyclometalated iridium(III) complexes, which included bis-N-heterocyclic carbene ligands as photodynamic and mitochondrial targeting groups, were also reported as theranostic agents.[271] All complexes were effectively localized in mitochondria and displayed higher cytotoxicity than cisplatin against all tested human tumor cell lines. The order of complexes for active transport with uptake was **108c** > **108b** > **108a**. The mechanism for apoptosis was mitochondrial damage caused by overproduction of reactive oxygen species (Fig. 18).

Farrell *et al.* presented Ru complexes **109a–c** and **110a,b**, which showed high cellular and uptake antitumor activity.[272] Ru complex **109a** showed high cytotoxicity to HCT116 $p53^{+/+}$ cells and HCT116 $p53^{-/-}$ cells with IC_{50} values of 0.1 and 0.7 μM, respectively, which indicated that the hydrogen bond of the imidazole units strongly affected antitumor activity. Fluorescence imaging indicated that **109a** and **109b** localized in the cytoplasm and in the nucleus, respectively. Flow cytometry and western blotting indicated that complex **109a** inhibited the G1 and S phases of the cell cycle.

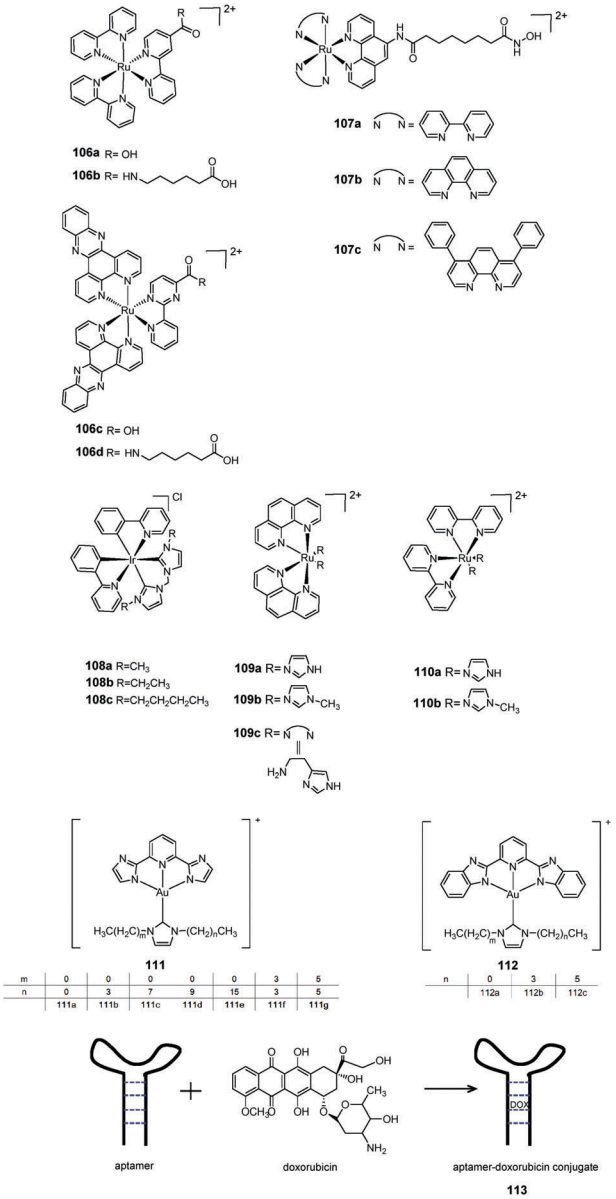

Fig. 18 Theranostics based on metal complexes and aptamers.

Che *et al.* developed a class of antitumor Au(III) complexes containing N-heterocyclic carbene and 2,6-bis(imidazol-2-yl)-pyridine or 2,6-bis(benzimidazol-2-yl)pyridine ligands (**111a–g**, **112a–c**).[273] The biothiols reduced the Au(III) complexes to the Au(I) state with release of the fluorescent ligand. These Au(III) complexes could suppress tumor growth in mice bearing HeLa xenografts. **112a** was easily taken up by cells and localized in the mitochondria of HeLa cells. **111e** exhibited significant suppression of tumor volume *in vivo*.

3.10 Aptamer-based theranostics

Aptamers are structured single-stranded DNA or RNA molecules that have a high affinity for small molecules, peptides, proteins, and oligosaccharides. Therefore, aptamers have attracted great attention because of their potential application for therapeutic or diagnostic targeted-delivery.[274–279]

Published on 20 marzo 2017. Downloaded on 11/05/2026 19:46:09.

Jon *et al.* reported an A10 RNA aptamer–doxorubicin conjugate (**113**) for the targeted delivery of doxorubicin to tumor cells.[280] The conjugate could bind to the PSMA protein on the surface of prostate cancer cells. The anticancer drug intercalated into the CG sequence of the A10 aptamer following maximal quenching of the fluorescence of doxorubicin at an approximately 1 : 1.2 molar equivalence of doxorubicin to the aptamer. Microscopy and flow cytometry studies showed that conjugate **113** could preferentially accumulate in PSMA-expressing LNCaP prostate epithelial cells compared with PSMA-negative PC3 prostate epithelial cells.

4. Challenges and perspectives for optical chemical probes

This review focuses on small molecular ligand-targeted fluorescent imaging probes and fluorescent theranostics for tumor diagnosis and therapy. It does not include nanoparticles, polymers, or liposomes, even though small molecular targeting groups and/or cytotoxic drugs have been attached and loaded to these transport carriers. The general tumor treatment methods include surgery, radiotherapy and chemotherapy. However, surgery is the preferred modality for the treatment of most solid tumors. The primary challenge for surgical intervention is how to distinguish the surgical margin between the lesion and its healthy surrounding tissue at the cellular level. Fluorescence bioimaging technologies for delimiting the surgical margin are able to precisely discern diseased tissues in patients. With current fluorescence imaging instruments, fluorescent imaging probes can be exploited for intraoperative decisions concerning which tissues need to be resected and which tissues need to be preserved during surgery. Successful surgical fluorescent navigation for tumor lesions is achieved by significantly minimizing the background and maximizing the target-to-background ratio to increase contrast. The general requirements and objectives of imaging probes are designed to achieve optimal visualization.

In general, there are two approaches for targeting imaging probes to tumor lesions (Fig. 1 and 19). Passive targeting benefits from the enhanced permeability and retention (EPR) effect, in which the defects or gaps in the tumor vasculature are typically 200 to 2000 nm in diameter. The EPR effect allows the extravasation and accumulation of both small molecules and larger particles (mainly with diameters <600 nm). Small molecules can easily diffuse back into the blood circulation by way of the defects or gaps, but larger particles (>4 nm or 30 kDa) are retained in solid tumors. This effect results in the preferential accumulation of larger particles around tumors. However, deep penetration of larger particles is hampered by the dense tumor interstitial space. This tumor backpressure strongly misrepresents diffusion patterns of larger particles in solid tumors. Obstacles to tumor penetration originating from the tumor backpressure should be overcome, as small molecules can be released and integrated into the tumor independently. This strategy belongs to the second category of active targeting, which requires the involvement of targeting moieties such as ligands, peptides, proteins, and antibodies. These targeting moieties are used to implement the identifying features (*i.e.*, tumor-specific receptors) that uniquely exist on the surface of tumor cells, such as proteins, sugars, and lipids. That is why the design focus for active targeting

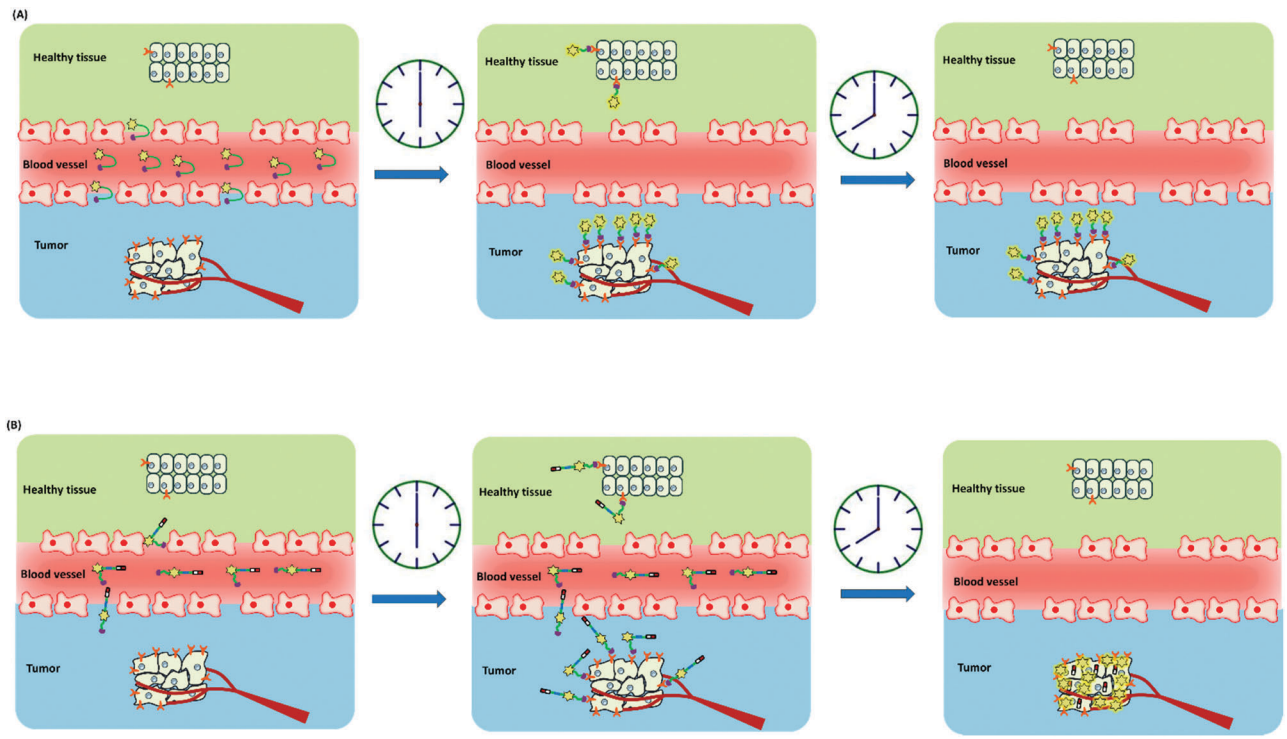

Fig. 19 Schematic of the *in vivo* imaging process using an imaging fluorescent probe (A) and fluorescent theranostics (B).

 This journal is © The Royal Society of Chemistry 2017

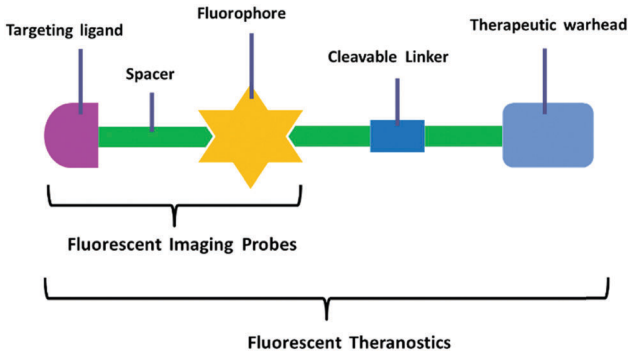

Fig. 20 Schematic of the design strategy for fluorescent imaging probes and fluorescent theranostics.

Published on 20 marzo 2017. Downloaded on 11/05/2026 19:46:09.

is seeking the right targeting moiety. These imaging probes are often represented as targeting moiety–spacer–fluorophore conjugates (Fig. 20). As the overall design approach, we first investigate the tumor-specific receptor that is the binding site of the imaging probes. To effectively capture the targeting moiety, the desirable receptor must meet the following criteria. First, the receptor is overexpressed on cancer cells. Relative to normal cells, the absolute level of the expressed receptor on cancer cells must be at least 3-fold higher. Second, the candidate receptor is fixed on the cell surface and should not be cleaved or shed into the circulation. Here, receptor-mediated endocytosis does not need to be considered. The critical need is a fluorescent imaging probe that accurately labels the tumor lesions. The candidate receptor is required to have a high affinity for the imaging probe, as this is a major contributing factor to the target-to-background ratio, tumor accumulation, and residence time. Any unbound imaging probe must be rapidly cleared by the circulation. If the targeted receptor is overexpressed within the cytoplasm or nucleus, the imaging conjugate should be designed to be nonspecifically permeable across cell membranes. The design of the targeting moiety must sufficiently take into account the affinity, specificity, molecular size, and functional-group modifiability. The dissociation constant (K_d) of the targeting moiety for its receptor is suggested to be lower than 10 nM. The spacer between the targeting moiety and the fluorophore *via* the derivatizable functional group must not severely reduce the affinity. The derivatizable functional group of the spacer is required to be chemically stable. Removal of the unbound imaging probe is controlled by the diffusion and clearance rate from the circulation. A NIR fluorophore is preferred for the selection of the fluorophore, in part because the low biological background is conducive to bioimaging. To date, fluorescent imaging probes that are applied to assist intraoperative dissection have been untargeted fluorescent dyes including methylene blue, indocyanine green, fluorescein, and 5-aminolevulinic acid. Although numerous targeting moiety–fluorophore conjugates have been reported only a few are in the process of clinical translation, such as IRDye 800CW,[281] ZW800-1,[282] EC17,[283] and OTL-0038.[95] In terms of increasing the target-to-background ratio, an activatable imaging probe is better than an active imaging probe due to the controllable change in fluorescence.

Anticancer drugs have made chemotherapy an indispensable therapeutic intervention for inhibiting the rapid growth of tumor cells. Chemotherapeutic drugs have achieved great advances, but their non-specific distribution in normal and tumor cells leads to low efficacy and severe side effects. Additionally, drug resistance is another factor that should be considered. The mechanisms of drug resistance involve sub-therapeutic concentrations and upregulation of efflux transporters and metabolizing enzymes. In order to improve the effectiveness of cancer treatment, it is essential to develop new strategies for the effective delivery of chemotherapeutic drugs to cancer cells. It seems that the targeted delivery of drugs can improve pharmacokinetics and increase efficacy. Passive targeting employs polymeric structures as carriers, such as nanoparticles, polymers, or liposomes.[284–291] This strategy is highly dependent on the enhanced permeability and retention effect. The direct conjugation of a chemotherapeutic drug to a certain tumor cell targeting ligand represents active targeting. The structure of this kind of drug delivery system generally includes a targeting moiety linked to a potent chemotherapeutic drug *via* a linker that embodies a cleavable bond.[292] The above-mentioned targeted delivery strategies have provided great advantages over traditional non-targeted chemotherapeutic drugs.[292] However, the progression and treatment of tumors involves many complicated stages including initiation, progression, metastasis, recurrence, and resistance to therapy. A precise diagnosis is indispensable for tumor staging and early therapy. To meet this demand, diagnostics and therapeutics are being integrated to provide promising tools for tumor diagnosis and therapy (Fig. 19). This newly emerging combined system has been termed theranostics. Small-molecule fluorescent theranostics are conceived and synthesized as three or four moieties. A targeting moiety is covalently labeled with a fluorophore *via* a spacer, and then a chemotherapeutic drug is introduced into the molecular structure through a cleavable linker. This can be represented as a targeting moiety–spacer–fluorophore–linker–drug (Fig. 20). For the design of small-molecule fluorescent theranostics, the issues to be considered combine the requirements of both diagnostics and therapeutics. However, one must also pay attention to receptor-mediated endocytosis. The candidate receptors on the cell surface must be sufficient to meet the precise delivery of theranostics into tumor tissues. The theranostics are intended to be retained within the tumor cells and achieve the desired steady-state concentrations. Another focal point is the manipulation of drug release at tumor lesions because non-targeted drug release will result in systemic toxicity. Structural constraints on the introduction of chemotherapeutic drugs are often imposed by the linkers therefore the design of cleavable linkers using tumor factors is a key element for drug triggering release. The tumor physiological microenvironment is different from that of normal tissues. Insufficient and defective vascular structures of the tumors result in hypoxia, low pH, and high interstitial fluid pressure. Some other unique characteristics of tumors, such as high levels of reactive oxygen species, high concentrations of glutathione, as well as overexpressed enzymes, also act as advantageous stimulants. External stimulators, such as light and heat, are good releasing triggers. It is worth noting that no residues of the linker can remain in the released

Published on 20 marzo 2017. Downloaded on 11/05/2026 19:46:09.

chemotherapeutic drug. In terms of the design requirements of the overall small-molecule fluorescent theranostic agents, they are expected to have low cytotoxicity, excellent pharmacokinetics, and chemical stability before reaching their destination. At the same time, we require the linker to play a role in regulation of the fluorescence changes that function as non-invasive, real-time, *in situ*, and direct detection signals.

Theranostics have been developed to target the primary tumor and metastases for early diagnosis and therapy. After being specifically activated by tumor factors, the cytotoxic drugs are released to inhibit the growth of tumor cells. High accumulation in tumor lesions allows cytotoxic drugs to act as effectively as possible. These expected effects allow patients to be administered lower doses, thus reducing overall systemic toxicity. Fluorescence signals provide an imaging modality that can both address the tumor lesions (by overexpressed receptors) and directly indicate the administered drugs (for distribution and accumulation). Fluorescence imaging of theranostics can allow visual evaluation and normalization of the efficacies of targeted drugs at tumor lesions. The results facilitate drug development by offering more information on the tumor stage, targeting ability, pharmacokinetics, and dosage. To date, there are no small-molecule fluorescent theranostics in clinical trials.

Imaging technologies are essential for the detection and visualization of tumor lesions. Current clinical imaging modalities include positron emission tomography (PET), single photon emission computed tomography (SPECT), magnetic resonance imaging/spectroscopy (MRI/MRS), computed tomography (CT), and ultrasound (US). Most of these have no depth sensitivity limit, but they cannot provide a real-time response for intraoperative diagnosis. Fluorescence imaging technology is expected to overcome some of the limitations of conventional therapeutics and improve tumor treatments. For fluorescence imaging tools, excellent selectivity and high sensitivity are the key parameters for visualizing physiological and pathological factors at a molecular level. These tools are also required to have sufficient spatial resolution for *in vivo* imaging. Unfortunately, the narrow tissue penetration of fluorescence has become the main obstacle to deep body scanning. Therefore, fluorescence imaging is performed at different spatial and temporal resolutions, ranging from micrometers (<5 mm) to centimeters (<10 cm).[48] Which imaging modality is chosen depends on the purpose of the examination and the site of the tumor lesion. To better understand the comprehensive nature of the tumor, development of this field has advanced toward combining fluorescence imaging with other radioactive imaging modalities, as well as intraoperative ultrasonography (termed as photoacoustic imaging). This strategy is expected to coordinate the individual benefits of each imaging technology, and thus overcome the limitations. In addition, attention must be paid to the cost and regulatory requirements for imaging reagents.

5. Conclusions

Cancer has been identified as a dominant cause of death. Surgery and chemotherapy drugs play vital roles in the treatment of tumors. Fluorescence imaging provides an exceptional approach to imaging and quantification of cellular dynamic events that have an enormous impact on the tumor. Fluorescence imaging is achieved by maximizing the target-to-background ratio. The availability of fluorescently labeled probes for targeting tumor lesions, including tumor margins, nerves, lymph nodes, and lymphatics, greatly benefit intraoperative diagnosis. Such small molecular fluorescent probe-based therapeutic systems, composed of an antitumor drug, an imaging unit, and a tumor targeting ligand linked by a cleavable bond, show high accumulation at tumor cells and low toxicity to normal cells. The therapeutic agents are responsive to physiological factors, such as GSH, H_2O_2, enzymes, and pH, and to external stimulators such as phototriggers to specifically release the incorporated prodrug. Such agents are not only used to examine the necessary dose and timing and the pharmacokinetics of chemotherapy drugs, but are also applied in real time to indicate the biodistribution and efficacy of chemotherapy drugs. Future generations of smart fluorescent imaging and theranostic agents should incorporate a specific tumor-targeting unit and cleavable bond to achieve enhanced cellular selectivity and targeted drug release. The ultimate goal of tumor therapy is to improve the quality of life and prolong the survival time.

Acknowledgements

We thank the National Nature Science Foundation of China (grant numbers: 21405172, 21575159, 31470415, 81670064), the National Research Foundation of Korea (grant numbers: 2008-0061891, 2009-00426), the Korea Health Industry Development Institute (grant number: HI16C2129), the program of Youth Innovation Promotion Association, CAS (Grant 2015170), and State Key Laboratory of Environmental Chemistry and Ecotoxicology, Research Center for Eco-Environmental Scienc-es, CAS (Grant KF2016-22).

References

1 R. Siegel, J. M. Ma, Z. H. Zou and A. Jemal, *Ca-Cancer J. Clin.*, 2014, **64**, 9–29.
2 J. Ferlay, H. R. Shin, F. Bray, D. Forman, C. Mathers and D. M. Parkin, *Int. J. Cancer*, 2010, **127**, 2893–2917.
3 H. Kobayashi, M. Ogawa, R. Alford, P. L. Choyke and Y. Urano, *Chem. Rev.*, 2010, **110**, 2620–2640.
4 C. A. Boswell and M. W. Brechbiel, *Nucl. Med. Biol.*, 2007, **34**, 757–778.
5 S. Salipalli, P. K. Singh and J. Borlak, *BMC Cell Biol.*, 2014, **15**, 26.
6 I. R. Correa, *Curr. Opin. Chem. Biol.*, 2014, **20**, 36–45.
7 K. M. Dean and A. E. Palmer, *Nat. Chem. Biol.*, 2014, **10**, 512–523.
8 M. Baker, *Nature*, 2010, **466**, 1137–1142.
9 X. Q. Chen, K. A. Lee, X. T. Ren, J. C. Ryu, G. Kim, J. H. Ryu, W. J. Lee and J. Yoon, *Nat. Protoc.*, 2016, **11**, 1219–1228.

 This journal is © The Royal Society of Chemistry 2017

Published on 20 marzo 2017. Downloaded on 11/05/2026 19:46:09.

10 F. Yu, P. Li, B. Wang and K. Han, *J. Am. Chem. Soc.*, 2013, **135**, 7674–7680.
11 M. de Jong, J. Essers and W. M. van Weerden, *Nat. Rev. Cancer*, 2014, **14**, 481–493.
12 M. Olivo, C. J. H. Ho and C. Y. Fu, *Laser Photonics Rev.*, 2013, **7**, 646–662.
13 X. Chen, F. Wang, J. Y. Hyun, T. Wei, J. Qiang, X. Ren, I. Shin and J. Yoon, *Chem. Soc. Rev.*, 2016, **45**, 2976–3016.
14 J. Li, D. Yim, W. D. Jang and J. Yoon, *Chem. Soc. Rev.*, 2016, DOI: 10.1039/c6cs00619a.
15 J. Yin, Y. Hu and J. Yoon, *Chem. Soc. Rev.*, 2015, **44**, 4619–4644.
16 Y. Tang, D. Lee, J. Wang, G. Li, J. Yu, W. Lin and J. Yoon, *Chem. Soc. Rev.*, 2015, **44**, 5003–5015.
17 A. L. Vahrmeijer, M. Hutteman, J. R. van der Vorst, C. J. H. van de Velde and J. V. Frangioni, *Nat. Rev. Clin. Oncol.*, 2013, **10**, 507–518.
18 Y. Liu, R. Njuguna, T. Matthews, W. J. Akers, G. P. Sudlow, S. Mondal, R. Tang, V. Gruev and S. Achilefu, *J. Biomed. Opt.*, 2013, **18**, 101303.
19 E. M. Sevick-Muraca, *Annu. Rev. Med.*, 2012, **63**, 217–231.
20 G. M. van Dam, G. Themelis, L. M. A. Crane, N. J. Harlaar, R. G. Pleijhuis, W. Kelder, A. Sarantopoulos, J. S. de Jong, H. J. G. Arts, A. G. J. van der Zee, J. Bart, P. S. Low and V. Ntziachristos, *Nat. Med.*, 2011, **17**, 1315–1319.
21 Q. T. Nguyen, E. S. Olson, T. A. Aguilera, T. Jiang, M. Scadeng, L. G. Ellies and R. Y. Tsien, *Proc. Natl. Acad. Sci. U. S. A.*, 2010, **107**, 4317–4322.
22 M. A. Pysz, S. S. Gambhir and J. K. Willmann, *Clin. Radiol.*, 2010, **65**, 500–516.
23 J. V. Frangioni, *Curr. Opin. Chem. Biol.*, 2003, **7**, 626–634.
24 S. A. Hilderbrand and R. Weissleder, *Curr. Opin. Chem. Biol.*, 2010, **14**, 71–79.
25 M. Gao, R. Wang, F. B. Yu, J. M. You and L. X. Chen, *Analyst*, 2015, **140**, 3766–3772.
26 P. Liu, X. T. Jing, F. B. Yu, C. J. Lv and L. X. Chen, *Analyst*, 2015, **140**, 4576–4583.
27 X. Jing, F. Yu and L. Chen, *Chem. Commun.*, 2014, **50**, 14253–14256.
28 K. Yin, F. Yu, W. Zhang and L. Chen, *Biosens. Bioelectron.*, 2015, **74**, 156–164.
29 X. Han, F. Yu, X. Song and L. Chen, *Chem. Sci.*, 2016, **7**, 5098–5107.
30 J. H. Park, S. Lee, J. H. Kim, K. Park, K. Kim and I. C. Kwon, *Prog. Polym. Sci.*, 2008, **33**, 113–137.
31 J. A. Hubbell and A. Chilkoti, *Science*, 2012, **337**, 303–305.
32 R. Tong and J. J. Cheng, *Polym. Rev.*, 2007, **47**, 345–381.
33 K. Riehemann, S. W. Schneider, T. A. Luger, B. Godin, M. Ferrari and H. Fuchs, *Angew. Chem., Int. Ed.*, 2009, **48**, 872–897.
34 J. V. Jokerst and S. S. Gambhir, *Acc. Chem. Res.*, 2011, **44**, 1050–1060.
35 W. Zhang, Y. Wang, X. Sun, W. Wang and L. Chen, *Nanoscale*, 2014, **6**, 14514–14522.
36 D. Lin, T. Qin, Y. Wang, X. Sun and L. Chen, *ACS Appl. Mater. Interfaces*, 2014, **6**, 1320–1329.
37 X. Niu, H. Chen, Y. Wang, W. Wang, X. Sun and L. Chen, *ACS Appl. Mater. Interfaces*, 2014, **6**, 5152–5160.
38 C. Vu Thanh, E. O. Ganbold, J. K. Saha, J. Jang, J. Min, J. Choo, S. Kim, N. W. Song, S. J. Son, S. B. Lee and S.-W. Joo, *J. Am. Chem. Soc.*, 2014, **136**, 3833–3841.
39 J. W. Singer, R. Bhatt, J. Tulinsky, K. R. Buhler, E. Heasley, P. Klein and P. de Vries, *J. Controlled Release*, 2001, **74**, 243–247.
40 P. V. Paranjpe, S. Stein and P. J. Sinko, *Anti-Cancer Drugs*, 2005, **16**, 763–775.
41 J. J. Khandare, P. Chandna, Y. Wang, V. P. Pozharov and T. Minko, *J. Pharmacol. Exp. Ther.*, 2006, **317**, 929–937.
42 A. Nel, T. Xia, L. Mädler and N. Li, *Science*, 2006, **311**, 622–627.
43 U. Resch-Genger, M. Grabolle, S. Cavaliere-Jaricot, R. Nitschke and T. Nann, *Nat. Methods*, 2008, **5**, 763–775.
44 M. Garland, J. J. Yim and M. Bogyo, *Cell Chem. Biol.*, 2016, **23**, 122–136.
45 S. Luo, E. Zhang, Y. Su, T. Cheng and C. Shi, *Biomaterials*, 2011, **32**, 7127–7138.
46 M. H. Lee, J. L. Sessler and J. S. Kim, *Acc. Chem. Res.*, 2015, **48**, 2935–2946.
47 J. H. Rao, A. Dragulescu-Andrasi, H. Q. Yao and H. Q. Yao, *Curr. Opin. Biotechnol.*, 2007, **18**, 17–25.
48 M. Rudin and R. Weissleder, *Nat. Rev. Drug Discovery*, 2003, **2**, 123–131.
49 M. Srinivasarao, C. V. Galliford and P. S. Low, *Nat. Rev. Drug Discovery*, 2015, **14**, 203–219.
50 R. Kumar, W. S. Shin, K. Sunwoo, W. Y. Kim, S. Koo, S. Bhuniya and J. S. Kim, *Chem. Soc. Rev.*, 2015, **44**, 6670–6683.
51 J. O. Escobedo, O. Rusin, S. Lim and R. M. Strongin, *Curr. Opin. Chem. Biol.*, 2010, **14**, 64–70.
52 F. Yu, X. Han and L. Chen, *Chem. Commun.*, 2014, **50**, 12234–12249.
53 J. R. van der Vorst, B. E. Schaafsma, F. P. R. Verbeek, M. Hutteman, J. S. D. Mieog, C. Lowik, G. J. Liefers, J. V. Frangioni, C. J. H. van de Velde and A. L. Vahrmeijer, *Ann. Surg. Oncol.*, 2012, **19**, 4104–4111.
54 Y. Ashitate, C. S. Vooght, M. Hutteman, R. Oketokoun, H. S. Choi and J. V. Frangioni, *Mol. Imaging*, 2012, **11**, 301–308.
55 W. Stummer, A. Novotny, H. Stepp, C. Goetz, K. Bise and H. J. Reulen, *J. Neurosurg.*, 2000, **93**, 1003–1013.
56 G. C. Gurtner, G. E. Jones, P. C. Neligan, M. I. Newman, B. T. Phillips, J. M. Sacks and M. R. Zenn, *Ann. Surg. Innov. Res.*, 2013, **7**, 1–14.
57 M. Gao, F. Yu, H. Chen and L. Chen, *Anal. Chem.*, 2015, **87**, 3631–3638.
58 F. Yu, M. Gao, M. Li and L. Chen, *Biomaterials*, 2015, **63**, 93–101.
59 Y. Huang, F. Yu, J. Wang and L. Chen, *Anal. Chem.*, 2016, **88**, 4122–4129.
60 C. Zhang, S. Wang, J. Xiao, X. Tan, Y. Zhu, Y. Su, T. Cheng and C. Shi, *Biomaterials*, 2010, **31**, 1911–1917.
61 X. Yang, C. Shi, R. Tong, W. Qian, H. E. Zhau, R. Wang, G. Zhu, J. Cheng, V. W. Yang and T. Cheng, *Clin. Cancer Res.*, 2010, **16**, 2833–2844.

Published on 20 marzo 2017. Downloaded on 11/05/2026 19:46:09.

62 C. Shi, J. B. Wu, G. C. Chu, Q. L. Li, R. Wang, C. Zhang, Y. Zhang, H. L. Kim, J. Wang, H. E. Zhau, D. Pan and L. W. Chung, *Oncotarget*, 2014, **5**, 10114–10126.
63 G. S. Hong, J. C. Lee, J. T. Robinson, U. Raaz, L. M. Xie, N. F. Huang, J. P. Cooke and H. J. Dai, *Nat. Med.*, 2012, **18**, 1841–1846.
64 G. S. Hong, J. T. Robinson, Y. J. Zhang, S. Diao, A. L. Antaris, Q. B. Wang and H. J. Dai, *Angew. Chem., Int. Ed.*, 2012, **51**, 9818–9821.
65 S. Diao, G. S. Hong, J. T. Robinson, L. Y. Jiao, A. L. Antaris, J. Z. Wu, C. L. Choi and H. J. Dai, *J. Am. Chem. Soc.*, 2012, **134**, 16971–16974.
66 A. L. Antaris, H. Chen, K. Cheng, Y. Sun, G. S. Hong, C. R. Qu, S. Diao, Z. X. Deng, X. M. Hu, B. Zhang, X. D. Zhang, O. K. Yaghi, Z. R. Alamparambil, X. C. Hong, Z. Cheng and H. J. Dai, *Nat. Mater.*, 2016, **15**, 235–242.
67 E. R. Trivedi, A. S. Harney, M. B. Olive, I. Podgorski, K. Moin, B. F. Sloane, A. G. M. Barrett, T. J. Meade and B. M. Hoffman, *Proc. Natl. Acad. Sci. U. S. A.*, 2010, **107**, 1284–1288.
68 H. S. Choi, S. L. Gibbs, J. H. Lee, S. H. Kim, Y. Ashitate, F. B. Liu, H. Hyun, G. Park, Y. Xie, S. Bae, M. Henary and J. V. Frangioni, *Nat. Biotechnol.*, 2013, **31**, 148–153.
69 M. H. Park, H. Hyun, Y. Ashitate, H. Wada, G. Park, J. H. Lee, C. Njiojob, M. Henary, J. V. Frangioni and H. S. Choi, *Theranostics*, 2014, **4**, 823–833.
70 M. Kawakami and J. Nakayama, *Cancer Res.*, 1997, **57**, 2321–2324.
71 R. E. Carter, A. R. Feldman and J. T. Coyle, *Proc. Natl. Acad. Sci. U. S. A.*, 1996, **93**, 749–753.
72 W. T. Tino, M. J. Huber, T. P. Lake, T. G. Greene, G. P. Murphy and E. H. Holmes, *Hybridoma*, 2000, **19**, 249–257.
73 S. E. Lupold, B. J. Hicke, Y. Lin and D. S. Coffey, *Cancer Res.*, 2002, **62**, 4029–4033.
74 S. E. Lupold and R. Rodriguez, *Mol. Cancer Ther.*, 2004, **3**, 597–603.
75 C. Liu, H. N. Huang, F. Donate, C. Dickinson, R. Santucci, A. El-Sheikh, R. Vessella and T. S. Edgington, *Cancer Res.*, 2002, **62**, 5470–5475.
76 M. G. Pomper, J. L. Musachio, J. Zhang, U. Scheffel, Y. Zhou, J. Hilton, A. Maini, R. F. Dannals, D. F. Wong and A. P. Kozikowski, *Mol. Imaging*, 2002, **1**, 96–101.
77 H. Tang, M. Brown, Y. Ye, G. Huang, Y. Zhang, Y. Wang, H. Zhai, X. Chen, T. Y. Shen and M. Tenniswood, *Biochem. Biophys. Res. Commun.*, 2003, **307**, 8–14.
78 V. Humblet, R. Lapidus, L. R. Williams, T. Tsukamoto, C. Rojas, P. Majer, B. Hin, S. Ohnishi, A. M. De Grand and A. Zaheer, *Mol. Imaging*, 2005, **4**, 448.
79 T. Liu, L. Wu, M. Kazak and C. E. Berkman, *Prostate*, 2008, **68**, 955–964.
80 T. Liu, L. Wu, M. R. Hopkins, J. K. Choi and C. E. Berkman, *Bioorg. Med. Chem. Lett.*, 2010, **20**, 7124–7126.
81 Y. Chen, S. Dhara, S. R. Banerjee, Y. Byun, M. Pullambhatla, R. C. Mease and M. G. Pomper, *Biochem. Biophys. Res. Commun.*, 2009, **390**, 624–629.
82 S. Jayaprakash, X. Wang, W. D. Heston and A. P. Kozikowski, *ChemMedChem*, 2006, **1**, 299–302.
83 C. E. Eberhart, R. J. Coffey, A. Radhika, F. M. Giardiello, S. Ferrenbach and R. N. Dubois, *Gastroenterology*, 1994, **107**, 1183–1188.
84 M. J. Uddin, B. C. Crews, A. L. Blobaum, P. J. Kingsley, D. L. Gorden, J. O. McIntyre, L. M. Matrisian, K. Subbaramaiah, A. J. Dannenberg, D. W. Piston and L. J. Marnett, *Cancer Res.*, 2010, **70**, 3618–3627.
85 M. J. Uddin, B. C. Crews, K. Ghebreselasie and L. J. Marnett, *Bioconjugate Chem.*, 2013, **24**, 712–723.
86 M. J. Uddin, B. C. Crews, I. Huda, K. Ghebreselasie, C. K. Daniel and L. J. Marnett, *ACS Med. Chem. Lett.*, 2014, **5**, 446–450.
87 M. J. Uddin, B. C. Crews, K. Ghebreselasie, C. K. Daniel, P. J. Kingsley, S. Xu and L. J. Marnett, *J. Biomed. Opt.*, 2015, **20**, 50502.
88 H. Zhang, J. Fan, J. Wang, S. Zhang, B. Dou and X. Peng, *J. Am. Chem. Soc.*, 2013, **135**, 11663–11669.
89 H. Zhang, J. Fan, J. Wang, B. Dou, F. Zhou, J. Cao, J. Qu, Z. Cao, W. Zhao and X. Peng, *J. Am. Chem. Soc.*, 2013, **135**, 17469–17475.
90 H. Zhang, J. L. Fan, K. Wang, J. Li, C. X. Wang, Y. M. Nie, T. Jiang, H. Y. Mu, X. J. Peng and K. Jiang, *Anal. Chem.*, 2014, **86**, 9131–9138.
91 B. Wang, J. Fan, X. Wang, H. Zhu, J. Wang, H. Mu and X. Peng, *Chem. Commun.*, 2015, **51**, 792–795.
92 W. Xia and P. S. Low, *J. Med. Chem.*, 2010, **53**, 6811–6824.
93 M. D. Kennedy, K. N. Jallad, D. H. Thompson, D. Ben-Amotz and P. S. Low, *J. Biomed. Opt.*, 2003, **8**, 636–641.
94 M. D. Kennedy, K. N. Jallad, J. Lu, P. S. Low and D. Ben-Amotz, *Pharm. Res.*, 2003, **20**, 714–719.
95 S. M. Mahalingam, S. A. Kularatne, J. Roy and P. S. Low, *Abstracts of Papers of the American Chemical Society*, 2013, vol. 246.
96 J. Yang, H. Chen, I. R. Vlahov, J. X. Cheng and P. S. Low, *Proc. Natl. Acad. Sci. U. S. A.*, 2006, **103**, 13872–13877.
97 H. Lee, J. Kim, H. Kim, Y. Kim and Y. Choi, *Chem. Commun.*, 2014, **50**, 7507–7510.
98 J. Levi, Z. Cheng, O. Gheysens, M. Patel, C. T. Chan, Y. B. Wang, M. Namavari and S. S. Gambhir, *Bioconjugate Chem.*, 2007, **18**, 628–634.
99 S. P. ZamoraLeon, D. W. Golde, I. I. Concha, C. I. Rivas, F. DelgadoLopez, J. Baselga, F. Nualart and J. C. Vera, *Proc. Natl. Acad. Sci. U. S. A.*, 1996, **93**, 15522.
100 K. Savage, H. A. Waller, M. Stubbs, K. Khan, S. A. Watson, P. A. Clarke, S. Grimes, D. Michaeli, A. P. Dhillon and M. E. Caplin, *Int. J. Oncol.*, 2006, **29**, 1429–1435.
101 D. S. Weinberg, B. Ruggeri, M. T. Barber, S. Biswas, S. Miknyocki and S. A. Waldman, *J. Clin. Invest.*, 1997, **100**, 597–603.
102 J. C. Reubi and B. Waser, *Int. J. Cancer*, 1996, **67**, 644–647.
103 T. Sethi, T. Herget, S. V. Wu, J. H. Walsh and E. Rozengurt, *Cancer Res.*, 1993, **53**, 5208–5213.
104 J. C. Reubi, J. C. Schaer and B. Waser, *Cancer Res.*, 1997, **57**, 1377–1386.

 This journal is © The Royal Society of Chemistry 2017

Published on 20 marzo 2017. Downloaded on 11/05/2026 19:46:09.

105 K. Hur, M. K. Kwak, H. J. Lee, D. J. Park, H. Lee, H. S. Lee, W. H. Kim, D. Michaeli and H. K. Yang, *J. Cancer Res. Clin. Oncol.*, 2006, **132**, 85–91.
106 J. Zhou, M. Chen, Q. Zhang, J. Hu and W. Wang, *Recept. Channels*, 2004, **10**, 185–188.
107 C. Wayua and P. S. Low, *Mol. Pharmaceutics*, 2014, **11**, 468–476.
108 S. Kossatz, M. Behe, R. Mansi, D. Saur, P. Czerney, W. A. Kaiser and I. Hilger, *Biomaterials*, 2013, **34**, 5172–5180.
109 M. A. Proescholdt, M. J. Merrill, E. M. Stoerr, A. Lohmeier, F. Pohl and A. Brawanski, *Neuro-Oncology*, 2012, **14**, 1357–1366.
110 A. M. Niemela, P. Hynninen, J. P. Mecklin, T. Kuopio, A. Kokko, L. Aaltonen, A. K. Parkkila, S. Pastorekova, J. Pastorek, A. Waheed, W. S. Sly, T. F. Orntoft, M. Kruhoffer, H. Haapasalo, S. Parkkila and A. J. Kivella, *Cancer Epidemiol., Biomarkers Prev.*, 2007, **16**, 1760–1766.
111 S. A. Hussain, R. Ganesan, G. Reynolds, L. Gross, A. Stevens, J. Pastorek, P. G. Murray, B. Perunovic, M. S. Anwar, L. Billingham, N. D. James, D. Spooner, C. J. Poole, D. W. Rea and D. H. Palmer, *Br. J. Cancer*, 2007, **96**, 104–109.
112 N. Krall, F. Pretto, W. Decurtins, G. J. L. Bernardes, C. T. Supuran and D. Neri, *Angew. Chem., Int. Ed.*, 2014, **53**, 4231–4235.
113 N. Krall, F. Pretto and D. Neri, *Chem. Sci.*, 2014, **5**, 3640–3644.
114 G. M. Thurber, K. S. Yang, T. Reiner, R. H. Kohler, P. Sorger, T. Mitchison and R. Weissleder, *Nat. Commun.*, 2013, **4**, 1504.
115 G. M. Thurber, T. Reiner, K. S. Yang, R. H. Kohler and R. Weissleder, *Mol. Cancer Ther.*, 2014, **13**, 986–995.
116 C. P. Irwin, Y. Portorreal, C. Brand, Y. C. Zhang, P. Desai, B. Salinas, W. A. Weber and T. Reiner, *Neoplasia*, 2014, **16**, 432–440.
117 R. J. Bernacki and U. Kim, *Science*, 1977, **195**, 577–580.
118 J. Dennis, C. Waller, R. Timpl and V. Schirrmacher, *Nature*, 1982, **300**, 274–276.
119 X. Wu, Y. Tian, M. Yu, B. Lin, J. Han and S. Han, *Biomater. Sci.*, 2014, **2**, 1120–1127.
120 X. Wu, M. Yu, B. Lin, H. Xing, J. Han and S. Han, *Chem. Sci.*, 2015, **6**, 798–803.
121 R. Andreesen, M. Modolell, H. U. Weltzien, H. Eibl, H. H. Common, G. W. Lohr and P. G. Munder, *Cancer Res.*, 1978, **38**, 3894–3899.
122 W. J. van Blitterswijk and M. Verheij, *Biochim. Biophys. Acta, Mol. Cell Biol. Lipids*, 2013, **1831**, 663–674.
123 J. P. Weichert, P. A. Clark, I. K. Kandela, A. M. Vaccaro, W. Clarke, M. A. Longino, A. N. Pinchuk, M. Farhoud, K. I. Swanson, J. M. Floberg, J. Grudzinski, B. Titz, A. M. Traynor, H. E. Chen, L. T. Hall, C. J. Pazoles, P. J. Pickhardt and J. S. Kuo, *Sci. Transl. Med.*, 2014, **6**, 240ra75.
124 K. I. Swanson, P. A. Clark, R. R. Zhang, I. K. Kandela, M. Farhoud, J. P. Weichert and J. S. Kuo, *Neurosurgery*, 2015, **76**, 115–123.
125 M. Stefanidakis and E. Koivunen, *Curr. Pharm. Des.*, 2004, **10**, 3033–3044.
126 Y. B. Kang, W. He, S. Tulley, G. P. Gupta, I. Serganova, C. R. Chen, K. Manova-Todorova, R. Blasberg, W. L. Gerald and J. Massague, *Proc. Natl. Acad. Sci. U. S. A.*, 2005, **102**, 13909–13914.
127 W. Wang, S. Ke, S. Kwon, S. Yallampalli, A. G. Cameron, K. E. Adams, M. E. Mawad and E. M. Sevick-Muraca, *Bioconjugate Chem.*, 2007, **18**, 397–402.
128 R. O. Hynes, *Cell*, 1992, **69**, 11–25.
129 R. Seftor, E. A. Seftor, K. R. Gehlsen, W. G. Stetler-Stevenson, P. D. Brown, E. Ruoslahti and M. Hendrix, *Proc. Natl. Acad. Sci. U. S. A.*, 1992, **89**, 1557–1561.
130 C. L. Gladson and D. Cheresh, *J. Clin. Invest.*, 1991, **88**, 1924.
131 K. R. Gehlsen, G. E. Davis and P. Sriramarao, *Clin. Exp. Metastasis*, 1992, **10**, 111–120.
132 E. J. Filardo, P. C. Brooks, S. L. Deming, C. Damsky and D. A. Cheresh, *J. Cell Biol.*, 1995, **130**, 441–450.
133 W. Wang, S. Ke, Q. Wu, C. Charnsangavej, M. Gurfinkel, J. G. Gelovani, J. L. Abbruzzese, E. M. Sevick-Muraca and C. Li, *Mol. Imaging*, 2004, **3**, 343–351.
134 S. Kwon, S. Ke, J. P. Houston, W. Wang, Q. Wu, C. Li and E. M. Sevick-Muraca, *Mol. Imaging*, 2005, **4**, 75–87.
135 R. M. Huang, J. Vider, J. L. Kovar, D. M. Olive, I. K. Mellinghoff, P. Mayer-Kuckuk, M. F. Kircher and R. G. Blasberg, *Clin. Cancer Res.*, 2012, **18**, 5731–5740.
136 X. Chen, P. S. Conti and R. A. Moats, *Cancer Res.*, 2004, **64**, 8009–8014.
137 Z. Cheng, Y. Wu, Z. Xiong, S. S. Gambhir and X. Chen, *Bioconjugate Chem.*, 2005, **16**, 1433–1441.
138 E. Garanger, D. Boturyn, Z. H. Jin, P. Dumy, M. C. Favrot and J. L. Coll, *Mol. Ther.*, 2005, **12**, 1168–1175.
139 Z. H. Jin, V. Josserand, J. Razkin, E. Garanger, D. Boturyn, M. C. Favrot, P. Dumy and J. L. Coll, *Mol. Imaging*, 2006, **5**, 188–197.
140 Z. H. Jin, V. Josserand, S. Foillard, D. Boturyn, P. Dumy, M. C. Favrot and J. L. Coll, *Mol. Cancer*, 2007, **6**, 41.
141 S. Lanzardo, L. Conti, C. Brioschi, M. P. Bartolomeo, D. Arosio, L. Belvisi, L. Manzoni, A. Maiocchi, F. Maisano and G. Forni, *Contrast Media Mol. Imaging*, 2011, **6**, 449–458.
142 F. Li, J. Liu, G. S. Jas, J. Zhang, G. Qin, J. Xing, C. Cotes, H. Zhao, X. Wang, L. A. Diaz, Z. Shi, D. Y. Lee, K. C. Li and Z. Li, *Bioconjugate Chem.*, 2010, **21**, 270–278.
143 W. Pham, Z. Medarova and A. Moore, *Bioconjugate Chem.*, 2005, **16**, 735–740.
144 R. Hussain, N. Courtenay-Luck and G. Siligardi, *Biomed. Pept., Proteins Nucleic Acids*, 1995, **2**, 67–70.
145 R. S. Herbst, *Int. J. Radiat. Oncol., Biol., Phys.*, 2004, **59**, 21–26.
146 H. Modjtahedi and C. Dean, *Int. J. Oncol.*, 1994, **4**, 277–296.
147 E. Chung, J. Lee, J. Yu, S. Lee, J. H. Kang, I. Y. Chung and J. Choo, *Biosens. Bioelectron.*, 2014, **60**, 358–365.
148 S. Ke, X. Wen, M. Gurfinkel, C. Charnsangavej, S. Wallace, E. M. Sevick-Muraca and C. Li, *Cancer Res.*, 2003, **63**, 7870–7875.

Published on 20 marzo 2017. Downloaded on 11/05/2026 19:46:09.

149 R. S. Agnes, A. M. Broome, J. Wang, A. Verma, K. Lavik and J. P. Basilion, *Mol. Cancer Ther.*, 2012, **11**, 2202–2211.
150 A. M. Burgoyne, J. M. Palomo, P. J. Phillips-Mason, S. M. Burden-Gulley, D. L. Major, A. Zaremba, S. Robinson, A. E. Sloan, M. A. Vogelbaum, R. H. Miller and S. M. Brady-Kalnay, *Neuro-Oncology*, 2009, **11**, 767–778.
151 S. M. Burden-Gulley, M. Q. Qutaish, K. E. Sullivant, M. Q. Tan, S. E. L. Craig, J. P. Basilion, Z. R. Lu, D. L. Wilson and S. M. Brady-Kalnay, *Int. J. Cancer*, 2013, **132**, 1624–1632.
152 S. E. L. Craig, J. Wright, A. E. Sloan and S. M. Brady-Kalnay, *World Neurosurg.*, 2016, **90**, 154–163.
153 L. Soroceanu, Y. Gillespie, M. B. Khazaeli and H. Sontheimer, *Cancer Res.*, 1998, **58**, 4871–4879.
154 M. Veiseh, P. Gabikian, S. B. Bahrami, O. Veiseh, M. Zhang, R. C. Hackman, A. C. Ravanpay, M. R. Stroud, Y. Kusuma, S. J. Hansen, D. Kwok, N. M. Munoz, R. W. Sze, W. M. Grady, N. M. Greenberg, R. G. Ellenbogen and J. M. Olson, *Cancer Res.*, 2007, **67**, 6882–6888.
155 M. Akcan, M. R. Stroud, S. J. Hansen, R. J. Clark, N. L. Daly, D. J. Craik and J. M. Olson, *J. Med. Chem.*, 2011, **54**, 782–787.
156 J. L. Kovar, E. Curtis, S. F. Othman, M. A. Simpson and D. M. Olive, *Anal. Biochem.*, 2013, **440**, 212–219.
157 P. V. Butte, A. Mamelak, J. Parrish-Novak, D. Drazin, F. Shweikeh, P. R. Gangalum, A. Chesnokova, J. Y. Ljubimova and K. Black, *Neurosurg. Focus*, 2014, **36**, E1.
158 A. Walia, J. F. Yang, Y. H. Huang, M. I. Rosenblatt, J. H. Chang and D. T. Azar, *Biochim. Biophys. Acta, Gen. Subj.*, 2015, **1850**, 2422–2438.
159 D. Citrin, A. K. Lee, T. Scott, M. Sproull, C. Menard, P. J. Tofilon and K. Camphausen, *Mol. Cancer Ther.*, 2004, **3**, 481–488.
160 Y. Matsumura and H. Maeda, *Cancer Res.*, 1986, **46**, 6387–6392.
161 A. Becker, B. Riefke, B. Ebert, U. Sukowski, H. Rinneberg, W. Semmler and K. Licha, *Photochem. Photobiol.*, 2000, **72**, 234–241.
162 H. I. Kim, D. Hwang, S. J. Jeon, S. Lee, J. H. Park, D. Yim, J. K. Yang, H. Kang, J. Choo, Y. S. Lee, J. Chung and J. H. Kim, *Nanoscale*, 2015, **7**, 6363–6373.
163 R. Atreya, H. Neumann, C. Neufert, M. J. Waldner, U. Billmeier, Y. Zopf, M. Willma, C. App, T. Munster, H. Kessler, S. Maas, B. Gebhardt, R. Heimke-Brinck, E. Reuter, F. Dorje, T. T. Rau, W. Uter, T. D. Wang, R. Kiesslich, M. Vieth, E. Hannappel and M. F. Neurath, *Nat. Med.*, 2014, **20**, 313–318.
164 J. A. Bonner, K. P. Raisch, H. Q. Trummell, F. Robert, R. F. Meredith, S. A. Spencer, D. J. Buchsbaum, M. N. Saleh, M. A. Stackhouse, A. F. LoBuglio, G. E. Peters, W. R. Carroll and H. W. Waksal, *J. Clin. Oncol.*, 2000, **18**, 47–53.
165 E. L. Rosenthal, B. D. Kulbersh, T. King, T. R. Chaudhuri and K. R. Zinn, *Mol. Cancer Ther.*, 2007, **6**, 1230–1238.
166 J. M. Warram, E. de Boer, M. Korb, Y. Hartman, J. Kovar, J. M. Markert, G. Y. Gillespie and E. L. Rosenthal, *Br. J. Neurosurg.*, 2015, **29**, 850–858.
167 H. M. Luo, R. Hernandez, H. Hong, S. A. Graves, Y. N. Yang, C. G. England, C. P. Theuer, R. J. Nickles and W. B. Cai, *Proc. Natl. Acad. Sci. U. S. A.*, 2015, **112**, 12806–12811.
168 M. Ogawa, N. Kosaka, P. L. Choyke and H. Kobayashi, *Cancer Res.*, 2009, **69**, 1268–1272.
169 T. Nakajima, M. Mitsunaga, N. H. Bander, W. D. Heston, P. L. Choyke and H. Kobayashi, *Bioconjugate Chem.*, 2011, **22**, 1700–1705.
170 K. Sano, M. Mitsunaga, T. Nakajima, P. L. Choyke and H. Kobayashi, *Breast Cancer Res.*, 2012, **14**, R61.
171 K. Sano, T. Nakajima, K. Miyazaki, Y. Ohuchi, T. Ikegami, P. L. Choyke and H. Kobayashi, *Bioconjugate Chem.*, 2013, **24**, 811–816.
172 R. Watanabe, K. Sato, H. Hanaoka, T. Harada, T. Nakajima, I. Kim, C. H. Paik, A. M. Wu, P. L. Choyke and H. Kobayashi, *ACS Med. Chem. Lett.*, 2014, **5**, 411–415.
173 K. Sato, A. P. Gorka, T. Nagaya, M. S. Michie, R. R. Nani, Y. Nakamura, V. L. Coble, O. V. Vasalatiy, R. E. Swenson, P. L. Choyke, M. J. Schnermann and H. Kobayashi, *Bioconjugate Chem.*, 2016, **27**, 404–413.
174 Z. Yang, J. Cao, Y. He, J. Yang, T. Kim, X. Peng and J. S. Kim, *Chem. Soc. Rev.*, 2014, **43**, 4563–4601.
175 Y. Liu, Y. Xu, X. Qian, Y. Xiao, J. Liu, L. Shen, J. Li and Y. Zhang, *Bioorg. Med. Chem. Lett.*, 2006, **16**, 1562–1566.
176 T. Guo, L. Cui, J. Shen, W. Zhu, Y. Xu and X. Qian, *Chem. Commun.*, 2013, **49**, 10820–10822.
177 Z. Li, X. Li, X. Gao, Y. Zhang, W. Shi and H. Ma, *Anal. Chem.*, 2013, **85**, 3926–3932.
178 Z. Li, X. Gao, W. Shi, X. Li and H. Ma, *Chem. Commun.*, 2013, **49**, 5859–5861.
179 Q. Wan, X. Gao, X. He, S. Chen, Y. Song, Q. Gong, X. Li and H. Ma, *Chem. – Asian J.*, 2014, **9**, 2058–2062.
180 K. Okuda, Y. Okabe, T. Kadonosono, T. Ueno, B. G. M. Youssif, S. Kizaka-Kondoh and H. Nagasawa, *Bioconjugate Chem.*, 2012, **23**, 324–329.
181 K. Xu, F. Wang, X. Pan, R. Liu, J. Ma, F. Kong and B. Tang, *Chem. Commun.*, 2013, **49**, 2554–2556.
182 Y. Li, Y. Sun, J. Li, Q. Su, W. Yuan, Y. Dai, C. Han, Q. Wang, W. Feng and F. Li, *J. Am. Chem. Soc.*, 2015, **137**, 6407–6416.
183 K. Tanabe, N. Hirata, H. Harada, M. Hiraoka and S. I. Nishimoto, *ChemBioChem*, 2008, **9**, 426–432.
184 H. Komatsu, H. Harada, K. Tanabe, M. Hiraoka and S. i. Nishimoto, *MedChemComm*, 2010, **1**, 50–53.
185 K. Kiyose, K. Hanaoka, D. Oushiki, T. Nakamura, M. Kajimura, M. Suematsu, H. Nishimatsu, T. Yamane, T. Terai and Y. Hirata, *J. Am. Chem. Soc.*, 2010, **132**, 15846–15848.
186 W. Piao, S. Tsuda, Y. Tanaka, S. Maeda, F. Liu, S. Takahashi, Y. Kushida, T. Komatsu, T. Ueno and T. Terai, *Angew. Chem., Int. Ed.*, 2013, **52**, 13028–13032.
187 H. Sies, *Free Radical Biol. Med.*, 1999, **27**, 916–921.
188 F. Yu, P. Li, P. Song, B. Wang, J. Zhao and K. Han, *Chem. Commun.*, 2012, **48**, 4980–4982.
189 Z. Zheng, G. Zhu, H. Tak, E. Joseph, J. L. Eiseman and D. J. Creighton, *Bioconjugate Chem.*, 2005, **16**, 598–607.

 This journal is © The Royal Society of Chemistry 2017

Published on 20 marzo 2017. Downloaded on 11/05/2026 19:46:09.

190 L. R. Jones, E. A. Goun, R. Shinde, J. B. Rothbard, C. H. Contag and P. A. Wender, *J. Am. Chem. Soc.*, 2006, **128**, 6526–6527.
191 S. Santra, C. Kaittanis, O. J. Santiesteban and J. M. Perez, *J. Am. Chem. Soc.*, 2011, **133**, 16680–16688.
192 Z. Yang, J. H. Lee, H. M. Jeon, J. H. Han, N. Park, Y. He, H. Lee, K. S. Hong, C. Kang and J. S. Kim, *J. Am. Chem. Soc.*, 2013, **135**, 11657–11662.
193 W. A. Henne, D. D. Doorneweerd, A. R. Hilgenbrink, S. A. Kularatne and P. S. Low, *Bioorg. Med. Chem. Lett.*, 2006, **16**, 5350–5355.
194 C. P. Leamon, J. A. Reddy, I. R. Vlahov, M. Vetzel, N. Parker, J. S. Nicoson, L.-C. Xu and E. Westrick, *Bioconjugate Chem.*, 2005, **16**, 803–811.
195 C. A. Ladino, R. V. Chari, L. A. Bourret, N. L. Kedersha and V. S. Goldmacher, *Int. J. Cancer*, 1997, **73**, 859–864.
196 I. Ojima, *Acc. Chem. Res.*, 2007, **41**, 108–119.
197 J. Chen, S. Chen, X. Zhao, L. V. Kuznetsova, S. S. Wong and I. Ojima, *J. Am. Chem. Soc.*, 2008, **130**, 16778–16785.
198 S. Chen, X. Zhao, J. Chen, J. Chen, L. Kuznetsova, S. S. Wong and I. Ojima, *Bioconjugate Chem.*, 2010, **21**, 979–987.
199 J. G. Vineberg, E. S. Zuniga, A. Kamath, Y.-J. Chen, J. D. Seitz and I. Ojima, *J. Med. Chem.*, 2014, **57**, 5777–5791.
200 J. G. Vineberg, T. Wang, E. S. Zuniga and I. Ojima, *J. Med. Chem.*, 2015, **58**, 2406–2416.
201 S. Maiti, N. Park, J. H. Han, H. M. Jeon, J. H. Lee, S. Bhuniya, C. Kang and J. S. Kim, *J. Am. Chem. Soc.*, 2013, **135**, 4567–4572.
202 S. Bhuniya, M. H. Lee, H. M. Jeon, J. H. Han, J. H. Lee, N. Park, S. Maiti, C. Kang and J. S. Kim, *Chem. Commun.*, 2013, **49**, 7141–7143.
203 H. MiáJeon, H. ThiáLe, T. WooáKim and J. SeungáKim, *Chem. Commun.*, 2014, **50**, 7690–7693.
204 S. Bhuniya, S. Maiti, E. J. Kim, H. Lee, J. L. Sessler, K. S. Hong and J. S. Kim, *Angew. Chem.*, 2014, **126**, 4558–4563.
205 A. El Alaoui, F. Schmidt, M. Amessou, M. Sarr, D. Decaudin, J. C. Florent and L. Johannes, *Angew. Chem., Int. Ed.*, 2007, **46**, 6469–6472.
206 M. H. Lee, J. Y. Kim, J. H. Han, S. Bhuniya, J. L. Sessler, C. Kang and J. S. Kim, *J. Am. Chem. Soc.*, 2012, **134**, 12668–12674.
207 X. Wu, X. Sun, Z. Guo, J. Tang, Y. Shen, T. D. James, H. Tian and W. Zhu, *J. Am. Chem. Soc.*, 2014, **136**, 3579–3588.
208 M. Ye, X. Wang, J. Tang, Z. Guo, Y. Shen, H. Tian and W. Zhu, *Chem. Sci.*, 2016, **7**, 4958–4965.
209 J. Wu, R. Huang, C. Wang, W. Liu, J. Wang, X. Weng, T. Tian and X. Zhou, *Org. Biomol. Chem.*, 2013, **11**, 580–585.
210 Y. Zhang, Q. Yin, J. Yen, J. Li, H. Ying, H. Wang, Y. Hua, E. J. Chaney, S. A. Boppart and J. Cheng, *Chem. Commun.*, 2015, **51**, 6948–6951.
211 O. Oktyabrsky and G. Smirnova, *Biochemistry*, 2007, **72**, 132–145.
212 M. López-Lázaro, *Cancer Lett.*, 2007, **252**, 1–8.
213 S. Reuter, S. C. Gupta, M. M. Chaturvedi and B. B. Aggarwal, *Free Radical Biol. Med.*, 2010, **49**, 1603–1616.
214 J. Fang, H. Nakamura and A. Iyer, *J. Drug Targeting*, 2007, **15**, 475–486.
215 Y. Kuang, K. Balakrishnan, V. Gandhi and X. Peng, *J. Am. Chem. Soc.*, 2011, **133**, 19278–19281.
216 E. J. Kim, S. Bhuniya, H. Lee, H. M. Kim, C. Cheong, S. Maiti, K. S. Hong and J. S. Kim, *J. Am. Chem. Soc.*, 2014, **136**, 13888–13894.
217 R. Kumar, J. Han, H. J. Lim, W. X. Ren, J. Y. Lim, J. H. Kim and J. S. Kim, *J. Am. Chem. Soc.*, 2014, **136**, 17836–17843.
218 R. Weinstain, E. Segal, R. Satchi-Fainaro and D. Shabat, *Chem. Commun.*, 2010, **46**, 553–555.
219 S. Danson, T. H. Ward, J. Butler and M. Ranson, *Cancer Treat. Rev.*, 2004, **30**, 437–449.
220 K. Sharma, A. Iyer, K. Sengupta and H. Chakrapani, *Org. Lett.*, 2013, **15**, 2636–2639.
221 P. Liu, J. Xu, D. Yan, P. Zhang, F. Zeng, B. Li and S. Wu, *Chem. Commun.*, 2015, **51**, 9567–9570.
222 S. G. Awuah, Y.-R. Zheng, P. M. Bruno, M. T. Hemann and S. J. Lippard, *J. Am. Chem. Soc.*, 2015, **137**, 14854–14857.
223 J. Y. Winum, M. Rami, A. Scozzafava, J. L. Montero and C. Supuran, *Med. Res. Rev.*, 2008, **28**, 445–463.
224 S. Y. Li, L. H. Liu, H. Z. Jia, W. X. Qiu, L. Rong, H. Cheng and X. Z. Zhang, *Chem. Commun.*, 2014, **50**, 11852–11855.
225 K. L. Dao, R. R. Sawant, J. A. Hendricks, V. Ronga, V. P. Torchilin and R. N. Hanson, *Bioconjugate Chem.*, 2012, **23**, 785–795.
226 D. E. Dolmans, D. Fukumura and R. K. Jain, *Nat. Rev. Cancer*, 2003, **3**, 380–387.
227 J. Lai, B. P. Shah, E. Garfunkel and K.-B. Lee, *ACS Nano*, 2013, **7**, 2741–2750.
228 T. Liu, L. Y. Wu, J. K. Choi and C. E. Berkman, *Prostate*, 2009, **69**, 585.
229 T. Liu, L. Y. Wu, J. K. Choi and C. E. Berkman, *Int. J. Oncol.*, 2010, **36**, 777–784.
230 J. Tian, J. Zhou, Z. Shen, L. Ding, J. Yu and H. Ju, *Chem. Sci.*, 2015, **6**, 5969–5977.
231 J. Kim, C. H. Tung and Y. Choi, *Chem. Commun.*, 2014, **50**, 10600–10603.
232 A. M. Hossion, M. Bio, G. Nkepang, S. G. Awuah and Y. You, *ACS Med. Chem. Lett.*, 2012, **4**, 124–127.
233 M. Bio, P. Rajaputra, G. Nkepang, S. G. Awuah, A. M. Hossion and Y. You, *J. Med. Chem.*, 2013, **56**, 3936–3942.
234 M. Bio, P. Rajaputra, G. Nkepang and Y. You, *J. Med. Chem.*, 2014, **57**, 3401–3409.
235 G. Nkepang, M. Bio, P. Rajaputra, S. G. Awuah and Y. You, *Bioconjugate Chem.*, 2014, **25**, 2175–2188.
236 S. Karthik, B. P. Kumar, M. Gangopadhyay, M. Mandal and N. P. Singh, *J. Mater. Chem. B*, 2015, **3**, 728–732.
237 D. J. Yamashiro, X. G. Liu, C. P. Lee, A. Nakagawara, N. Ikegaki, L. M. McGregor, S. B. Baylin and G. M. Brodeur, *Eur. J. Cancer*, 1997, **33**, 2054–2057.
238 G. M. Brodeur, A. Nakagawara, D. J. Yamashiro, N. Ikegaki, X. G. Liu, C. G. Azar, C. P. Lee and A. E. Evans, *J. Neuro-Oncol.*, 1997, **31**, 49–55.

Published on 20 marzo 2017. Downloaded on 11/05/2026 19:46:09.

239 Y. Wang, C. Hagel, W. Hamel, S. Muller, L. Kluwe and M. Westphal, *Acta Neuropathol.*, 1998, **96**, 357–364.
240 S. Kumar and J. deVellis, *J. Neurosci. Res.*, 1996, **44**, 490–498.
241 L. M. McGregor, B. K. McCune, J. R. Graff, P. R. McDowell, K. E. Romans, G. D. Yancopoulos, D. W. Ball, S. B. Baylin and B. D. Nelkin, *Proc. Natl. Acad. Sci. U. S. A.*, 1999, **96**, 4540–4545.
242 X. W. Xu, S. R. Tahan, T. L. Pasha and P. J. Zhang, *J. Cutaneous Pathol.*, 2003, **30**, 318–322.
243 M. J. Blasco-Gutierrez, I. J. S. Jose-Crespo, E. Zozaya-Alvarez, R. Ramos-Sanchez and N. Garcia-Atares, *Cancer Invest.*, 2007, **25**, 405–410.
244 W. Jin, G. M. Kim, M. S. Kim, M. H. Lim, C. Yun, J. Jeong, J. S. Nam and S. J. Kim, *Carcinogenesis*, 2010, **31**, 1939–1947.
245 A. Kamkaew and K. Burgess, *J. Med. Chem.*, 2013, **56**, 7608–7614.
246 H. Yuan, H. Chong, B. Wang, C. Zhu, L. Liu, Q. Yang, F. Lv and S. Wang, *J. Am. Chem. Soc.*, 2012, **134**, 13184–13187.
247 R. R. Nani, A. P. Gorka, T. Nagaya, H. Kobayashi and M. J. Schnermann, *Angew. Chem., Int. Ed.*, 2015, **54**, 13635–13638.
248 C. Zhang, L. Gao, Y. Cai, H. Liu, D. Gao, J. Lai, B. Jia, F. Wang and Z. Liu, *Biomaterials*, 2016, **84**, 1–12.
249 L. Liu, W. Qiu, B. Li, C. Zhang, L. Sun, S. Wan, L. Rong and X. Zhang, *Adv. Funct. Mater.*, 2016, **26**, 6257–6269.
250 W. Feng, C. Gao, W. Liu, H. Ren, C. Wang, K. Ge, S. Li, G. Zhou, H. Li, S. Wang, G. Jia, Z. Li and J. Zhang, *Chem. Commun.*, 2016, **52**, 9434–9437.
251 Y. Hong, J. W. Lam and B. Tang, *Chem. Soc. Rev.*, 2011, **40**, 5361–5388.
252 Y. Yuan, R. T. Kwok, B. Tang and B. Liu, *J. Am. Chem. Soc.*, 2014, **136**, 2546–2554.
253 Y. Yuan, Y. Chen, B. Tang and B. Liu, *Chem. Commun.*, 2014, **50**, 3868–3870.
254 Y. Yuan, R. T. Kwok, R. Zhang, B. Tang and B. Liu, *Chem. Commun.*, 2014, **50**, 11465–11468.
255 D. R. Green, L. Galluzzi and G. Kroemer, *Science*, 2011, **333**, 1109–1112.
256 M. Ross, G. Kelso, F. Blaikie, A. James, H. Cocheme, A. Filipovska, T. Da Ros, T. Hurd, R. Smith and M. Murphy, *Biochemistry*, 2005, **70**, 222–230.
257 Q. Hu, M. Gao, G. Feng and B. Liu, *Angew. Chem., Int. Ed.*, 2014, **53**, 14225–14229.
258 W. Sun, S. G. Guo, C. Hu, J. L. Fan and X. J. Peng, *Chem. Rev.*, 2016, **116**, 7768–7817.
259 C. Zhang, T. Liu, Y. Su, S. Luo, Y. Zhu, X. Tan, S. Fan, L. Zhang, Y. Zhou and T. Cheng, *Biomaterials*, 2010, **31**, 6612–6617.
260 E. Zhang, C. Zhang, Y. Su, T. Cheng and C. Shi, *Drug Discovery Today*, 2011, **16**, 140–146.
261 X. Tan, S. Luo, D. Wang, Y. Su, T. Cheng and C. Shi, *Biomaterials*, 2012, **33**, 2230–2239.
262 S. Luo, X. Tan, Q. Qi, Q. Guo, X. Ran, L. Zhang, E. Zhang, Y. Liang, L. Weng and H. Zheng, *Biomaterials*, 2013, **34**, 2244–2251.
263 Y. Wang, T. Liu, E. Zhang, S. Luo, X. Tan and C. Shi, *Biomaterials*, 2014, **35**, 4116–4124.
264 S. Luo, X. Tan, S. Fang, Y. Wang, T. Liu, X. Wang, Y. Yuan, H. Q. Sun, Q. R. Qi and C. M. Shi, *Adv. Funct. Mater.*, 2016, **26**, 2826–2835.
265 Y. Huang, J. Zhou, S. Luo, Y. Wang, J. He, P. Luo, Z. Chen, T. Liu, X. Tan, J. Ou, H. Miao, H. Liang and C. Shi, *Gut*, 2016, DOI: 10.1136/gutjnl-2016-311909.
266 J. B. Wu, T. P. Lin, J. D. Gallagher, S. Kushal, L. W. Chung, H. E. Zhau, B. Z. Olenyuk and J. C. Shih, *J. Am. Chem. Soc.*, 2015, **137**, 2366–2374.
267 J. B. Wu, C. Shi, G. C. Y. Chu, Q. Xu, Y. Zhang, Q. Li, S. Y. John, H. E. Zhau and L. W. Chung, *Biomaterials*, 2015, **67**, 1–10.
268 I. Bratsos, S. Jedner, T. Gianferrara and E. Alessio, *Chimia*, 2007, **61**, 692–697.
269 V. Pierroz, T. Joshi, A. Leonidova, C. Mari, J. Schur, I. Ott, L. Spiccia, S. Ferrari and G. Gasser, *J. Am. Chem. Soc.*, 2012, **134**, 20376–20387.
270 R. Ye, Z. Ke, C. Tan, L. He, L. Ji and Z. Mao, *Chem. – Eur. J.*, 2013, **19**, 10160–10169.
271 Y. Li, C. P. Tan, W. Zhang, L. He, L. N. Ji and Z. W. Mao, *Biomaterials*, 2015, **39**, 95–104.
272 C. R. Cardoso, M. V. Lima, J. Cheleski, E. J. Peterson, T. Venancio, N. P. Farrell and R. M. Carlos, *J. Med. Chem.*, 2014, **57**, 4906–4915.
273 T. Zou, C. T. Lum, S. S. Y. Chui and C. M. Che, *Angew. Chem.*, 2013, **125**, 3002–3005.
274 A. D. Keefe, S. Pai and A. Ellington, *Nat. Rev. Drug Discovery*, 2010, **9**, 537–550.
275 O. C. Farokhzad, J. Cheng, B. A. Teply, I. Sherifi, S. Jon, P. W. Kantoff, J. P. Richie and R. Langer, *Proc. Natl. Acad. Sci. U. S. A.*, 2006, **103**, 6315–6320.
276 O. C. Farokhzad and R. Langer, *Adv. Drug Delivery Rev.*, 2006, **58**, 1456–1459.
277 D. Shangguan, Y. Li, Z. Tang, Z. C. Cao, H. W. Chen, P. Mallikaratchy, K. Sefah, C. J. Yang and W. Tan, *Proc. Natl. Acad. Sci. U. S. A.*, 2006, **103**, 11838–11843.
278 X. Fang and W. Tan, *Acc. Chem. Res.*, 2009, **43**, 48–57.
279 Z. Tang, D. Shangguan, K. Wang, H. Shi, K. Sefah, P. Mallikratchy, H. W. Chen, Y. Li and W. Tan, *Anal. Chem.*, 2007, **79**, 4900–4907.
280 V. Bagalkot, O. C. Farokhzad, R. Langer and S. Jon, *Angew. Chem., Int. Ed.*, 2006, **45**, 8149–8152.
281 H. S. Choi, K. Nasr, S. Alyabyev, D. Feith, J. H. Lee, S. H. Kim, Y. Ashitate, H. Hyun, G. Patonay and L. Strekowski, *Angew. Chem., Int. Ed.*, 2011, **50**, 6258–6263.
282 M. V. Marshall, D. Draney, E. M. Sevick-Muraca and D. M. Olive, *Mol. Imaging Biol.*, 2010, **12**, 583–594.
283 R. J. Amato, A. Shetty, Y. Lu, R. Ellis and P. S. Low, *J. Immunother.*, 2013, **36**, 268–275.
284 K. L. Kiick, *Science*, 2007, **317**, 1182.
285 C. C. Lee, J. A. MacKay, J. M. Fréchet and F. C. Szoka, *Nat. Biotechnol.*, 2005, **23**, 1517–1526.

 This journal is © The Royal Society of Chemistry 2017

286 Y. Zhou, W. Huang, J. Liu, X. Zhu and D. Yan, *Adv. Mater.*, 2010, **22**, 4567–4590.
287 S. M. Lee, H. Chen, C. M. Dettmer, T. V. O'Halloran and S. T. Nguyen, *J. Am. Chem. Soc.*, 2007, **129**, 15096–15097.
288 L. Linderoth, P. Fristrup, M. Hansen, F. Melander, R. Madsen, T. L. Andresen and G. n. H. Peters, *J. Am. Chem. Soc.*, 2009, **131**, 12193–12200.
289 R. Mo, T. Jiang, R. DiSanto, W. Tai and Z. Gu, *Nat. Commun.*, 2014, **5**, 3364.
290 R. Mo, T. Jiang, J. Di, W. Tai and Z. Gu, *Chem. Soc. Rev.*, 2014, **43**, 3595–3629.
291 R. Mo and Z. Gu, *Mater. Today*, 2015, **19**, 276–284.
292 C. S. Kue, A. Kamkaew, K. Burgess, L. V. Kiew, L. Y. Chung and H. B. Lee, *Med. Res. Rev.*, 2016, **36**, 494–575.

Published on 20 marzo 2017. Downloaded on 11/05/2026 19:46:09.